Application of Extended DLVO Theory: Modeling of Flotation and Hydrophobicity of Dodecane

Laiqun Mao

Dissertation submitted to the Faculty of the
Virginia Polytechnic Institute and State University
in partial fulfillment of the requirements for the degree of

Doctor of Philosophy
in
Mining and Minerals Engineering

Roe-Hoan Yoon, Chair
Gerald H. Luttrell
Gregory T. Adel
Richey M. Davis
Zhenghe Xu

May 23, 1998
Blacksburg, Virginia

Keywords: Extended DLVO theory, Flotation Modeling, Hydrophobic force, Dodecane

Application of Extended DLVO Theory: Modeling of Flotation and Hydrophobicity of Dodecane

Laiqun Mao

(ABSTRACT)

The extended DLVO theory was used to develop a flotation model by considering both hydrodynamic and surface forces involved in the process. A stream function was used to estimate the kinetic energies for thinning the water films between bubbles and particles, which were compared with the energy barriers, created by surface forces, to determine the probability of adhesion. A general expression for the probability of detachment was derived from similar mechanism for chemical reaction, and the kinetic energy for detachment was estimated with French and Wilson's model. The hydrophobic force parameter (K_{132}) calculated from the rate constants of single bubble flotation tests showed that, K_{132} for bubble-particle interaction were close to the geometric means of K_{131} for particle-particle interactions and K_{232} for bubble-bubble interaction, indicating that the combining rules developed for dispersion forces may be useful for hydrophobic forces.

The model was used to predict flotation results as functions of several important parameters such as contact angle, double-layer potentials, particle size, bubble size, etc. The predictions were consistent with experience, and could be explained in view of the various subprocesses considered in the model development. Furthermore, the model suggested optimum conditions for achieving the maximum separation efficiency.

The extended DLVO theory was also used to determine the hydrophobic force between two oil/solution interfaces from the equilibrium film thicknesses of dodecylammonium chloride (RNH_3Cl) solutions obtained using Thin Film Balance (TFB) technique. The

results showed that, the oil droplets were inherently hydrophobic, and the hydrophobic force played an important role in the stability of emulsions. This force decreased with increasing surfactant concentration, and also changed with pH and the addition of electrolyte. The interfacial area occupied by molecules indicated that, the dodecane molecules might present between two surfactant ions at interface, thus the hydrophobicity of oil/solution interface was less sensitive to the addition of the surfactant than that of air/solution interface. Thermodynamic analysis suggested that, there might exist a relationship between the interfacial hydrophobicity and the interfacial tension.

ACKNOWLEDGMENTS

The utmost appreciation is expressed to my advisor, Dr. Roe-Hoan Yoon, for his guidance, suggestions, criticism and support throughout the course of this investigation. Special thanks are also given to Dr. Gerald H. Luttrell, Dr. Gregory T. Adel, Dr. Yakov, Rabinovich for their continuous interest and invaluable suggestions, and other committee members Dr. Richey Davis, Dr. Zhenghe Xu and Dr. William Ducker for reviewing this dissertation and their constructive comments.

The financial support from the Department of Mining and Minerals Engineering is gratefully acknowledged.

Sincere gratitude is expressed to the surface force group Dr. B. Suha Aksoy, X. Chen, Subramanian Vivek, Sohn Seungman Ramozan Asmatulu, Ismail Yildirim and Rajesh Pazhianur for their useful suggestions and comments, as well as the rest of his fellow graduate students at Holden Hall and Plantation road for their assistance and friendship. Additional gratitude is given to Alisa Alls, Roy Hill, Wayne Slusser, Lee Rasnake, Barbara Hess and Keith Kutz for their help and support.

My special appreciation is also given to my parent for their understanding, continued support and encouragement. Finally, deepest thanks are expressed to my wife, Hong Liu, for her endless confidence, patient and unconditional love.

TABLE OF CONTENTS

LIST OF FIGURES

LIST OF TABLES

CHAPTER 1: INTRODUCTION

1.1 General

Froth flotation is a physico-chemical separation process extensively used in a wide variety of processing plants. The success of this process depends on the difference in the surface properties of the raw materials. Usually, most species contained in the raw materials are hydrophilic (water-loving), but some of them, such as talc or freshly mined coal are hydrophobic (water-hating), and others can be rendered a hydrophobic surface by collector, a chemical components which selectively adsorb on the minerals to be floated. If a mixture of particles having different surface properties with respect to water is prepared in water and air bubbles are introduced into the pulp, the hydrophobic particles will attach to buoyant bubbles, which "float" away from the suspension to the froth layer at the top of the slurry where the particle-laden bubbles are collected as product. The hydrophilic minerals or tailings are rejected from the bottom of the flotation cell.

Owing to its efficiency, flotation has become a major process in the minerals industry. It is estimated that over two billion tons of ore, representing over one hundred different minerals, are processed annually by flotation worldwide (1) and the proportion of base-metals won by flotation is 95% (2). In the United States, four to five hundred million tons of ore and raw coal are subjected to flotation each year (3). However, with the continued depletion of high-grade ores, low-grade ores, which are usually fine-grained and complex, have to be mined and processed. Beneficiation of these low-grade ores requires the optimization of design and operation of the flotation facility that make separation economically feasible on a large scale. Modeling and simulation are essential engineering tools for such optimization which can maximize the process recoveries and minimize the costs of both tests and operation.

Sastry (4) summarized the purposes and advantages associated with the process models as follows:

- Provide a formal, structured qualitative and quantitative definition and understanding of the process;
- provide a basis for planning and evaluation of laboratory, pilot and plant experiments, for determining process parameters (and scale-up criteria), and for process control;
- enable simulation for process analysis leading to process and plant design, operation, control, optimization and improvement; and
- constitute excellent teaching, learning and training tools.

Computer simulation based on such physical and symbolic models provides efficient and economic investigation on the effects of different design and operating variables with reproducible results whenever the experiments are repeated.

In the initial flotation model of 1935 (5), the flotation process was described as a rate process, and the flotation recovery was expressed as an exponential function of time. Since that time, many flotation models have been proposed and published in the literature (6, 7), which are classified by Lynch *et al* (7) into three categories: empirical models, probability models and kinetic models. Due to the complexities involved in the three-phase phenomenon, most of the proposed models are empirical or semi-empirical (7-9), developing a fundamental model of flotation from first principles has been considered to be very difficult (4). Such model must include both hydrodynamic and surface chemistry parameters in the flotation system, but the information concerning the latter has been in lacking, and thus elementary processes of bubble-particle interactions have not been well understood. The surface forces considered in the classic DLVO theory can not explain the bubble-particle adhesion in most flotation system (10-12).

Recent development in direct force measurement revealed that, non-DLVO force forces such as hydration and hydrophobic forces play an important role in coagulation and dispersion of particles (13-16) , and the hydrophobic force is often considered as the only driving force for bubble-particle adhesion (10-12, 17). These forces are then included into the classic DLVO theory, named extended DLVO theory, which makes it possible to develop a fundamental model of flotation.

The extended DLVO theory can also be used to describe other phenomena in colloid and surface chemistry. In many industrial processes such as liquid-liquid extraction, alkaline flooding operation, flotation of hydrocarbons, etc., the stability of the oil droplets in the emulsion is often one of the most important factors which determine the efficiency of the processes (18-25). Many investigators showed that, the stability of the oil droplets can not be reasonably explained without the consideration of an attractive force, now recognized as hydrophobic force, in addition to electrostatic double layer force and van der Waals dispersion force included in classic DLVO theory (26-30). Obviously, this force is dependent on the hydrophobicity of the oil/solution interface which can be changed by addition of various chemicals (in which surfactant are most commonly used in practice). In order to accurately describe the stability of the emulsion, further investigation must be conducted to quantify the hydrophobicity of oil droplets under different conditions.

1.2 Literature Review

1.2.1 Extended DLVO theory

The DLVO theory (31, 32) has been used to predict the stability of colloidal suspensions of lyophobic particles and served as a backbone of colloid chemistry for the past half a century. According to this theory, stability of colloidal suspensions in a

dielectric medium is determined by the sum of repulsive electrostatic interaction energy (V_e) and the attractive London-van der Waals (dispersion) energy (V_d). Thus, the total energy (V_t) is given by:

$$V_t = V_e + V_d \qquad [1.1]$$

Fig. 1.1 shows the typical values of V_e, V_d and V_t as a function of distance between two surfaces. At an intermediate distance, V_e can exceed V_d, in which case an energy barrier (E_1) exists. If particles collide with each other with sufficient kinetic or thermal energies to overcome E_1, the coagulation will occur and the suspension will be destabilized. Changing the ionic strength of the solution may obviously alter V_e, which can be used to control the stability of colloidal suspensions.

Despite the time-honored success, it is now well established that the classical DLVO theory has its limitation. It is applicable only for those particles that are neither hydrophobic nor hydrophilic. When the advancing water contact angle on the surface (θ_a) is less than 15°, the hydration force becomes significant which may greatly stabilizes the colloidal suspension (13,14, 33-36), while the hydrophobic force becomes appreciable when θ_a>64° which provides main driving force for particle coagulation (37, 38). Recognizing this fact, Xu and Yoon (15, 16) included third term V_s to the classical DLVO theory, so called extended DLVO theory, to consider the contribution from the non-DLVO forces (or structural force) . Thus the total energy becomes:

$$V_t = V_e + V_d + V_s. \qquad [1.2]$$

This equation has been successfully used to quantitatively describe interactions between two symmetric interfaces (30-42) and further extended to describe the bubble-particle interaction in flotation systems (43-44), as discussed in the following sections.

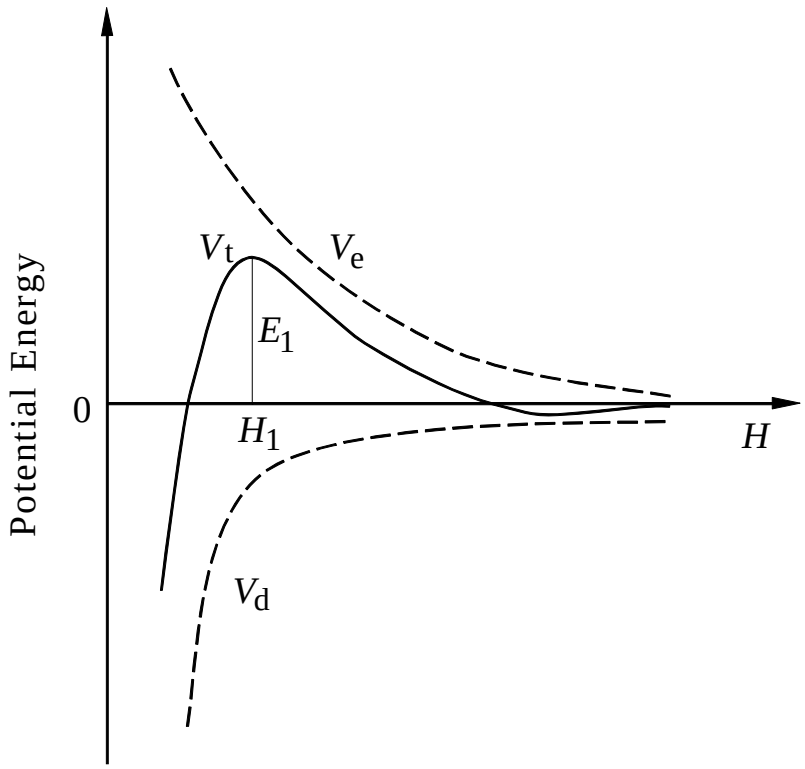

Figure 1.1. Interaction energy between two identical macroscopic bodies as described by the classic DLVO theory.

1.2.1.1 Electrical Double Layer Component (V_e)

The electrostatic double layer force develops due to the interaction between the electrical double layers of the bubble and particle. Overlap between the double layers gives a rise to attraction or repulsion, depending on their relative signs. If the double layers are of opposite charge, the force is attractive, which assists in thinning and finally rupture of the film between bubble and particle. When the double layers are of like charge, the resulting force is repulsive, which resists film thinning. The magnitude of the double layer force is a function of the double layer characteristics, if the bubble and particle are considered as two spheres with radii R_1 and R_2, respectively, the expression for V_e is given as (45, 46):

$$V_e = P\left[Q\ln\left(\frac{1+e^{-\kappa H}}{1-e^{-\kappa H}}\right)+\ln\left(1-e^{-2\kappa H}\right)\right] \qquad [1.3]$$

where H is the closest distance between two surfaces, P and Q are given by:

$$P = \frac{\varepsilon R_1 R_2\left(\psi_1{}^2+\psi_2{}^2\right)}{4\left(R_1+R_2\right)} \qquad [1.4]$$

$$Q = \frac{2\psi_1\psi_2}{\psi_1{}^2+\psi_2{}^2} \qquad [1.5]$$

ψ_1 and ψ_2 are the surface potentials of the particle and bubble, respectively, ε is the dielectric constant. κ is the Debye reciprocal length which represents the thickness of the electrical double layer and is mainly determined by the electrolyte concentration. According to the classic Debye-Hucel theory (47), the $1/\kappa$ is given as following:

$$\frac{1}{\kappa} = \sqrt{\frac{\varepsilon kT}{8\pi n_0 e^2}} \approx \frac{3}{Z\sqrt{C}} \qquad \text{[Å] in water at 25°C} \qquad [1.6]$$

in which k is the Boltzmann constant, T is the temperature, n_0 is the number density of ions, e is the elementary charge, and C is the electrolyte concentration (mol/l). Eq. [1.6] indicates that increasing the electrolyte concentration will compress the electrical double layer, resulting in decreasing of the double layer force.

Several mechanisms may be responsible for the charging at the particle/liquid interfaces, including unequal distribution of the lattice-forming ions, dissociation of the surface groups, preferential adsorption and substitution of crystal ions. In a given system, the predominate mechanism is dependent on the material characteristics. At bubble/liquid interface, the preferential adsorption of ions in the solution is commonly considered as the charging mechanism of bubble surface, the sign of the charge is determined by the polar head of the surfactant and pH when an ionic surfactant is used to stabilize bubbles. In the presence of non-ionic surfactants the bubble can be charged either positively or negatively, depending on pH of the solution, and the Isoelectric Point (i.e.p) appears to be related to the oxygen-to-carbon ratio of the surfactant molecule (48, 49).

It should be pointed out that, the derivation of Eq. [1.3] is based on the Derjaguin approximation. Recently, from the linearized Poisson-Boltzmann equation, Ohshima and Kondo (50) proposed an exact expression for the interaction between two charged spheres as :

$$V_e = \frac{4\pi R_1 R_2 \rho_1 \rho_2}{\varepsilon_r \varepsilon_0 \kappa^4} \frac{\exp(-\kappa R)}{R} \left[\cosh(\kappa R_1) - \frac{\sinh(\kappa R_1)}{\kappa R_1} \right] \left[\cosh(\kappa R_2) - \frac{\sinh(\kappa R_2)}{\kappa R_2} \right] \quad [1.7]$$

where, ρ_1 and ρ_2 are the fixed charge densities of sphere 1 and 2 respectively, ε_r and ε_0 are the relative permittivities of electrolyte solution and vacuum, R is the sum of a_1, a_2 and H. They checked the validity of the Derjaguin approximation and showed that

Derjaguin method was quite a good approximation in the case of two interacting charged spheres. Similar conclusions were obtained in the derivation of analytical expressions for electric double layer force, although in some cases, this force even becomes attractive between two similarly charged surfaces (51, 52).

When the double layers of bubble and particle are of like charge, increasing the potentials of bubble or particle can increase the difference of rate constants for minerals with different hydrophobicity, which can be used to enhance the selectivity of flotation (53).

1.2.1.2 Dispersion Component

Dispersion force arises from the van der Waals forces which operate between nonpolar atoms and molecules. The calculation of V_d has been attempted by two different approaches; one is based on a molecular model attributed to Hamaker, and the other based on a model of condensed media attributed to Lifshitz (54). The former approach is also known as the microscopic approach, it uses the well-known London's expression for the dispersion attraction between two isolated molecules, and integrates it for all molecules to obtain the dispersion energy of interaction between two macroscopic bodies. For two spherical bodies with radius R_1 and R_2, the V_d is given as (55):

$$V_d = -\frac{R_1 R_2 A_{132}}{6(R_1 + R_2)H} f \qquad [1.8]$$

where, f is a factor included to account for the retardation effect. A_{132} is the complex Hamaker constant which is used to characterize the interaction between sphere 1 (particle) and sphere 2 (bubble) with the intervening medium 3 (aqueous solution). Hamaker (56) has shown that:

$$A_{132} = \left(\sqrt{A_{11}} - \sqrt{A_{33}}\right)\left(\sqrt{A_{22}} - \sqrt{A_{33}}\right) \quad [1.9]$$

where A_{11}, A_{22} and A_{33} refer to the Hamaker constants of the particle, bubble and medium respectively. Eq. [1.9] indicates that, when the Hamaker constants for the two objects are either both greater than or less than the medium's Hamaker constant, A_{132} is positive and the dispersion force is attractive. When the Hamaker constant of the medium is between those of the two objects, however, A_{132} is negative and a repulsive dispersion force is produced, as observed by Milling *et al* using Atomic Force Microscope (AFM) (57). Typically, the Hamaker constant for water is less than that of the particle, but greater than that of the air bubble (for which the Hamaker constant is assumed to be zero if the bubble surface is not significantly coated by surfactant). Then A_{132} becomes negative for most flotation systems. In this case, V_d becomes positive according to Eq. [1.8], which means that the dispersion force is repulsive in bubble-particle interaction.

1.2.1.3 Structural Component

The origin of the structural force is still not completely understood, but its existence has been confirmed in many experiments. For a hydrophilic surface, V_s is positive, demonstrating a repulsive structural force which is often referred to as hydration force. For a hydrophobic surface, V_s is negative, and an attractive structural force can be observed which is usually referred to as hydrophobic force. In 1982, Israelachvili and Pashley (58, 59) showed that direct force measurements between mica surfaces immersed in cetyltrimethylammonium bromide (CTAB) solution could not be explained by the classical DLVO theory, an additional attractive force presented in 0-10 nm range, which was much stronger than the van der Waals dispersion force. This hydrophobic force (F_h) was clearly attributed to the hydrophobic interaction between the surfactant-coated surfaces and decayed exponentially with the separation distance (H) as follows:

$$\frac{F_h}{R} = -C_0 \exp\left(-\frac{H}{D_0}\right) \quad [1.10]$$

where R is the radius of the curved mica surfaces, C_0 is a constant (-140 mN/m) and D_0 is the decay length (1.0±0.1 nm). Similar hydrophobic force was observed in subsequent measurements of mica surfaces in surfactant solutions with decay length from 1.0 to 2.5 nm (39, 60-62).

Direct force measurements conducted later showed that the hydrophobic forces can be 10-1000 times stronger than the van der Waals force and effective in the range of more than 100 nm. Such long-range attractive forces were found between surfaces coated with surfactants by Langmuir-Blodgett (LB) deposition (63-68) or silanated with trimethylchlorosilane (TMCS) and octadecyltrichlorosilane (ODTCS) (69-72). A double exponential function:

$$\frac{F_h}{R} = -C_1 \exp\left(-\frac{H}{D_1}\right) - C_2 \exp\left(-\frac{H}{D_2}\right) \quad [1.11]$$

is often used to account for this long-range hydrophobic force. In which, C_1 and C_2 are the pre-exponential parameters. D_1 and D_2 are decay lengths of short-range and long-range hydrophobic force. In general, the short-range forces are discernible at H<10 nm with D_1 in the range of 1-2 nm, while the long-range forces are measured at H>10 nm with D_2 in the range of 10-32 nm, depending on the hydrophobicity of the surfaces involved. In some cases, experimentally measured hydrophobic forces can be fitted by a power law (65, 73):

$$\frac{F_h}{R} = -\frac{K}{6H^2} \quad [1.12]$$

where K is the hydrophobic force parameter. Eq. [1.12] is of the same forms as the van der Waals dispersion forces, therefore the values of its only parameter K can be directly compared with the Hamaker constants.

Several investigators proposed the theoretical rationales for the single exponential form (Eq. [1.10]) (74-76) and the power law (Eq. [1.12]) (77). However, since the origin of hydrophobic force is still not completely understood, these rationales are quite questionable, and therefore all expressions for hydrophobic force (Eq. [1.10]- [1.12]) are still empirical functions without theoretical basis.

1.2.1.4 Disjoining Pressures

In 1939, Derjaguin and Kussakov (78) observed that, when an air bubble is pressed against a hydrophilic glass plate immersed in aqueous solution, the intervening liquid slowly thins to leave a uniform equilibrium film of considerable thickness. The film behaviors as though there were an excessive pressure Π, acting normally to the film and opposing the further reduction in film thickness. This excessive pressure, termed as disjoining pressure, represents the difference between the pressure within the bubble (P^b) and that in the bulk liquid adjacent to the solid surface (P^l), i.e.

$$\Pi = P^b - P^l \qquad [1.13]$$

The thermodynamic analysis gives a more rigorous definition Π (44):

$$\Pi = \frac{d\mu_{H_2O}}{\overline{V}^{\sigma}} \qquad [1.14]$$

where μ_{H_2O} is the chemical potential of water, $\bar{V}^{\sigma}$ is the partial molar volume of water. Eq. [1.14] indicates that the disjoining pressure results from the difference in chemical potential of water in the bulk and the interface which is the function of distance between two surfaces.

It is widely accepted that, the disjoining pressure is produced by three types of forces: electrostatic double layer force, van der Waals dispersion force and structure force, as discussed in previous section. Similarly, the total pressure can be expressed as the summation of three components (79):

$$\Pi = \Pi_e + \Pi_d + \Pi_s . \qquad [1.15]$$

Π_e can be obtained by solving the Poisson-Boltzmann (PB) equation under a variety of different boundary conditions (80-83). Typically, when the surface charge is low enough to satisfy the linearization of the PB equation, in presence of univalent electrolyte, the constant surface potential (80, 81) and constant surface charge (80-83) models for Π_e are respectively given by:

$$\Pi_e = \frac{\varepsilon \psi_0^{\,2}}{8\pi}\left[\sec h^2(\kappa H)\right] \qquad [1.16]$$

and

$$\Pi_e = \frac{2\pi\sigma_0^{\,2}}{\varepsilon}\left[\frac{1+\sec h\left(\frac{\kappa H}{2}\right)}{\tanh\left(\frac{\kappa H}{2}\right)}\right]^2 \qquad [1.17]$$

in which ψ_0 is the potential and σ_0 is the charge density at the interface. Eq. [1.17] can be further simplified for large distances and low potential as (84):

$$\Pi_e = 64CRT\tanh^2\left(\frac{e\psi_0}{4kT}\right)\exp(-\kappa H) \qquad [1.18]$$

where R is the gas constant and T the absolute temperature. Eq. [1.18] is also applicable for constant charge systems since discharge is ignorable for small overlap of double layers. More elaborate models for Π_e include, charge regulation boundary conditions at the interface (85, 86) and effects due to ionic correlation and image forces (87, 88).

Similar to V_d, Π_d was determined in the microscopic approach of Hamaker or macroscopic approach of Liftshitz. For interaction between two plane parallel surfaces (**2**) separated by another phase (**3**), it was given by (56):

$$\Pi_d = -\frac{A_{232}}{6\pi H^3} \qquad [1.19]$$

where A_{232} is the Hamaker constant.

Corresponding to Eq. [1.10] - [1.12], the expression for Π_s can be given as single exponential (58) or double exponential functions (62, 63, 68), but for the same advantages of Eq. [1.12], it is commonly represented by a power law (70, 73):

$$\Pi_s = -\frac{K_{232}}{6\pi H^3} \qquad [1.20]$$

in which K_{232} is the hydrophobic force parameter which can be directly compared with A_{232}.

1.2.1.5 Origin of Hydrophobic Force

Several theories have been proposed over the past decade to describe the origin of the hydrophobic force. It was proposed that the hydrophobic attraction is a entropic force due to configurational orientation and rearrange of water molecules when two surfaces approach to each other (37, 74, 89-92). The molecular dynamics and Monte Carlo simulation (93-96) give different structures of water layers close to hydrophilic and hydrophobic surface. The dipoles of water molecules near the hydrophilic walls are predominately oriented normally to the surface, which causes the appearance of a dipole potential and reduces the tangential mobility of water molecules, as the results, the density and viscosity of this boundary layer is increased, while the dielectric permittivity is reduced and excess energy is required to disrupt this ordered water structure as two surfaces approach to each other (92). While for the hydrophobic surfaces, the dipoles and the planes of water molecules are oriented predominantly in parallel with the surface, which causes an increase in their tangential mobility and thus reduction in both density and viscosity of the boundary layer, consequently, the water molecules are readily displaced from the interface. The importance of water molecules was confirmed by Parker and Claesson (97). They measured the attractive force between two hydrophobic surfaces in the solutions with different water/ethylene glycol ratio, and found that the range and strength of the attractive force was dramatically increased with increasing water content. After the water content reached 51%, the force approximated to that observed in pure water. However, simulation results showed that these peculiar structures can propagate 5 to 6 layers water molecules from the surface at most (98), thus this theory can only explain short-range hydrophobic forces (74).

Many investigators observed that the long-range hydrophobic force is sensitive to the addition of some electrolytes even in low concentration, indicating that there are some electrostatic contributions, direct or indirect, to the attractive force (63, 66, 99, 100). The magnitude of the hydrophobic force decreases with increasing electrolyte concentration, and the 2:2 electrolytes such as $MgSO_4$ have a stronger effect than the 1:1 electrolyte like NaCl (99), but this effect of the salt mainly reduces the amplitude but not the decay

length of the hydrophobic force (100). At a low electrolyte concentration, the Zeta-potential does not change obviously, and no simple relationship is found between the decay length of the hydrophobic force and the Debye screening length κ^{-1}, indicating that the decrease of the long range attractive force upon addition of salt does not arise from the generation of the double layer interaction. Based on experimental observations, Attard (75) proposed that the long-range hydrophobic force may be due to the anomalous polarization of the water molecules near the hydrophobic surface. Podgornik (76) suggested that the fluctuating electric field due to the lateral mobility of the ions at the solid/liquid interfaces may attribute to the long-range hydrophobic forces. The correlation of the large in-plane dipoles formed by the domains of adsorbed hydrocarbons produces electric fields which was also considered as a possible origin of the hydrophobic force (68, 70, 71, 99, 101-103), the size of the domains and the order of the hydrocarbon chains are important factors determining the magnitude and range of the attractive forces. Tsao *et al* (68) measured the hydrophobic forces at different temperatures and suggested that, the force is most long-ranged when the alkyl chains are in a well-ordered "frozen" states, when the hydrophobic monolayer becomes disordered at higher temperature, the attractive force is decreased to the extent that it could not distinguished from the van der Waals force. Their results were further correlated with the order parameter by Rabinovich *et al* (102) demonstrating a linear relationship between the force parameters and the order parameter of the hydrocarbon chains, which clearly supports the domain theory. However, this theory can not explain the force measurement data which show the independence of the hydrophobic force on the electrolyte concentration (66, 69, 99).

It is very interesting to observe that (99, 104), the long-range attraction between a hydrophobic surface and a polar surface of mica is stronger than that between two hydrophobic surfaces, where the attractive force results from one surface generating the electrical field due to the domains on the hydrophobic surface, and the second surface responding to this field through its polarization. However, similar surface force

measurements conducted on the silica surfaces showed only short-range attractive forces (71, 105).

Thermodynamically, when the receding contact angle of the solid surfaces exceeds 90°, vapor cavities can be spontaneously formed due to the metastability of the water film near the hydrophobic surfaces, the capillary forces resulting from these cavities can be an origin of the long-range hydrophobic forces (106). This phenomenon can also occur between the surface with contact angle less than 90°, in this case, the voids produced by lateral thermal fluctuation of water molecules near hydrophobic surface may align themselves to form a vapor bridge between the surfaces at sufficiently close distance (77). Obviously, the presence of dissolved gas in the solution facilitates cavitation and thus increases the hydrophobic force, which is observed in many experiments (71, 107-109). However, the macroscopic vapor cavities have not been observed between two surfaces approaching to each other, instead, they have been found between surfaces in contact (64, 110). Also, cavitation should be enhanced at higher temperature due to a lower solubility of gases in solution, and thus the hydrophobic force should be increased, however, the experimental result showed decrease of hydrophobic force with increasing temperature (32, 68). Recognizing these facts, Ruckenstein and Churaev suggested that the fluctuations of metastable water molecules at two solid-liquid interfaces can correlate hydrodynamically to produce a long-range attractive force (111).

1.2.2 Bubble-Particle Interactions in Flotation

1.2.2.1 Criteria of Bubble-Particle Interactions

From the fundamental viewpoint, it is well recognized that a successful flotation must satisfy both thermodynamic and kinetic criteria (112). The general thermodynamic condition for three-phase contact between the particle, solution and air bubble is a finite

contact angle at the three-phase boundary, as shown in Figure 1.2. From Young's equation, modified to take account saturation of the gas phase with water vapor, there is (113):

$$\cos\theta = \frac{\gamma_{sv} - \gamma_{sl}}{\gamma_{lv}} \qquad [1.21]$$

where θ is the contact angle, γ_{sv}, γ_{sl} and γ_{lv} are the surface tensions at solid/vapor, solid/liquid and liquid/vapor interfaces, respectively. The change in free energy (ΔG) for the process of bubble-particle attachment is given by:

$$\Delta G = \gamma_{sl} - (\gamma_{sv} + \gamma_{lv}) \qquad [1.22]$$

Substituting Eq. [1.21] into Eq. [1.22] produces the thermodynamic criteria of flotation:

$$\Delta G = \gamma_{lv}(\cos\theta - 1), \qquad [1.23]$$

which suggest that, only when the contact angle has a finite value, the particles can attach to the bubble surface. However, a minimum contact angle is required in practice for successful flotation, which depends on hydrodynamic and physico-chemical properties of both bubble and particle (114).

Obviously, larger contact angle implies better flotability of the particle. Eq. [1.21] indicates that, in order to obtain the maximum contact angle, γ_{sv} should be minimized which can be achieved by adsorption of surfactant at solid/vapor interface. (115). On the other hand, the value of γ_{lv} should be as large as possible, indicating that the dosage of the frother which is used to stabilize bubbles in pulp should be limited, because the presence

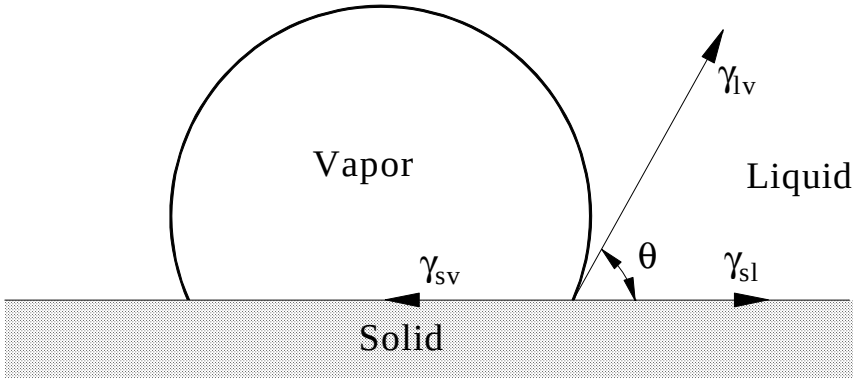

Figure 1.2 Three-phase contact for an air bubble attached to a solid surface in liquid medium.

of the frother may obviously reduce γ_{lv} , which in turn decreases the probability of flotation.

From a dynamic viewpoint, the process involved in flotation are usually considered to have three distinct stages (116, 117):

a) Bubble-particle collision with the formation of a thin wetting film, called disjoining film;

b) Thinning of the disjoining film which separates the colliding bubble and particle, and film ruptures at the critical thickness which depend on surface forces between bubble and particle;

c) Formation of a stable bubble-particle aggregate capable of withstanding considerable disruptive forces operating in the flotation machines.

The hydrodynamics of flotation system, such as size of bubble and particle, Reynolds number, viscosity of fluid, etc. determine the first stage, bubble-particle collision, while the other two stages depend on both hydrodynamics and surface forces between bubble and particle, in which the hydrophobicity of the solid surface plays a particularly important roles in the bubble-particle interaction. The second stage, the thinning and rupture of the wetting film, is often considered as the most important stage in flotation (117-120), because it is a slow process and therefore is the rate-determining step.

Most of the early research in froth flotation was primarily devoted to the chemistry and model of actions of the collectors, activators, depressants and frothers, which are used to increase the difference of hydrophobicity between valuable minerals and gangue or stabilize bubbles in solid suspension. It was not until the 1930's that the

importance of the physical and chemical interactions between bubble and particle becomes recognized, and are increasingly interested by many investigators (118-123). They attempt to quantitatively describe the rate of flotation through physico-chemical mechanisms involved in flotation process. In 1948, Sutherland (124) developed the first theoretical approach into the investigation of flotation by considering the capture mechanism of a single particle by a single rising bubble. He suggested that the overall probability of particle flotation (P) could be represented by:

$$P = P_c \; P_a \; (1 - P_d) \qquad [1.24]$$

where P_c is the probability of collision between bubbles and particles, P_a is the probability of adhesion after collision and P_d is the probability of subsequent detachment of particles from bubble surface.

1.2.2.2 Probability of Collision (P_c)

Of all terms in the Eq. [1.24], P_c has been the most extensively investigated, and generally the collision process between a bubble and particle is considered as hydrodynamic event which is related to particle and bubble size, particle and liquid density, liquid viscosity and relative particle-bubble velocity. From the principles of fluid mechanics, numerous fundamental analyses have been conducted to quantify the collision process. Sutherland (124) derived the first expression for P_c by assuming the potential streamline flow around the bubble and inertialess particle:

$$P_c = 3\left(\frac{D_p}{D_b}\right) \qquad [1.25]$$

where D_p and D_b are the particle and bubble diameters. This equation is applicable only for very large Reynolds numbers (Re) which is rarely found in flotation. Gaudin (125)

investigated the opposite flow regime, i.e. creeping flow, and derived an expression for P_c for low Reynolds numbers:

$$P_c = \frac{3}{2}\left(\frac{D_p}{D_b}\right)^2 \qquad [1.26]$$

This equation is valid only for extremely small bubbles which may be found in microbubble flotation column.

Recognizing the limited applicability of Eq. [1.25] and Eq. [1.26], Flint and Howarth (126) numerically solved the Navier-Stokes equations to determine P_c. This approach was modified by Ready and Ratcliff (127) to show that:

$$P_c \propto \left(\frac{D_p}{D_b}\right)^2 \qquad [1.27]$$

This relationship indicates that, theoretically P_c is increased using smaller bubbles and larger particles, as has been observed in many flotation experiments.

More recently, Weber (128) and Weber and Paddock (129) derived an analytical expression for P_c for bubbles of low Reynolds numbers. For the case of large Reynold numbers, the Navier-Stokes equations were solved numerically using a curve-fitting techniques (130, 131). In this way, Weber and Paddock developed an expression for P_c:

$$P_c = \frac{3}{2}\left[1+\frac{(3/6)\,\mathrm{Re}}{1+0.249\,\mathrm{Re}^{0.56}}\right]\left(\frac{D_p}{D_b}\right)^2 \qquad [1.28]$$

This is the first of its kind that can predict P_c for wide ranges of bubble and particles. However, Weber and Paddock did not verify this relationship experimentally.

The derivation of expression for P_c requires appropriate stream functions for different flow conditions. For Stokes and potential flow conditions, the stream functions had been known for a long time. However, for most flotation applications, the Reynolds number is intermediate between these two extremes. Recognizing this fact, Yoon and Lutterell (132) derived a empirical stream function for this range by combining those for Stokes flow and potential flow, then the probability of collision could be obtained as:

$$P_c = \left[\frac{3}{2} + \frac{4\,\mathrm{Re}^{0.72}}{15}\right]\left(\frac{D_p}{D_b}\right)^2 \qquad [1.29]$$

which shows that P_c varies as D_b^{-2} for small bubble with Re ≈0. However, as the bubble size becomes larger, P_c will become less dependent on D_b. It can be readily shown that for very large bubble, P_c varies as $D_b^{-0.45}$. Eq. [1.29] has been verified in many flotation system (132-135).

Jiang and Holtham (136) included the inertia force into their collision model, A forth-order Runge-Kutta numerical technique was used to solve the equation of motion. They found the following relationship:

$$P_c = A\left(\frac{D_p}{D_b}\right)^n \qquad [1.30]$$

where A and n are function of Re. For bubble size between 280 and 860 μm, n is essentially a constant 2 and A varies between 6 and 12. However, they did not obtain a generalized expression for P_c.

Yoon (10) compared the calculation results of P_c using four different models outlined above to the experimental data for D_p = 11.4 μm. He found that for the bubble sizes used in flotation practice, Sutherland's equation (Eq. [1.25]) overestimates P_c, while Gaudin's (Eq. [1.26]) underestimates. However, Gaudin's equation can still be used for

bubble smaller than 100 μm. Beyond this limit, two equations developed by Weber and Paddock (Eq. [1.28]) and Yoon and Luttrell (Eq. [1.29]) fit the experimental data much better.

1.2.2.3 Probability of Adhesion (P_a)

It is obvious that bubble-particle collision does not guarantee attachment and subsequent flotation. Adhesion, whereby the particle establishes three-phase contact with bubble, must be considered as well. It is the differences in P_a of species in ore that forms the foundation for selective separation involved in flotation.

However, developing an expression for P_a has been a challenging problem. Induction time, which is defined as the time required for the disjoining film between bubble and particle to thin and rupture, and sliding time, which is the time for particle sliding over the bubble surface, were commonly used in earlier investigation to assess the bubble-particle adhesion (124, 137-144). If the sliding time is longer than the induction time, the particle will have long enough time to thin the disjoining film to a critical thickness where the film spontaneously ruptures and three-phase contact is established. Obviously, the induction time represents the flotability of particles, particle with a short induction time can be easily floated with fast flotation rate. Experimental results showed that, the induction time is also a function of many variables, such as temperature, reagent addition, pH, etc. (1, 48, 145-149).

Based on the concepts of induction/sliding time, Finch and Dobby (150) defined the probability of adhesion as the fraction of particles whose sliding time are longer than induction time which can be determined from the closest streamline approach angle (θ_c) and the maximum angle of contact (θ_n) using following equation:

$$P_a = \frac{\sin^2 \theta_n}{\sin^2 \theta_c} \qquad [1.31]$$

where θ_n is a function of induction time and hydrodynamics of a system. Luttrell and Yoon (151) conducted a more theoretic analysis and derived an expression for P_a directly from the stream function for intermediate Reynold number range in the following form:

$$P_a = \sin^2\left[2 \arctan \exp\left(\frac{-\left(45 + 8\,\mathrm{Re}^{0.72}\right)U_b t_i}{15 D_b \left(D_b / D_p + 1\right)}\right)\right] \qquad [1.32]$$

where t_i is the induction time and U_b is the rising velocity of bubble.

An alternate investigation is considering that the bubble-particle interaction is analogous to the chemical reaction. The particle must possess sufficient kinetic energy to overcome the energy barrier which is created by surface forces between bubble and particle, then the disjoining film spontaneously rupture and adhesion occurs. This is incorporated into an Arrhenius-type equation for P_a (152, 153):

$$P_a = \exp\left(-\frac{E_1}{E_k}\right) \qquad [1.33]$$

where E_1 is the energy barrier for bubble-particle adhesion, and E_k is the kinetic energy of collision. E_1 can be determined by the surface forces involved in the bubble-particle interaction which is described by extended DLVO theory. However, the explicit method for determining E_k is still lacking.

Computer simulation using force balance is another way to analyze bubble-particle adhesion (11, 136, 153). It is direct, easy to be understood, but usually no generalized expression can be obtained, which limits its application in practice.

1.2.2.4 Probability of Detachment (P_d)

Quantifying the probability of detachment P_d is even more difficult than P_a. The experimental observation showed that (1, 154-158), the combination of gravitational forces, turbulent forces and bubble oscillations acting on attached particles are considered as attributions of detachment, which determines the upper limit of particle size of floatability (159, 160). P_d is higher for larger particles due to the greater inertia (155-157) and also increased with increasing number of particles attached on the bubble surface (155, 158). Woodburn *et al* (161) analyzed the tension developed in the surface of bubble when it is subjected to a sudden acceleration in turbulent fluid and showed that:

$$P_d = \left(\frac{D_p}{D_{p,\max}} \right)^{1.5} \qquad [1.34]$$

in which D_p is the particle diameter and $D_{p,\,max}$ is the maximum particle size that will remain attached under the prevailing turbulent conditions. Holtham and Cheng (158) proposed a empirical relationship between P_d and the ratio of particle size (D_p) to bubble size (D_b) of the form:

$$P_d = a + b\frac{D_p}{D_b} \qquad [1.35]$$

where a and b are constants which decrease with particle size. However, explicit theoretic expression for P_d is not available. Although P_d is approximately unity for fine particle flotation (162), it is necessary for a complete flotation model.

Once P in Eq. [1.24] is known from the detailed knowledge of the microprocesses, the first order flotation rate constant (k) can be obtained using following relationship (163, 164):

$$k = \frac{3P}{2D_b} V_g \qquad [1.36]$$

where V_g is the superficial gas rate which is defined as the gas flow rate per cross sectional area of the flotation cell. Thus the flotation rate equation can be predicted from the hydrodynamics and surface chemistry.

1.2.3 Interactions between Two Oil/Solution Interfaces

Oil droplets dispersed in aqueous solution are thermodynamically unstable. Given sufficient time, they will aggregate or coalesce until ultimately two liquid layers are formed. It has been recognized that the coalescence process, as summarized in an early review paper by Jeffreys and Davies (18), depends on the physical properties and hydrodynamics of the system, such as drop size, curvature of the interface, density, viscosity, interfacial tension, temperature, etc. In the past 50 years, numerous theoretical analysis and experimental investigations have been accomplished on various aspects of emulsion films to understand and generalize the nature and mechanism of the coalescence process (18, 19, 22, 162-174). However, only a few investigators described the interactions between two oil/solution interfaces in terms of surface forces including in the classic DLVO theory or the extended DLVO theory.

Chen (175) developed a model for the dynamics of an axisymmetric, dimpled film which includes the effects of London-van der Waals and electric double layer force. The former was considered to destabilize the film, whereas the later stabilized it. The dimpled film either formed a flat film or ruptured at the rim depending on net disjoining pressure of two components. The predictions on the film stability and its thickness were in good agreement with experimental results of thin films of aqueous KCl solutions between two oil drops in a capillary. Sanders *et al* (26) modeled the deposition

experiments by solving the governing mass transfer and flow field equations, using analytical expressions from classic DLVO theory. They found that, the behavior of the bitumen droplets dispersed in aqueous solution could be accurately predicted from the classic DLVO theory. However, the calculated deposition rates for the mineral oil emulsions stabilized by asphaltene were inconsistent with the observed values, indicating that the classic DLVO theory failed to describe the stability of the mineral oil emulsions. Deshiikan *et al* (29, 30) visually observed the coalescence of n-hexadecane oil drops suspended in the aqueous solutions with different pH and ionic strength. They found that, the coalescence of oil drops occurred in some cases when the classic DLVO theory gave very high energy barrier, indicating that some important characteristics which determined the stability of the thin film interfaces should be included in the classic DLVO theory.

Hazlett (28) investigated the coalescence of water drops in emulsion stabilized by sodium dodecyl sulfate (SDS), and showed that, in presence of surfactant, the stability could not be predicted by the classic DLVO theory, an addition attractive force existed between two oil/solution interfaces. He considered that this force is attributed to a continuous percolating network formed by the swollen micelle spheres in the continuous phase. Groeneweg *et al* (27) measured the dynamic stability of water/oil emulsions prepared from vegetable oil in presence of the emulsifier monolinoleylglycerol, and found that, an additional attractive force was necessary to explain the experimental results, which might be related to the expulsion of the oil molecules out of the film. Nevertheless what mechanism is involved, these attractive force may be considered as the hydrophobic force related to the surfactant or the emulsifier. On the other hand, some non-ionic polymer (176) can uniformly coated on the surface of oil droplets with a crystalline structure, this protective layer prevents the coalescence of the oil droplets and stabilize the emulsion. Similar conclusion was obtained by Meller and Stavans (21). These repulsive forces may be considered as a steric force, one of the structure forces included in the extended DLVO theory.

Recently, Aveyard *et al* (177) designed a new apparatus to determine the disjoining pressure isotherm between two liquid/liquid interfaces. An oil drop is formed at the tip of a thin flexible micropipette and pressed up to an oil/solution interface by piezo translator capable of vertical movement of 40 μm. The disjoining pressure was measured by the hydrostatic pressure applied to the oil contained in the micropipet, and film thickness was determined from the optical interference pattern obtained using a microscope. Experimental results for dodecane-water-dodecane emulsion film stabilized by the anionic surfactant sodium bis (2-ethylhexyl) sulfosuccinate (AOT) showed that, the data of Π versus distance can be reasonable fitted by considering double layer component of disjoining pressure with the surface potential as an adjustable parameter. Using same apparatus, Cho *et al* (178) conducted similar experiment for dodecane-water-dodecane emulsion films stabilized by the anionic surfactant sodium dodecyl sulfate (SDS) in presence of different concentration of NaCl. An attractive force was observed, which was explained by imperfect 'pining' of the three-phase contact line at the inner diameter of the micropipette instead of the line tension at the perimeter of the thin emulsion film formed as the oil drop is pressed up to the oil/water interface. The contribution of structure force was not considered in both of these two investigations, which was most probably the mechanism of the attractive force.

1.3 Research Objectives

The primary objects of the present work are to explore the applications of the extended DLVO theory in different systems. Specifically, a theoretic flotation model is to be developed based on the elementary subprocess of bubble-particle interactions in flotation which correlates flotation rate constant with various hydrodynamic and surface chemistry parameters involved in the system. The surface forces described in the extended DLVO theory are essential in derivation of the model. This model is then used to predict the flotation rate from all hydrodynamic and surface chemistry variables and

determine the hydrophobic force parameter based on the experimental results of simplified flotation test. The effects of several important parameters on the flotation response are to be investigated with derived model which provides detail explanation of the simulation results. The extended DLVO theory is also to be used to describe the interactions between two oil droplets in aqueous solution of surfactant. The hydrophobicity of oil/solution interface will be quantified, and compared with that of free film to find the relationship between hydrophobicity and surface chemistry parameters of liquids.

1.4 Report Organization

Due to the relatively independent nature of each of the topics in this report, they will be presented as separate, stand-alone chapters. Each chapter has its own introduction, theoretical analysis, experimental or simulation, results, discussion and conclusion sections.

In Chapter 2, a first order rate equation is developed using extended DLVO theory by consider both hydrodynamic and surface forces involved in flotation process. The structure of the model is described in detail, and a sample application of the model is presented. The experimental results of single bubble flotation, contact angle and ζ potential measurements are used to determine the hydrophobic force parameter between bubble and particle which is correlated with those of other interfaces. Also, various methods of improving flotation performance are suggested based on theoretical analysis of the derived rate equation.

Chapter 3 deals with the simulation of the bubble-particle interaction in flotation using the model developed in Chapter 2. The flotation rate constants are predicted as functions of several important hydrodynamic and surface chemistry parameters, such as

contact angle, surface potential, bubble size, etc. The simulations show consistent results with experience, and are explained in the view of various subprocesses considered in the model.

In Chapter 4, Thin-Film-Balance (TFB) technique is used to determine the equilibrium film thickness of dodecane film presented in the DAH solutions. With the data from interfacial tension measurements, the surface potentials of the oil/solution interface are calculated and thus the values of hydrophobic force parameter (K_{232}) are determined using extended DLVO theory. These results are compared with those of the free film to investigate the possible relationship between hydrophobicity and the physico-chemical properties of liquids. The effects of pH and electrolyte concentration on K_{232} are also investigated.

In Chapter 5, the overall conclusions obtained in present investigation are summarized. The recommendations for future research are discussed in Chapter 6.

1.5 References

1. Schulze, H. J., "Phyico-chemical Elementary Processes in Flotation, An Analysis from the point of view of Colloid Science including Process Engineering Considerations. Elsevier, New York, 1984.

2. Kitchener, J. A., "The Froth Flotation Process: past, Present and Future-in Brief" in The Scientific Basis of Flotation, K. Ives Ed., NATO ASI Series, Series E: Applied Scienced. No. 75, P. 3 (1984).

3. Mineral Industry Survey, "Froth Flotation in the United States, 1985", U.S. Department of the Interior, Bureau of Mines, Washington, D. C., (1987).

4. Sastry, Kal V. S., "Principles and Methodology of Mineral Process Modeling" in proceedings of Control'90-Mineral and Metallurgical Processing, Salt Lake City, UT, USA, p. 3(1990).

5. Garcia-Zungia, H., *Bol. Soc. Nac. Min*. Santiago, **47**, 83(1935).

6. Dowling, E. C., Klimpel, R. R., and Aplan, F. F., *Miner. Metallurgy Process*. **2**, 87(1985).

7. Lynch, A. J., Johnson, N. W., Nanlapig, E. V. and Thorne, C. G., Mineral and Coal Flotation Circuits, Chapter 3, Mathematical Models of Flotation, In: D. W. Fuerstenau, Ed., Development in Mineral Processing, Elsevier, Amsterdam, 57(1981).

8. Kelsall, D. F., *Trans. Inst. Min. Met*. **70**, 191(1961).

9. Bushell, C. H., *Trans. A.I.M.E*. **223**, 266(1962).

10. Yoon, R. H., in "Proceedings, XVII Int. Miner. Process. Congr., Dresden, German", Vol. II, p. 17(1991); *LES Techniques* **74** (1992).

11. Schimmoller, B. K., Luttrell, G. H. and Yoon, R. H., Proceed. VXIIth Int. Miner. Process. Congr., Sydney, Australia, p. 751(1993).

12. Yoon, R. H. and Yordan, J. L., *J. Colloid Interface Sci*. **146**, 2(1991).

13. Yotsumoto, H. and Yoon, R.-H., *J. Colloid Interface Sci*. **157**, 426(1993).

14. Yotsumoto, H. and Yoon, R.-H., *J. Colloid Interface Sci*. **157**, 434(1993).

15. Xu, Z. and Yoon, R.-H., *J. Colloid Interface Sci*. **132**, 532(1989).

16. Xu, Z. and Yoon, R.-H., *J. Colloid Interface Sci*. **134**, 427(1989).

17. Yoon, R.-H. and Mao, L., *J. Colloid Interface Sci*. **181**, 613(1996).

18. Jeffreys, G. V., and Davies, G. A., in: Recent Advances in Liquid-Liquid Extraction, Hanson, C. Ed., Pergamon, New York, p. 495(1971).

19. Dahami, M. A., Constant, W. D., and Wolcott, M., *Fuel* **67**, 1242(1988).

20. Wolfgang, R., Eckhart, B., and Walter, M., *Chem. Eng. Sci*. **47**, 555(1992).

21. Meller, A., and Stavans, J., *Langmuir* **12**, 301(1996).

22. Tambe, D. E., and Sharma, M. M., *Advances in Colloid and Interface Sci*. **52**, 1(1994).

23. Anon, *J. Colloid Interface Sci*., **163**, 512(1994).

24. Harald, F., Yannick, S., Johan, S., and Luc, V. J., *Colloids and Surfaces A: Physiochemical and Engineering Aspects* **106**, 33(1996).

25. Medrzycka, K., and Zwiezykowski, W., *Sep. Sci. Technol*. **22**, 1637(1987).

26. Sanders, R. S., Chow, R. S. and Masliyah, J. H., *J. Colloid Interface Sci*. **174**, 230(1995).

27. Groeneweg, F., Vader, F. van V., and Agterof, W. G. M., *Chemical Engineering Sci*. **48**, 229(1993).

28. Hazlett, R. D., and Schechter, R. S., *Colloids Surf*. **29**, 53(1988).

29. Deshiikan, S. R., and Paradopoulos, K. D., *J. Colloid Interface Sci*. **174**, 302(1995).

30. Deshiikan, S. R., and Paradopoulos, K. D., *J. Colloid Interface Sci*. **174**, 313(1995).

31. Derjaguin, B. V. and Landau, L., *Acta Physicochim. URSS* **14**, 633(1941).

32. Verwey, E. J. W. and Overbeek, J. Th. G., "Theory of the Stability of Lyophobic Colloids", Elsevier, Amsterdam, (1948).

33. Allen, L. H. and Matijevic, E., *J. Colloid Interface Sci*. **31**, 287 (1969).

34. Derjaguin, B. V. and Churaev, N. V., *J. Colloid Interface Sci*. **49**, 249(1974).

35. Paunov, V. N., Diamova, R. I., Kralchevsky, P.A., Broze, G., and Mehreteab, A., *J. Colloid Interface Sci*. **182**, 239(1996).

36. Delgado-Calvo-Flores, J. M., Peula-Garcia, J. M., Martinez, R., and Callejas-Fernandez, J., *J. Colloid Interface Sci*. **188**, 58(1996).

37. Luzar, A., Svetina, S. and Zeks, B., *Chem. Phys. Lett*. **96**, 485(1983).

38. Duck, W. A. and Pashley, R. M., *Langmuir* **8**, 109(1992).

39. Yoon, R.-H. and Ravishankar, S. A., *J. Colloid Interface Sci*. **166**, 215(1996).

40. Yoon, R.-H. and Ravishankar, S. A., *J. Colloid Interface Sci*. **179**, 391(1996).

41. Yoon, R.-H. and Ravishankar, S. A., *J. Colloid Interface Sci*. **179**, 403(1996).

42. Aksoy, B. S., "Hydrophobic Forces in Free Thin Films of Water in the Presence and Absence of Surfactants", Ph. D. Thesis, Dept. of Mining Minerals Eng., Virginia Polytechnic Institute and State University, 1997.

43. Yordan, J. L., and Yoon, R.-H., Application of Heterocoagulation Theories to the Bubble-Particle Adhesion Process, 119th Annual SME Meeting, Salt Lake City, Utah, (1990).

44. Yordan, J. L., Studies on the Stability of Thinning Films in Bubble-Particle Adhesion. Ph. D. Thesis, Dept. Mining and Minerals Eng., Virginia Polytechnic Institute and State University, (1989).

45. Derjaguin, B. V., *Kolloid Z*. **69**, 155(1934).

46. Hogg, R., Healy, T. W. and Fuerstanau, D. W., *Trans. Faraday Soc*. **62**, 1638(1966).

47. Chu, B., Molecular Forces, Based on the Baker Lectures of Peter J. W. Debye, Interscience Publishers, John Wiley and Sons, New York, (1967).

48. Yordan, J. L., Kinetics of Bubble-Particle Adhesion in Flotation, MS Thesis, Dept. mining and Minerals Eng., Virginia Polytechnic Institute and State University, 1985.

49. Yoon, R. H. and Yordan, J. L., *J. Colloid Interface Sci*. **113**, 430(1986).

50. Ohshima, H and Kondo, T., *J. Colloid Interface Sci*. **155**, 499(1993).

51. Chu, X. and Wasan, D., *J. Colloid Interface Sci*. **184**, 268(1996).

52. Haughey, D. and Earnshaw, J. C., *Colloids and Surfaces A: Physicochemical and Engineering Aspects* 106, 237(1996).

53. Mao, L. and Yoon, R. H., *Int. J. Miner. Process*., **51**, 171(1997).

54. Visser, J., *Advances in Colloid and Interface Sci*. **3**, 331(1972).

55. Schenkel, J. H. and Kitchener, J. A., *Trans. Faraday Soc*. **56**, 161(1960).

56. Hamaker, H. C., *Physica* **4**, 1058(1937).

57. Milling, A., Mulvaney, P., and Larson, I., *J. Colloid Interface Sci*. **180**, 460(1996).

58. Israelachvili, J. N. and Pashley, R. M., *Nature* **300**, 341(1982).

59. Israelachvili, J. N. and Pashley, R. M., *J. Colloid Interface Sci*. **98**, 500(1984).

60. Kékicheff, P., Christenson, H. K. and Ninham, B. W., *Colloids Surf*. **40**, 31(1989).

61. Herder, P. C., *J. Colloid Interface Sci*. **134**, 346(1990).

62. Pashley, R. M., McGuiggan, P. M., Ninham, B. W. and Evans, D. F., *Science* **229**, 1088(1985).

63. Claesson, P. M., Blom, C. E., Herder, P. C. and Ninham, B. W., *J. Colloid Interface Sci*. **114**, 234(1986).

64. Christenson, H. K. and Claesson, P. M., *Science* **239**, 390(1988).

65. Claesson, P. M. and Christenson, H. K., *J. Phys. Chem*. **92**, 1650(1988).

66. Christenson, H. K., Claesson, P. M., Berg, J. and Herder, P. M., *J. Phys. Chem*. **93**, 1472(1989).

67. Christenson, H. K., Fang, J., Ninham, B. W. and Parker, J. L., *J. Phys. Chem*. **94**, 8004(1990).

68. Tsao, Y., Yang, S. X., Evans, D. F. and Wennerström, H., *Langmuir* **7**, 3154(1991).

69. Rabinovich, Y. I. and Derjaguin, B. V., *Colloids Surf*. **30**, 243(1988).

70. Rabinovich, Y. I. and Yoon, R.-H., *Langmuir* **10**, 1903(1994).

71. Rabinovich, Y. I. and Yoon, R.-H., *Colloids and Interfaces* **93**, 263(1994).

72. Parker, J. L. and Cleasson, P. M., *Langmuir* **10**, 635(1994).

73. Rabinovich, Y. I. and Derjaguin, B. V., in "Proceedings of the 5th Hungarian Conference on Colloid Chemistry", Loránd Eötvös University, Balatonfured, Hungary, 1988.

74. Eriksson, J. C., Ljunggren, S., and Claesson, P. M., *J. Chem. Soc. Faraday. Trans*. **85**, 163(1989).

75. Attard, P., *J. Phys. Chem*. **93**, 6441(1989).

76. Podgornik, V., Rau, D. M. and Parsegian, V. A., *J. Chem. Phys*. **91**, 5840(1989).

77. Yaminsky, V. V. and Ninham, B. W., *Langmuir* **9**, 3618(1993).

78. Derjaguin, B. V., and Kussakov, M., *Acta Physicochimica U.S.S.R*. **10**, 26(1939).

79. Churaev, N. V. and Derjaguin, B. V., *J. Colloid Interface Sci*. **103**, 542(1985).

80. Derjaguin, B. V., Churaev, N. V. and Muller, V. M., Surface Forces, Kichener, J. A. Ed., Consaltants Bureau, New York (1987).

81. Usui, S. and Hacjisu, S., Electrical Phenomena at Interfaces: Fundamental. Measurements and Applications, Kitahara, A. and Watanabe, A. Ed., Marcel Dekker Inc., Surfactant Science Series, **15**, 47(1980).

82. Ohshima, H., *Colloid and Polymer Sci*. **252**, 158(1974).

83. Ohshima, H., *Colloid and Polymer Sci*. **252**, 257(1974).

84. Hunter, R. J., Foundations of Colloid Science, Clarendon Press, Oxford Vol. 1, (1987).

85. Chan, D., Perram, J. W., White, L. R., and Healy, T. W., *J. Chem. Soc. Faraday. Trans*. **71**, 1046(1989).

86. Chan, D., White, L. R., and Healy, T. W., *J. Chem. Soc. Faraday. Trans*. **72**, 2844(1989).

87. Attard, P., Mitchell, D. J., and Ninham, B. W., *J. Chem. Phys*. **88**, 4987(1988).

88. Attard, P., Mitchell, D. J., and Ninham, B. W., *J. Chem. Phys*. **89**, 4358(1988).

89. Marcelja, S., Mitchell, D. J., Ninham, B. W. and Sculley, M. J., *J. Chem. Soc. Faraday Trans. 2* **73**, 630(1977).

90. Pratt, L.R. and Chandler, D. J., *J. Chem. Phys*. **67**, 3683(1977).

91. Rao, M., Pangali, C. and Berne, B. J., *J. Chem. Phys*. **71**, 2975(1979).

92. Derjaguin, B. V. and Churaev, N. V., *Langmuir* **3**, 607(1987).

93. Sonnenschein, P. and Heinzinger, K., *Chem. Phys. Lett*. **102**, 550(1983).

94. Anastasiou, N., Fincham, D. and Singer, K., *J. Chem. Soc., Faraday, Trans. 2* **79**, 1639(1983).

95. Kjellander, R., Marcelja, S., *Chem. Phys. Lett*. **120**, 393(1985).

96. Christou, N. I., Whitehouse, J. S., Nicholson, D. and Parsonage, N. G., *Mol. Phys*. **55**, 397(1985).

97. Parker, J. L., and Claesson, P. M., *Langmuir* **8**, 757(1992).

98. Lee, C. Y., McCammon, J. A. and Rossky, P. J., *J. Chem. Phys*. **80**, 4448(1984).

99. Tsao, Y. and Evans, D. F., *Langmuir* **9**, 779(1993).

100. Christensson, H. K., Claesson, P. M. and Parker, J. L., *J. Phys. Chem.* **96**, 6725(1992).

101. Tsao, Y., Evans, D. F. and Wennerström, H., *Science* **262**, 547(1993).

102. Rabinovich, Y. I., Guzonas, D. A. and Yoon, R.-H., *Langmuir* **9**, 1168(1993).

103. Miklavic, S. J., Chan, D. Y. C., White, L. R., and Healy, T. W., *J. Phys. Chem*. **98**, 9022(1994).

104. Claesson, P. M., Herder, P. C., Blom, C. E., and Ninham, B. W., *J. Colloid Interface Sci*. **118**, 68(1987).

105. Ducker, W. A., Xu, Z., and Israelachvili, J. N., *Langnuir* **10**, 3279(1994).

106. Yushchenko, V. S., Yaminsky, V. V., and Shchukin, E. D., *J. Colloid Interface Sci*. **96**, 307(1983).

107. Craig, S. J. V., Ninham, B. W., and Pashley, R. M., *J. Phys. Chem*. **97**, 10192(1993).

108. Craig, S. J. V., Ninham, B. W., and Pashley, R. M., *Nature* **364**, 317(1993).

109. Meagher, L., and Craig, S. J., *Langmuir* **10**, 2736(1994).

110. Yaminsky, V. V., Yushchenko, V. S., Amelina, E. A., and Shchukin, E. D., *J. Colloid Interface Sci*. **96**, 301(1983).

111. Ruckenstein, E., and Churaev, N., *J. Colloid Interface Sci*. **147**, 535(1991).

112. Laskowski, J., "The Relationship Between Floatability and Hydrophobicity", in: Advances in Mineral Processing, P. Somasundaran Ed. SME Publication, 1986.

113. Young, T., *Phil. Trans. Roy. Soc. London* **95**, 65(1805).

114. Shaw, D. J., "Introduction to Surface and Colloid Chemistry" 3rd Ed. Butterworths, Boston, 1989.

115. Iler, R. K., "The Chemistry of Silica", Wiley-Interscience, New York, 1979.

116. Derjaguin, B. V. and Dukhin, S. S., *Trans. IMM* **70**, 221(1961).

117. Laskowski, J., *Miner. Sci. Eng*. **6**, 223(1974).

118. Wark, J. W., *J. Phys. Chem*. **37**, 623(1933).

119. Bogdanov, O. S. and Filanovskij, M. S., *J. Phys. Chem. USSR* **14**, 244(1940).

120. Spedden, H. R. and Hanna, W. S., *Tech. Publ*. No. 2354, Amer. Inst. Mining Engrs., 1948.

121. Whelan, P. F. and Brown, D. J., *Bulletin Inst. Mining & Metall*. **65**, No. 591, 181(1956).

122. Gaudin, A. M., Flotation, McGraw Hill Book Company, New York, N. Y., 1932.

123. Schuhmann, R., *J. Phys. Chem.* **46**, 891(1942).

124. Sutherland, K. L., *J. Phys. Chem*. **52**, 394(1948).

125. Gaudin, A. M., Flotation, 2nd Edition, McGraw-Hill Book Company, New York, N. Y., 1957.

126. Flint, L. R. and Howarth, W. J., *Chem. Eng. Sci*. **26**, 1155(1971).

127. Reay, D. and Ratcliff, G. A., *Canadian J. Chem. Engrg*. **51**, 178(1973).

128. Weber, M. E., *J. Separation Process Technol.* **2**, 29(1981).

129. Weber, M. E. and Paddock, D., *J. colloid Interface Sci*. **94**, 328(1983).

130. Masliyah, J. H., Ph. D. Dissertation, University of British Columbia, Vancouver, 1970.

131. Woo, S. W., Ph. D. Dissertation, McMaster University, Hamilton, Ontario, 1971.

132. Yoon, R. H. and Luttrell, G. H., *Miner. Process. Extr. Metall. Rev*. **5**, 101(1988).

133. Luttrell, G. H. and Yoon, R. H., in "Proceedings, Engineering Foundation Conference, Benefication of Phosphate: Theory and Practice, Palm Coast, FL. Dec. 1993.

134. Yoon, R. H. and Luttrell, G. H., *Coal Preparation* **2**, 179(1986).

135. Yoon, R. H., Adel, G. T., Luttrell, G. H., Mankosa, M. J. and Weber, A. T., in "Interfacial Phenomena in Biotechnology and Materials Processing (Y. A. Attia, B. M. Moudgil, and S. Chander, Eds.), Elsevier, Amsterdam, 1988.

136. Jiang, Z. W. and Holtham, P. N., Trans. Ins. Mining.Metallurgy, 95, C187(1986).

137. King, R. P., Hatton, T. A. and Hulbert, D. G., *Trans. Inst. Mining & Metall*. Sect. C, C9(1974).

138. Schulze, H. J. and Gottschalk, G., Proceed., 13th International Mineral Processing Congress, Warsaw, Poland, (J. Laskowski, Ed.), Elsevier, New York, Part A, p. 63, 1981).

139. Luttrell, G. H., Hydrodynamic Studies and Mathematical Modeling of Fine Coal Flotation, Ph. D. Thesis, Dept. of Mining Eng., Virginia Polytechnic Institute and State University, 1986.

140. Dobby, G. S. and Finch, J. A., *J. Colloid Interface Sci*. **109**, 493(1986).

141. Philippoff, W., *Trans. AIME* **193**, 386(1952).

142. Evans, L. F., *Industrial and Engineering Chemistry* **46**, 2420(1954).

143. Ye, Y. and Miller, J. D., *Coal Preparation* **5**, 147(1988).

144. Jiang, Z. W., *Proceed. XVIIth Int. Miner. Process. Congr*., Vol. II, 429(1991).

145. Eigeles, M. A. and Volova, M. L., Proceed. 5th Inter. Miner. Process. Congr., London, 271(1960).

146. Dobby, G. S. and Finch, J. A., *Int. J. Miner. Process*. **21**, 241(1987).

147. Laskowski, J., *Mineral Processing and Extraction Metallurgy Review* **5**, 25(1989).

148. Laskowski, J. and Iskra, J., *Trans. Inst. Min. Metall*. **79**. C6(1970).

149. Yoon, R. H. and Yordan, J. L., *J. Colloid Interface Sci.* **141**, 374(1991).

150. Finch, J. A. and Dobby, G. S., Column Flotation, Pergamon Press, New York, N. Y. , 1990.

151. Luttrell, G. H. and Yoon, R. H., in: Production and Processing of Fine Particles, A. Plumpton Ed. Pergamon Press, Toronto, p. 159(1988).

152. Yoon, R. H., *Aufbereitungs Technik* **32**, 474(1991).

153. Luttrell, G. H. and Yoon, R.H., *J. Colloid Interface Sci*. **154**, 129(1992).

154. Philippoff, W., *Min. Engng*. N. Y., **4**, 386(1952).

155. Nutt, C. W., *Chem. Engng Sci*. **12(2)**, 133(1960).

156. Schulze, H. J., Wahl, B. and Gottschalk, G., *J. Colloid Interface Sci*. **128**, 57(1989).

157. Nishkov, I. and Pugh, R. *J., Int. J. Miner. Process*. **25**, 275(1989).

158. Holtham, P. N. and Cheng, T. W., *Mineral Processing and Extractive Metallurgy* **100**, C147(1991).

159. Schulze, H. J., *Int. J. Miner. Process*. **4**, 241(1977).

160. Crawford, R. and Ralston, *J., Int. J. Miner. Process*. **23**, 1(1988).

161. Woodburn, E. T., King, R. P., and Colburn, R. P., *Metallurgical Trans*. **2**, 3163(1971).

162. Derjaguin, B. V. and Dukhin, S. S., Proceed. 13th Int. Miner. Process. Congr., (J. Laskowski, Ed.), Warsaw, 21(1979).

163. Yoon, R. H., Luttrell, G. H., Adel, G. T. and Mankosa, M. J., in: Advances in Coal and Mineral Processing Using Flotation, S. Chander Ed., SME, Inc., Littleton, Colorado, 211(1989).

164. Luttrell, G. H., Weber, A. T., Adel, G. T. and Yoon, R. H., In: Column Flotation '88 (K. V. S. Sastry, Ed.), SME, Inc., Littleton, Colorado, 205(1988).

165. Lissant, K. J., *Colloids and Surfaces* **29**, 1(1988).

166. Menon, V. B. and Wasan, D. T., *Colloids and Surfaces* **29**, 7(1988).

167. Brooks, B. W. and Richmond, H. N., *Chemical Engineering Sci*. **49**, 1843(1994).

168. Roques, H. and Aurelle, Y., *Wat. Sci. Tech*. **18**, 91(1986).

169. Sokolovic, R. M. S. and Sokolovic, S. M., *Separation Science and Technology* **31**(15), 2089(1996).

170. Nakache, E., Longaive, P. Y., and Aiello, S., *Colloids and Surfaces A: Physicochemical and Engineering Aspects* **96**, 69(1995).

171. Mediboure, B., Dicharry, C., Marion, G., Morel, G., Salager, J. L., and Lachaise, J., *Progr. Colloid Polym. Sci*. **93**, 310(1993).

172. Draxier, J and Marr, R., *Inter. Chemical Eng*. **33**, 1(1993).

173. Engels, T., Förster, T. E. and Rybinski, W. V, *Colloids and Surfaces A: Physicochemical and Engineering Aspects* **99**, 141(1995).

174. Dickinson, E., *Colloids and Surfaces* **42**, 191(1989).

175. Chen, J., *J. Colloid Interface Sci*. **107**, 209(1985).

176. Aderangi, N. and Wasan, D. T., *Chem. Eng. Comm*. **132**, 207(1995).

177. Aveyard, R., Binks, B. P., Cho, W. G., Fisher, L. R., Fletcher, P. D. I., and Klinkhammer, F., *Langmuir* **12**, 6561(1996).

178. Cho, W. G. and Fletcher, P. D. I., *J. Chem. Soc. Faraday Trans*. **93**(7), 1389(1997).

CHAPTER 2: FLOTATION RATE EQUATION

2.1 Introduction

In froth flotation, air bubbles are injected into a moving stream of aqueous slurry containing a mixture of particles, so that only hydrophobic ones are collected on the bubble surface and exit the stream. Owing to its simplicity, the process is widely used for separating a variety of minerals, cleaning coals, deinking recycled paper fibers, removing oils from water, cleaning soils, etc. However, the process is difficult to model from the first principles because of the complexities involved in the three-phase phenomenon. For this reason, most of the flotation models developed in the past are empirical (1-3). A few investigators attempted to model the process by considering hydrodynamic parameters but ignoring surface chemistry parameters (4-7). Part of the difficulty lies in the lack of information concerning the latter. However, recent advances made in the measurement of surface forces using surface force apparatus (SFA) and atomic force microscope (AFM) revealed new information, particularly on those not considered in the DLVO theory, that is essential for modeling flotation. It has been shown that the non-DLVO forces such as hydration (8, 9) and hydrophobic forces (10, 11) play an important role in the coagulation and dispersion of fine particles in aqueous media, and that the hydrophobic force is the major driving force for bubble-particle adhesion (12-14). Therefore, modeling flotation without considering contributions from the hydrophobic force would be unrealistic. More recently, the role of long-range hydrophobic forces in flotation has been discussed (15), and the relationship between various hydrophobic force parameters and water contact angle (which is a more traditional measure of hydrophobicity) has been established (16-18). These recent developments may be conducive to develop a flotation model based on the first principles.

Derjaguin and Duhkin (19) were probably the first to consider surface forces in developing a model for bubble-particle interactions. According to their model, a particle must pass through three distinct zones sequentially, i.e., hydrodynamic, diffusio-phoretic and wetting zones, before it can adhere on the surface of an air bubble. Once the particle is in the wetting zone, the fate of the particle as to whether adhesion occurs or not is decided by three surface forces, namely, London-van der Waals, ion-electrostatic and structural forces. The third force was considered to be hydrophilic and thought to become zero when the bubble-particle adhesion is to occur. In a later investigation, Derjaguin and Duhkin (20) suggested that for very fine particles for which inertia force can be ignored, bubble-particle adhesion can occur *via* the van der Waals and ion-electrostatic forces only, without penetrating the wetting film. Thus, neither of the work of Derjaguin and Duhkin considered the possibility that there may be an attractive force that drives the process of bubble-particle adhesion.

The first evidence that there may exist an attractive force not considered in the DLVO theory that is responsible for the rupture of wetting films was given in 1969 by Laskowski and Kitchener (21). They showed that both double-layer and dispersion forces are repulsive, yet the wetting films on methylated silica surfaces rupture spontaneously. The rupture thicknesses measured by Blake and Kitchener (22) were in the range of 60-220 nm, which indicate that wetting films are destabilized by long-range attractive forces. It was not until 1982, when Israelachvili and Pashley (23) conducted force measurements with mica surfaces in equilibrium with CTAB solutions, that a direct evidence was given for the existence of a non-DLVO attractive force, which is referred to as hydrophobic force. The measured forces were more than ten-times stronger than the dispersion force and represented by a single exponential function:

$$\frac{F}{R} = C_0 \exp\left(-\frac{H}{D_0}\right), \qquad [2.1]$$

where F is the force measured between two curved mica surfaces with the radius of curvature of R, H the closest separation distance, D_0 the decay length, and C_0 is a constant. Many investigators measured later much stronger hydrophobic forces, for which a double-exponential function (24-26):

$$\frac{F}{R} = C_1 \exp\left(-\frac{H}{D_1}\right) + C_2 \exp\left(-\frac{H}{D_2}\right), \qquad [2.2]$$

is frequently used. It has been shown recently that for hydrophobic surfaces whose advancing water contact angles (θ_a) are less than 90^o, Eq. [2.1] is suitable with D_0 in the range of 1-2 nm, while those with θ_a>90^o require Eq. [2.2] with D_1 in the same range as D_0 and D_2 in the range of 3-24 nm (16). The hydrophobic forces can also be represented by a power law (18, 27):

$$\frac{F}{R} = -\frac{K}{6H^2}\ , \qquad [2.3]$$

in which K is the only parameter. An advantage of Eq. [2.3] is that it is of the same form as that for the dispersion interaction; therefore, the value of K can be directly compared with Hamaker constants.

Although the origin of hydrophobic force is still being debated, there are overwhelming evidences for its existence particularly between two hydrophobic solid surfaces. The extended DLVO theory, which includes hydrophobic force in the classic DLVO theory, makes it possible to modeling bubble-particle interaction (12, 14, 28-33). Furthermore, recent studies using the thin film balance (TFB) technique show evidence that hydrophobic force may also exist at the air/water interface particularly at very low surfactant concentrations (34-36). Therefore, there is likelihood that bubble-particle adhesion is controlled by hydrophobic interactions. In this chapter, a flotation rate equation is derived from the first principle by considering both hydrodynamic and surface

forces. Contributions from the hydrodynamic forces were calculated using a stream function derived for single bubbles rising under laminar conditions, while those from surface forces were determined using an extended DLVO theory, which incorporates hydrophobic forces in addition to the ion-electrostatic and dispersion forces.

As mentioned in Chapter 1, the process of bubble-particle adhesion can also be simulated using force balance. However, this approach usually does not produce an explicit expression, which limits its application. The model to be developed in the present work come up with a simple, explicit expression, therefore it can be easily used to do theoretic analysis and optimization.

2.2 Model Development

2.2.1 Theoretical Background

Figure 2.1 shows a single air bubble of radius, R_2, rising in an aqueous suspension of fine particles of radius, R_1, contained in a cylindrical flotation column with diameter, D. The height of the suspension inside the column is h and the total number of particles present in the suspension is N. The number of particles collected by the bubble during its residence time in the column will be the product of i) the volume swept by the bubble ($\pi R_2^2 h$), ii) the number density of particles ($4N/\pi D^2 h$) in the suspension, and iii) the fraction of the particles in front of the bubble that are actually collected by the bubble, which is referred to as probability of collection (P).

$$\frac{Number\ of\ \ particles\ collected}{Bubble} = \pi R_2^{\ 2} h \cdot \frac{4N}{\pi D^2 h} \cdot P\,, \qquad [2.4]$$

the number of bubbles passed through the flotation column per unit time is:

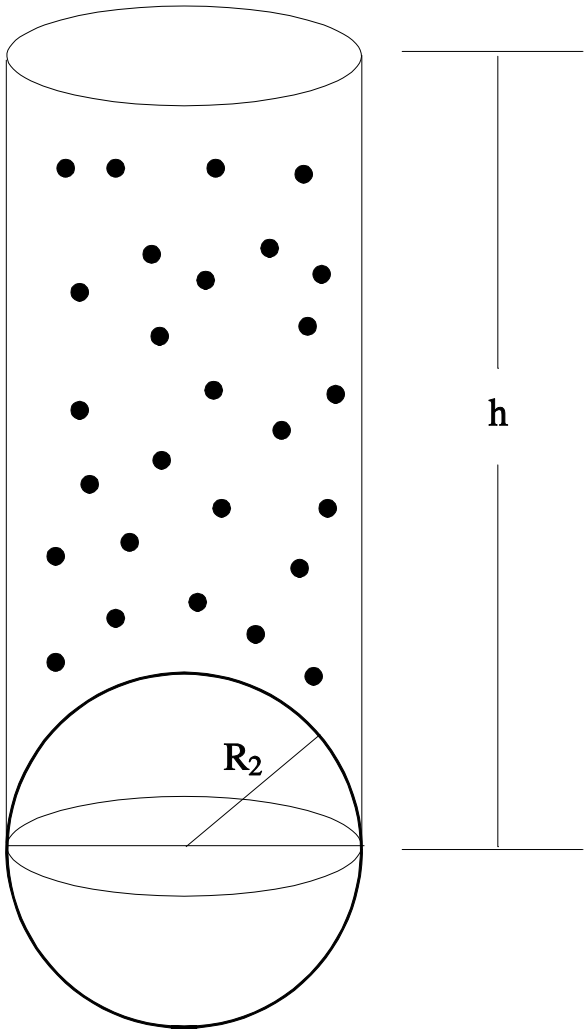

Figure 2.1. An air bubble rising in the flotation column and solid particles suspended in the solution.

$$\frac{Number\ of\ Bubbles}{Time} = \frac{Q}{\frac{4}{3}\pi R_2^{\,3}}, \qquad [2.5]$$

in which Q is the volumetric air flow rate. Multiplying Eq. [2.4] by Eq. [2.5], one can determine the rate at which the particles are removed by the flotation process as follows:

$$\begin{aligned}\frac{dN}{dt} &= -\left(\frac{3P}{4R_2}\frac{Q}{\frac{1}{4}\pi D^2}\right) \\ &= -\left(\frac{3P}{4R_2}V_g\right)N \\ &= -kN, \end{aligned} \qquad [2.6]$$

in which V_g is the superficial velocity of air, which is defined as volumetric air flow rate normalized by the cross sectional area of the flotation column.

Equation [2.6] is the first-order rate equation, in which k is its rate constant. Many investigators showed that mineral flotation could be described as a first-order process (1,37-45). The rate constant, k (=$(3P/4R_2)V_g$), can be reduced to:

$$k = \frac{1}{4}S_b P, \qquad [2.7]$$

where S_b is the superficial surface area rate of bubbles, which is defined as the bubble surface area moving out of the cell per unit time per unit cross-sectional area of the flotation column. It can be readily shown that

$$S_b = \frac{3V_g}{R_2}. \qquad [2.8]$$

The bubble-particle interaction can be considered as a statistical phenomenon (37, 46, 47). The probability of collection (P) in Eq. [2.7] can be obtained using the following relationship (37):

$$P = P_c P_a (1 - P_d) \ , \qquad [2.9]$$

in which P_c is the probability of bubble-particle collision, P_a the probability of adhesion, and P_d is the probability of detachment. In the following sections, analytical expressions for these probability functions will be derived and substituted into Eqs. [2.9] and [2.7] to obtain an expression for k based on first principles.

2.2.1.1 Probability of Bubble-Particle Collision (P_c)

As a bubble rises in a quiescent particle suspension, the liquid flows around the bubble, forming an infinite number of streamlines which can be represented mathematically by a stream function. If the particles in the suspension are small enough that they can be considered inertialess, the particle trajectory would correspond to the streamline (48). Once the particle trajectory is known, it is possible to derive an expression for P_c.

Figure 2.2 shows an inertialess particle of R_1 following the critical streamline, which is defined as the trajectory of a particle that grazes-off the bubble at its equator, i.e., $\alpha=\pi/2$. One can see that of the particles located in front of the bubble, only those within the critical radius r_c, as defined in Figure 2.2, will collide with the bubble. Thus, P_c becomes:

$$P_c = \left(\frac{r_c}{R_1 + R_2} \right)^2 . \qquad [2.10]$$

If the particle size is much smaller than the bubble size, i.e. $R_1 << R_2$, then Eq. [2.10] can be approximated as:

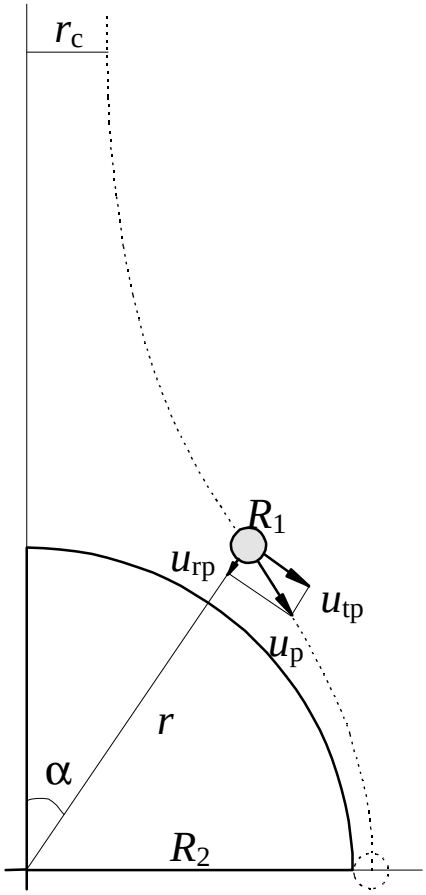

Figure 2.2. A grazing streamline for a particle of radius R_1 approaching the surface of a large bubble of radius R_2 given in polar coordinates, with r representing the distance from the center of the bubble to the center of the particle and α the angular coordinate. Only those particles within the critical radius r_c at far distances away from the bubble will collide with the bubble. The particle is considered to have no inertia, and has its velocity u_p, with u_{rp} and u_{tp} representing the radial and tangential velocity components, respectively.

$$P_c = \left(\frac{r_c}{R_2} \right)^2 \qquad [2.11]$$

For a given particle size (R_1) and bubble size (R_2), one can derive an expression for r_c from the stream function and substitute it into Eq. [2.10] for P_c.

The stream functions can be derived from solutions of the Navier-Stokes equations. When the Reynolds number of a bubble is much less than unity, the streamlines are described by the Stokes stream function as:

$$\Psi = u_2 R_2^{\,2} \sin^2 \alpha \left(\frac{1}{2} x^2 - \frac{3}{4} x + \frac{1}{4x} \right) \qquad [2.12]$$

in which u_2 is the bubble rise velocity, x is the radial coordinate, r, normalized by the bubble radius, R_2, (i.e. $x=r/R_2$), α the angular coordinate (see Figure 2.2), and the Reynolds number of the bubble Re is given as:

$$\mathrm{Re} = \frac{\rho_3 R_2 u_2}{\mu} \qquad [2.13]$$

where ρ_3 is the density and μ_2 is the viscosity of the medium. From Equations [2.11] and [2.12], the probability of collision for Stokes flow can be derived as:

$$P_c = \frac{3}{2} \left(\frac{R_1}{R_2} \right)^2 . \qquad [2.14]$$

When the Reynolds number is very large (potential flow), the stream function becomes:

$$\Psi = u_2 R_2^{\,2} \sin^2 \alpha \left(\frac{1}{2} x^2 - \frac{1}{2x} \right) \qquad [2.15]$$

then P_c can be obtained as:

$$P_c = 3\left(\frac{R_1}{R_2}\right). \qquad [2.16]$$

However, in most flotation systems, air bubbles have Reynolds numbers in-between those for Stokes and potential flow conditions, for which no analytical solution exists. Therefore, Yoon and Luttrell (49, 50) derived an empirical stream function as follows by analyzing a large number of experimental streamlines reported in the literature:

$$\Psi = u_2 R_2^{\,2} \sin^2\alpha\left[\frac{1}{2}x^2 - \frac{3}{4}x + \frac{1}{4x} + \frac{\mathrm{Re}^{0.72}}{15}\left(\frac{1}{x^2} + \frac{1}{x} + x - 1\right)\right], \qquad [2.17]$$

then P_c becomes:

$$P_c = \left[\frac{3}{2} + \frac{4\,\mathrm{Re}^{0.72}}{15}\right]\left(\frac{R_1}{R_2}\right)^2. \qquad [2.18]$$

Eq. [2.18] is similar to the expression derived by Webber and Paddock (51). It has been validated by many experimental results (49, 52-54).

2.2.1.2 Probability of Bubble-particle Adhesion (P_a)

Figure 2.3 shows a potential energy (V) *vs.* distance (H) diagram for bubble-particle interaction. According to the extended DLVO theory, V is the sum of the electrostatic (V_e), dispersion (V_d) and hydrophobic (V_h) interaction energies (8), i.e.,

$$V = V_e + V_d + V_h \ . \qquad [2.19]$$

Each term varies as a function of the closest separation distance (H) between the bubble and particle surfaces. The V *vs.* H diagram of Figure 2.3 shows an energy barrier (E_1) at H_1 and

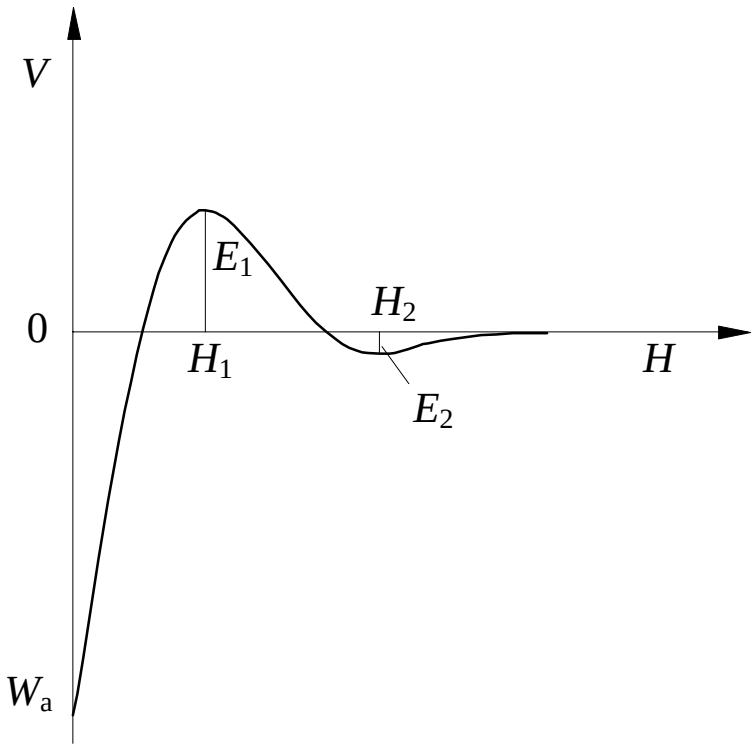

Figure 2.3. A potential energy (V) *vs.* distance (H) diagram for bubble-particle interaction, with E_1 representing the energy barrier and E_2 the secondary energy minimum. W_a is the work of adhesion.

a secondary energy minimum (E_2) at H_2. If the kinetic energy (E_k) of a particle approaching a bubble is smaller than E_1 and E_2, bubble-particle adhesion may occur at the secondary minimum with an equilibrium inter-particle distance of H_2. Derjaguin and Duhkin (20) suggested that bubble-particle adhesion could occur at the secondary minimum without forming a three-phase contact. This process was referred to as "contactless" flotation, which may be limited to the case of floating very small particles with relatively low hydrophobicity.

If E_k is larger than E_1 and E_2 but smaller than the sum of the work of adhesion (W_a) and E_1, then the thin film between the bubble and particle will rupture to form a three-phase contact, i.e., H becomes zero. W_a will be a function of the interfacial tension, contact angle and the contact area as will be shown in the following section. The particles with $E_k \geq E_1$ can approach the bubble within the distance of H_1, where the surface force between them ($F=-dV/dH$) becomes negative and, hence, the film ruptures spontaneously. H_1 is, therefore, referred to as critical rupture thickness. Thus, the necessary condition for bubble-particle adhesion is $E_k \geq E_1$. Although it is convenient to represent the kinetic energies of the particles colliding with a bubble with a single value of E_k, the fact of the matter is that particles have distributed E_k values. Therefore, it would be useful to represent the probability of bubble-particle adhesion (P_a) as (12, 14, 50):

$$P_a = \exp\left(-\frac{E_1}{E_k}\right), \qquad [2.20]$$

which is analogous to the probability functions used in the theory of chemical kinetics. In Eq. [2.20], E_k represents the kinetic energies of the macroscopic particles, while in chemical kinetics kT represents the thermal energies of molecules.

Eq. [2.20] suggests that P_a increase with a decrease in E_1 and an increase in E_k, which can be achieved by increasing the hydrophobicity of the particles and providing a

high-shear agitation, respectively. Weiss and Schubert (55) showed that the high-shear agitation is beneficial to fine particle flotation. E_1 can also be reduced by decreasing the electrostatic repulsion between particle and bubble. Derjaguin (56) showed that the floatability of a particle increases with a decrease in the magnitude of its ς-potential, which is consistent with the finding of Fuerstenau (57) which showed that a maximum flotation is achieved at the point of zero charge (p.z.c.) of the particle.

In determining E_1, it is necessary to accurately know the values of V_e, V_d and V_h of Eq. [2.19]. By considering particle and bubble as rigid spheres with radii R_1 and R_2, respectively, one can use the Hogg, Fuerstenau and Healy's expression (58) for V_e:

$$V_e = \frac{\varepsilon R_1 R_2 (\psi_1^{\,2} + \psi_2^{\,2})}{4(R_1 + R_2)} \left[\frac{2\psi_1 \psi_2}{\psi_1^{\,2} + \psi_2^{\,2}} \ln\left(\frac{1 + e^{-\kappa H}}{1 - e^{-\kappa H}} \right) + \ln(1 - e^{-2\kappa H}) \right], \qquad [2.21]$$

in which ε is the dielectric constant of the medium, ψ_1 and ψ_2 are Stern potentials of the bubble and particle, which are often substituted by ς-potentials as an approximation, and $1/\kappa$ is the Debye length.

The dispersion component (V_d) of the total interaction energy arises from the correlation of fluctuating electromagnetic dipoles at the particle and bubble surfaces. For two spherical macroscopic bodies of radii R_1 and R_2, V_d is given as (59):

$$V_d = -\frac{A_{132} R_1 R_2}{6H(R_1 + R_2)} \left[1 - \frac{1 + 2bl}{1 + bc / H} \right], \qquad [2.22]$$

where A_{132} is the Hamaker constant of particle **1** and bubble **2** interacting in a medium **3** (water). The second part of the equation represents a correction factor for the retardation effect, in which b is a parameter characterizing materials of interacting particles, l ($=3.3\times10^{15}$ s^{-1}) that of medium (water) and c ($=3\times10^{8}$ m/s) the velocity of light. For most materials, b is 3×10^{-17} s. Since the Hamaker constant for water ($A_{33}=4.38\times10^{-20}$ J) is less

than those of solid particles (A_{11}) but is greater than that of air bubble (A_{22}), A_{132} is usually negative. Therefore, the dispersion interaction between bubble and particle is repulsive.

The contribution from the hydrophobic interaction between the bubble and particle (V_h) to the total interaction energy (V) can be obtained by integrating Eq. [2.1]-[2.3] as follows:

$$V_h = -\frac{1}{2}\int_{\infty}^{H} F_h dH \,, \qquad [2.23]$$

in which F_h is the hydrophobic force between two like cylinders of equal radius of curvature as is done in direct force measurements using SFA or between a sphere and a flat surface when using AFM. For interactions between two dissimilar surfaces as in bubble-particle interactions, Eq. [2.23] becomes:

$$V_h = \frac{R_1 R_2}{R_1 + R_2}\left[C_1 D_1 \exp\left(-\frac{H}{D_1}\right) + C_2 D_2 \exp\left(-\frac{H}{D_2}\right)\right], \qquad [2.24]$$

when Eq. [2.2] is substituted into Eq. [2.23], or

$$V_h = -\frac{R_1 R_2}{6(R_1 + R_2)}\frac{K_{132}}{H}\,, \qquad [2.25]$$

when Eq. [2.3] is substituted. In the present work, Eq. [2.25] rather than Eq. [2.24] is used for two reasons. First, it has only one parameter (K_{132}), while Eq. [2.24] has four (C_1, D_1, C_2, D_2). Even when the short-range term (i.e., the first exponential term) is ignored, Eq. [2.24] has two parameters (C_2, D_2) that need to be fitted to experimental data. Second, Eq. [2.25] is in the same form as that for the non-retarded van der Waals interaction, which makes it possible to compare the K_{132} with the Hamaker constants (A_{132}).

2.2.2 Probability of Bubble-particle Detachment (P_d)

A particle can be detached from the surface of a bubble when the particle is subjected to a kinetic energy that exceeds the sum of the work of adhesion (W_a) and E_1 (60, 61) (see Figure 2.3). Therefore, the probability of detachment (P_d) may be given as:

$$P_d = \exp\left(-\frac{W_a + E_1}{E_k'}\right), \qquad [2.26]$$

in which E_k' represents the kinetic energy that tears the particles off the bubble surface. It should be noted that E_k' is not the same as E_k, which determines P_a. The logic behind using an exponential function to represent P_d is that particles on the surface of a bubble would have a distributed E_k' values, as will be discussed later.

Figure 2.4 shows a spherical particle of radius R_1 being attached onto the surface of a large bubble, whose surface may be considered flat relative to that of the particle. The work of adhesion can be determined as follows:

$$\begin{aligned} W_a &= \gamma_{sl} s_2 + \gamma_{lv} s_1 - \gamma_{sv} s_2 \\ &= \gamma_{lv} s_1 + s_2(\gamma_{sl} - \gamma_{sv}) \end{aligned} \qquad [2.27]$$

where γ_{sl}, γ_{lv} and γ_{sv} represent the surface free energies at the solid/liquid, liquid/vapor and solid/vapor interfaces, respectively; s_2 is the curved area of the particle inside the bubble after the bubble-particle attachment has taken place; and s_1 is the projected area of s_2 on the bubble surface.

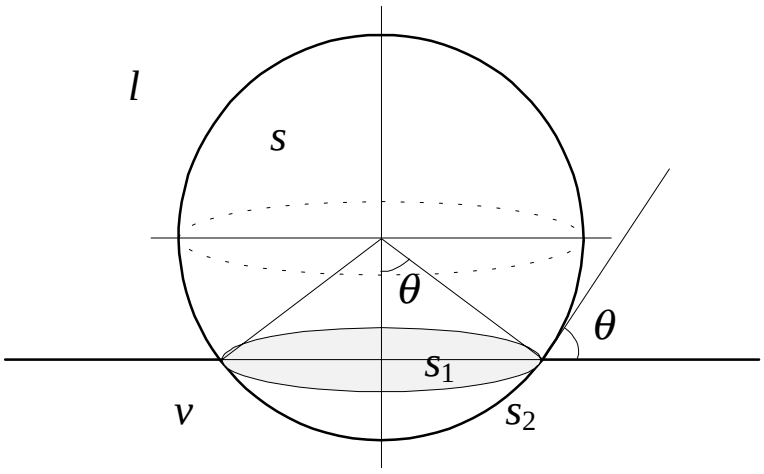

Figure 2.4. A spherical particle (*s*) of radius R_1 adhering on the surface of an air bubble (*v*) suspended in water (*l*). When R_1 is much smaller than the radius of the bubble, the bubble surface may be considered flat as compared to that of the particle. The curved area of the particle inside the bubble is represented by s_2, and s_1 is its projected area.

From the Young's equation,

$$\gamma_{sl} - \gamma_{sv} = -\gamma_{lv}\cos\theta\,, \qquad [2.28]$$

where θ is the contact angle. By substituting Eq. [2.28] into Eq. [2.27],

$$W_a = \gamma_{lv}\,(s_1 - s_2\cos\theta)\,. \qquad [2.29]$$

From Figure 2.4, one can obtain the following relationships:

$$s_1 = \pi (R_1 \sin\theta)^2\,, \qquad [2.30]$$

and

$$s_2 = 2\pi R_1^2\,(1 - \cos\theta)\,, \qquad [2.31]$$

which can be substituted into Eq. [2.28] to obtain:

$$W_a = \gamma_{lv}\,\pi R_1^2\,(1-\cos\theta)^2\,. \qquad [2.32]$$

Substituting Eq. [2.32] into Eq. [2.26], one obtains an expression for the probability of detachment as follows:

$$P_d = \exp\left(-\frac{\gamma_{lv}\pi R_1^2(1-\cos\theta)^2 + E_1}{E_k'}\right)\,. \qquad [2.33]$$

The combination of gravitational forces, turbulent forces and bubble oscillations acting on attached particles may attribute to the detachment of particles from bubble surface. Using high-speed photography, the strong oscillation of bubbles was observed in the impeller-driven flotation system due to the turbulence caused by rotor (62-64). Also, Bubble-particle collision may create bubble oscillation which is related to the

deformation of bubble surface and hence considerably influenced by particle size (65). A centrifuge technique (66-68), pendulum method (69) and vibration platform (70) have been used to investigate the bubble-particle detachment, most of the theoretic analysis is based on the force balance, however, the quantitative relationship between detachment force and probability of detachment has not been established. Equation [2.33] is the first fundamental expression for probability of bubble-particle detachment.

The expressions of P_a and P_d were developed by considering the bubble-particle interaction as a non-deterministic, probabilistic process. Apparently, they are applicable to the turbulent conditions usually found in the completely mixed cell. Even in the single bubble flotation cell, there is a degree of turbulence due to the rotation of particles, Wake phenomenon, etc. which makes the bubble-particle interaction to be a probabilistic process, and thus Eq. [2.20] and Eq. [2.26] can be used.

2.2.3 First-Order Rate Equation

The probability functions for the collision (Eq. [2.18]), adhesion (Eq. [2.20]) and detachment (Eq. [2.33]) can now be substituted into the expression for the first-order flotation rate constant (Eq. [2.7]) to obtain:

$$k = \frac{1}{4} S_b \left[\frac{3}{2} + \frac{4\,\mathrm{Re}^{0.72}}{15} \right] \left(\frac{R_1}{R_2} \right)^2 \exp\left(-\frac{E_1}{E_k} \right) \left\{ 1 - \exp\left[-\frac{\gamma_{lv} \pi R_1^{\,2} (1-\cos\theta)^2 + E_1}{E_k'} \right] \right\} \quad [2.34]$$

Eq. [2.34] shows that k is a function of both the hydrodynamic parameters, i.e., R_1, R_2, E_k, E_k', Re, and S_b, and the surface chemistry parameters, i.e., E_1, θ and γ_{lv}.

As shown by Eqs. [2.21]-[2.25] and schematically by Figure 2.2, E_1 is a complex function of ψ_1, ψ_2, A_{132}, and K_{132}, of which the first three can be readily determined

experimentally. (ψ_1 and ψ_2 are usually approximated by ς_1 and ς_2, respectively.) On the other hand, it is difficult to determine K_{132} experimentally. It has been shown that the hydrophobic force constant (K_{131}) between two solid surfaces of identical hydrophobicity can be estimated from advancing contact angles (17). However, it is unlikely that K_{131} can directly substitute for K_{132}. Recognizing that air bubble is one of the most hydrophobic entities (36), K_{132} should be greater than K_{131}, depending on the particle hydrophobicity and the amount of surfactant used to stabilize the air bubble in a given flotation system.

In using Eq. [2.34], it is necessary to have the values of the kinetic energies for attachment (E_k) and detachment (E_k'), which are difficult to be determined in an operating flotation cell where there is a considerable turbulence. If a flotation experiment were conducted under laminar condition, however, it would be possible to estimate the kinetic energies as follows.

2.2.4 Kinetic Energy for Attachment (E_k)

When a particle makes a head-on collision with a bubble (i.e., α=0), practically all of its kinetic energy would be consumed in thinning the film between the bubble and particle. However, only part of the total kinetic energy will be used for this process when α>0. Since the hydrodynamic and surface forces resisting to the film thinning process are acting only along the radial direction, the maximum kinetic energy available for this process may be determined from the radial velocity of the particle. For an inertialess particle located at a sufficient distance away from the bubble, the radial velocity of the particle (u_{rp}) would be the same as the radial velocity of the liquid (u_r), which can be determined from the stream function (Eq. [2.17]) as follows (50):

$$u_r = \frac{1}{r^2 \sin\alpha} \frac{\partial \Psi}{\partial \alpha}$$

$$= u_b \cos\alpha\left[1 - \frac{3}{2x} + \frac{1}{2x^3} + \frac{2\,\mathrm{Re}^{0.72}}{15}\left(\frac{1}{x^4} - \frac{1}{x^3} + \frac{1}{x} - \frac{1}{x^2}\right)\right]. \qquad [2.35]$$

As the particle approaches the bubble surface at a closer distance, u_{rp} will decrease due to the hydrodynamic resistance force (F_r):

$$F_r = 6\pi\mu R_1 u_{rp}\beta\ , \qquad [2.36]$$

where β is the Stokes correction factor. Thus, u_{rp} is reduced by a factor of 1/β as follows:

$$u_{rp} = u_r\ /\ \beta\ , \qquad [2.37]$$

as has been shown by Luttrell and Yoon (50) from a force balance. The values of β used in the present work were from Goren and O'Neill (71), and shown in Figure 2.5.

The maximum kinetic energy (E_k) that can be used for overcoming the energy barrier (E_1) created by the surface forces can then be obtained as follows:

$$\begin{aligned} E_k &= \frac{1}{2} m u_{rp}^{\ 2} \\ &= \frac{1}{2}(\rho_1 - \rho_3)\frac{4\pi R_1^{\ 3}}{3} u_{rp}^{\ 2} \\ &= \frac{2\pi R_1^{\ 3}(\rho_1 - \rho_3)}{3} u_{rp}^{\ 2}\ . \end{aligned} \qquad [2.38]$$

where ρ_1 and ρ_3 are the densities of solid and medium (water), respectively. Recall that the E_k used in Eq. [2.34] is the fraction of the kinetic energy of the particle that is used to thin the film at H_1. Therefore, Eq. [2.38] was used to calculate the E_k values at H_1 for the particles moving toward the bubble from various initial positions far away from the bubble under consideration. Consequently, there exist distributed E_k values at H_1. In the present work, a mean particle kinetic energy has been calculated and used for Eq. [2.34].

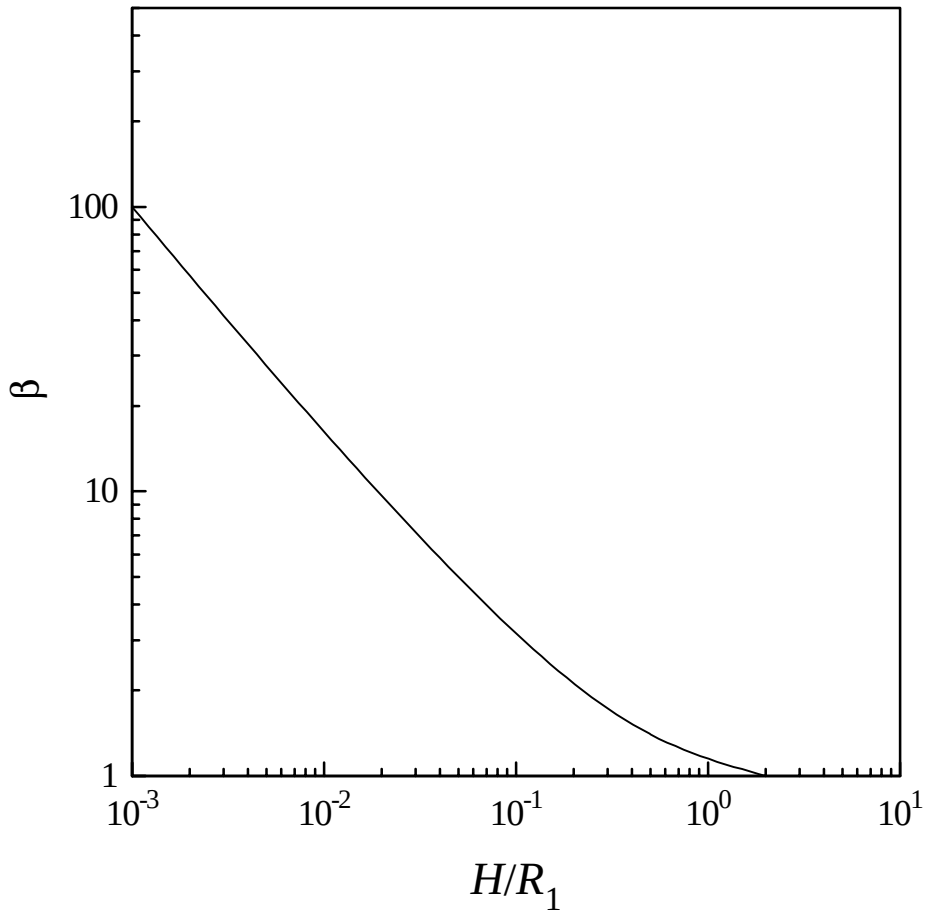

Figure 2.5. Relationships between β and H/R_1 determined by Goren and O'Neill(71).

The determination of E_k has been considered as a challenge problem. There is no appropriate solution so far. Although the method proposed in the present work is deterministic, it is the only way to evaluate E_k.

2.2.5 Kinetic Energy for Detachment (E_k')

As a bubble rises in a flotation column, more and more particles will be collected on the surface at the bottom and form a cap as shown in Figure 2.6. Let θ_0 be the angle representing the cap area. When θ_0 is large, the particles in the cap are subjected to increased pressure due to the drag force of the fluid flowing past the bubble. According to French and Wilson (72), when the bubble size is small enough to be in the creeping flow regime, the buoyant force on the bubble is given by:

$$f_b = \frac{3}{4}\pi R_2^{\,3}\rho_3 g\,, \qquad [2.39]$$

where ρ_3 is the density of the liquid, g the gravitational acceleration, and R_2 is the bubble radius. It is assumed that this force is counter-balanced by the drag force uniformly distributed over the area of the sphere, therefore the drag force per unit area is given by:

$$\frac{4\pi R_2^{\,3}\rho_3 g/3}{4\pi R_2^{\,2}} = \frac{\rho_3 g R_2}{3}\,. \qquad [2.40]$$

Thus the surface (tangential) stress at position θ_1 is:

$$p_s = \int_{\theta_0}^{\theta} \frac{\rho_3 g R_2}{3} R_2\, d\theta_1 = \frac{\rho_3 g R_2^{\,2}}{3}(\theta_0 - \theta_1) \qquad [2.41]$$

and the particle at the center of the cap is subject to a stress of p_1:

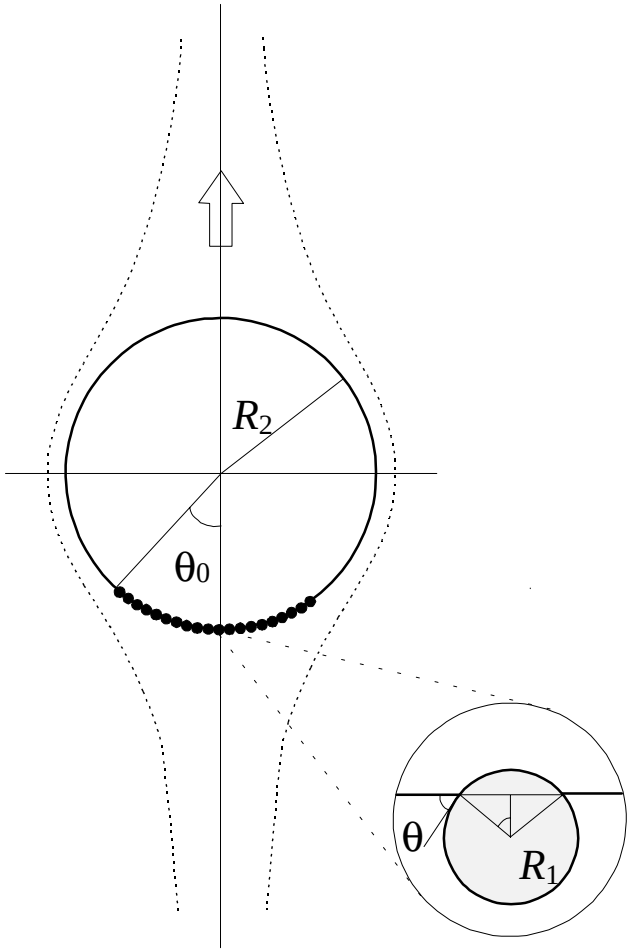

Figure 2.6. A cap of particles of radius R_1 collected at the bottom of a rising air bubble of radius R_2. The cap angle θ_0 is zero initially, and increases as more and more particles are collected on the bubble surface. The inset shows a particle at the center of the cap, whose contact angle is θ.

$$p_1 = \frac{\rho_3 g R_2^{\,2} \theta_0}{3} \ , \qquad [2.42]$$

θ_0 should be a function of the dimensions of the bubble and particle and the number of the particles in the cap.

If the area of contact between a particle of radius R_1 and the bubble is A, then the kinetic energy required to detach it from the bubble surface (E_k') is:

$$E_k' = p_1 A \ . \qquad [2.43]$$

From the inset in Figure 2.6, one can determine A as follows:

$$A = \pi R_1^{\,2} \sin^2 \theta \ , \qquad [2.44]$$

where θ is the contact angle of the particle at the three-phase contact. From Eqs. [2.42]-[2.44], one can derive a relationship for E_k' as follows:

$$E_k' = \frac{\rho_3 g R_2^{\,2} \theta_0}{3} \pi R_1^{\,2} \sin^2 \theta \ . \qquad [2.45]$$

When a fresh bubble is generated at the bottom of a flotation column, no particle will be present on the surface, i.e. θ_0 =0. As the bubble rises in a column of particle suspension, the number of particles collected on the bubble surface (n_s) will increase with time t, resulting in an increase in θ_0. From the value of n_s determined in a flotation experiment and the values of R_1 and R_2 employed in the experiment, one can generate a plot of θ_0 *vs*. t plot. In the present work, these plots were obtained for each experiment using the following assumptions, as illustrated in Figure 2.7. : i) the first particle collected will reside at the south pole of the bubble, and those collected subsequently form concentric rings sequentially around the first one, and ii) when there is not enough room to accommodate a whole particle in a concentric ring, it will begin to form a new concentric ring. Thus, the θ_0

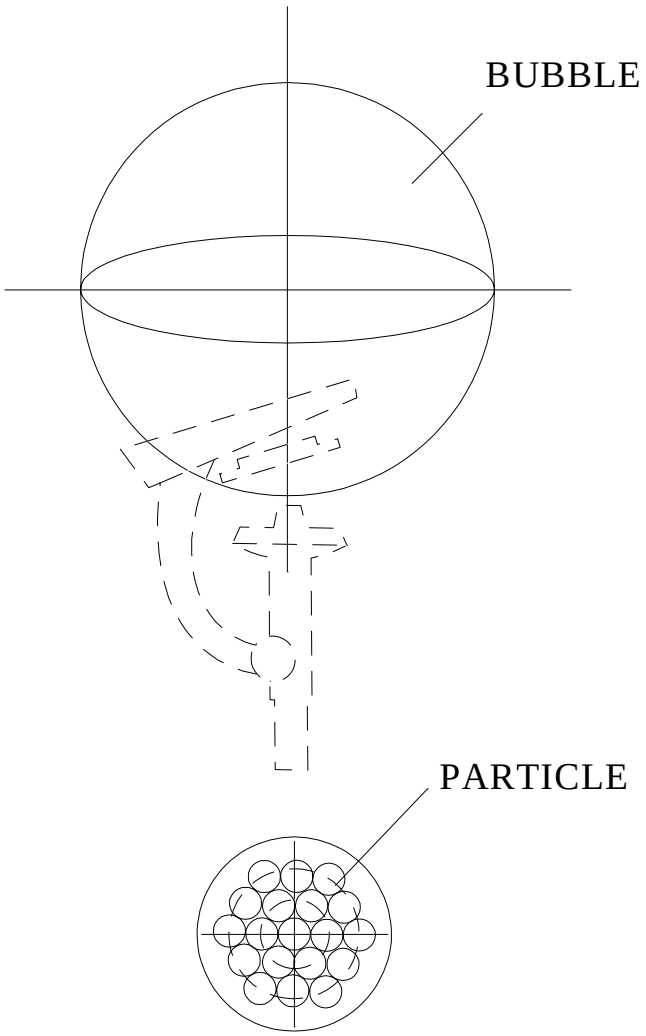

Figure 2.7. Accumulation of the particles collected by an air bubble.

must be a step-function with respect to the bubble rise time in a flotation column, as shown in Figure 2.8, and the particles in the cap area form approximately a close-packed monolayer. As θ_0 increases with t, E_k' will increase as suggested by Eq. [2.45]; therefore, there must exist a time at which the rate of hydrophobic particles being collected by the bubble is equal to the rate of detachment. At this point, θ_0 reaches a maximum, θ_0^{max}, which represents a maximum bubble loading. From each of the θ_0 *vs.* t plot constructed in this manner, a weighted mean of the θ_0 values for all of the particles adhering on a bubble surface was calculated and used for determining E_k' using Eq. [2.45].

Larger θ_0 indicates more particles collected by bubble, Eq. [2.45] and [2.26] suggest that P_d is increased with increasing number of particles in the bubble-particle aggregate. This is consistent with experimental results which shows that particles more easily detach from the bubble surface when more particles are in the bubble-particle aggregate (66).

The above analysis is appropriate for the creeping flow regime, the Reynolds number *R*e in this regime is less than 5 and the bubble size is less than 210 μm. For the larger bubble, the boundary layer separation must be taken into account, as shown in Figure 2.9 (73). In this case, the rise velocity of the bubble u_2 can be calculated from (74):

$$u_2 = \frac{2g\rho_3 R_2^{\,2}}{9\eta\left[1+\frac{1}{4}\left(\rho_3 R_2 u_2/2\eta\right)^{1/2}+0.34\rho_3 R_2 u_2/12\eta\right]}, \qquad [2.46]$$

where η is the viscosity of water. Eq. [2.46] is valid for *R*e ≤ 10^4 or the bubble of size ≤ 2.64 mm.

The stream function (ψ) and the velocity potential (ϕ) for inviscid ideal flow past a spherical object were given as (75):

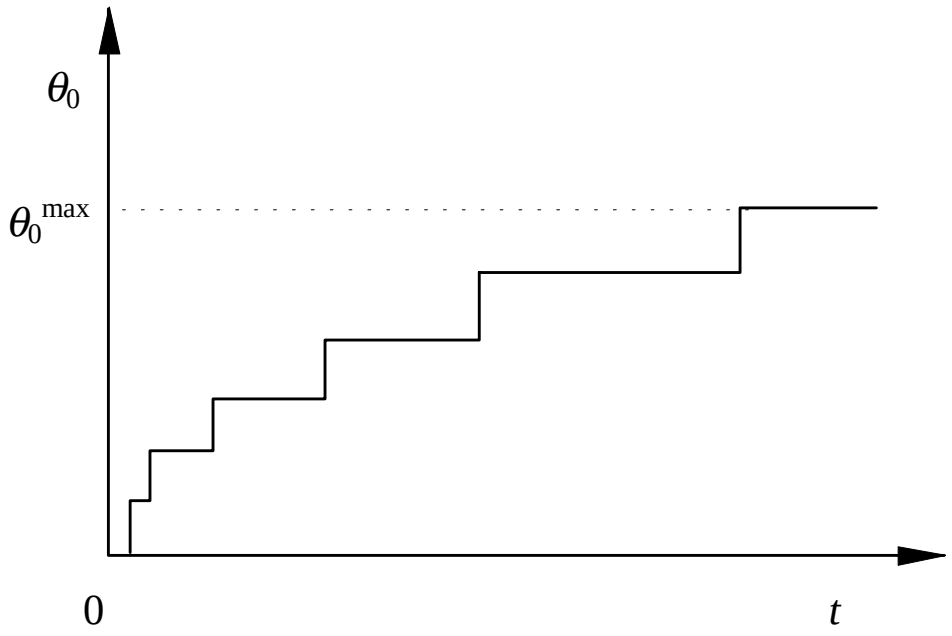

Figure 2.8. Step changes in the cap angle θ_0 (shown in Figure 2.6) with bubble rise time t in a flotation column. θ_0^{max} represents a maximum bubble loading, which is obtained when the rate of adhesion is equal to the rate of detachment.

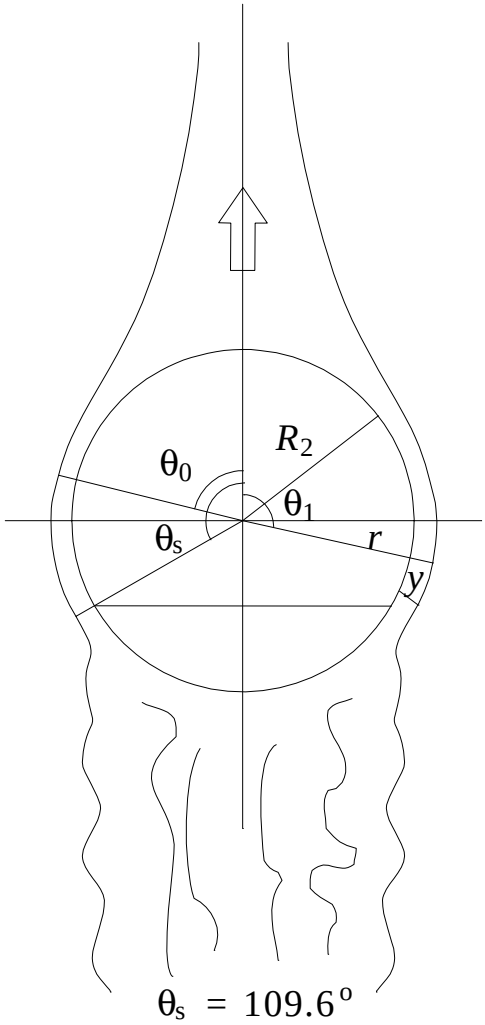

Figure 2.9. Boundary layer separation in the inviscid flow regime (73).

$$\psi = \frac{u_2}{2}\left(\frac{R_2^{\,3}}{r} - r^2\right)\sin^2\theta_1, \qquad [2.47]$$

$$\phi = u_2\left(\frac{R_2^{\,3}}{2r^2} + r\right)\cos\theta_1, \qquad [2.48]$$

where r and θ_1 are spherical coordinates with the polar axis in the direction of bubble motion. Thus the velocity components are:

$$U_r = -\frac{\partial\phi}{\partial r} = -u_2\left(-\frac{R_2^{\,3}}{r^3} + 1\right)\cos\theta_1 \qquad [2.49]$$

and

$$U_\theta = -\frac{1}{r}\frac{\partial\phi}{\partial\theta} = u_2\left(-\frac{R_2^{\,3}}{2r^3} + 1\right)\sin\theta_1. \qquad [2.50]$$

The viscous drag stress on the particles attached on the bubble surface is only dependent on u_θ which is a function of θ_1 and y (see Figure 2.9). There is (73):

$$u_\theta = U_\theta(\theta_1, y)\cdot f(\theta_1, Y) \qquad [2.51]$$

where f is a coefficient function which is determined by θ and Y, and Y is:

$$Y = \left(\frac{u_2 R_2 \rho_3}{\eta}\right)^{1/2}\frac{y}{R_2} \qquad y = r - R_2. \qquad [2.52]$$

Thus,

$$\frac{\partial u_\theta}{\partial r} = \frac{\partial u_\theta}{\partial y} = \frac{\partial U_\theta(\theta_1, y)}{\partial y} f(\theta_1, Y) + U_\theta(\theta_1, y)\frac{\partial f(\theta_1, Y)}{\partial Y}\frac{dY}{dy}. \qquad [2.53]$$

At $r = R$, or $y = Y = 0$, $f(\theta_1, 0) = 0$. Combining Eqs. [2.50], [2.52] and [2.53], there is:

$$\left.\frac{\partial u_\theta}{\partial r}\right|_{r=R} = \frac{3}{2} u_2^{3/2} \left(\frac{\rho_3}{R_2 \eta}\right)^{1/2} \frac{\partial f(\theta_1, 0)}{\partial Y} \sin\theta_1 . \qquad [2.54]$$

Therefore, the tangential surface stress at θ_2 is given by:

$$p_s = \eta \int_{\theta_0}^{\theta_2} \left.\frac{\partial u_\theta}{\partial r}\right|_{r=R} R\, d\theta_1 , \qquad [2.55]$$

and the maximum tangential surface stress at $\theta_2 = \theta_s$ is:

$$p_1 = \frac{3}{2} u_2^{3/2} (\rho_3 R_2 \eta)^{1/2} \int_{\theta_0}^{\theta_s} \frac{\partial f(\theta_1, 0)}{\partial Y} \sin\theta_1 \, d\theta_1 . \qquad [2.56]$$

Let

$$g(\theta_0) = \int_{\theta_0}^{\theta_s} \frac{\partial f(\theta_1, 0)}{\partial Y} \sin\theta_1 \, d\theta_1 \qquad [2.57]$$

and evaluate it as the function of θ_0 by numerical integration. Figure 2.10 shows the computation results (76). Substitute Eqs. [2.44] and [2.56] to Eq. [2.43], there is:

$$E_k' = \frac{3}{2} u_2^{3/2} (\rho_3 R_2 \eta)^{1/2} g(\theta_0) \pi R_1^2 \sin^2\theta . \qquad [2.58]$$

This equation is suitable for inviscid flow condition which is often found in typical flotation systems.

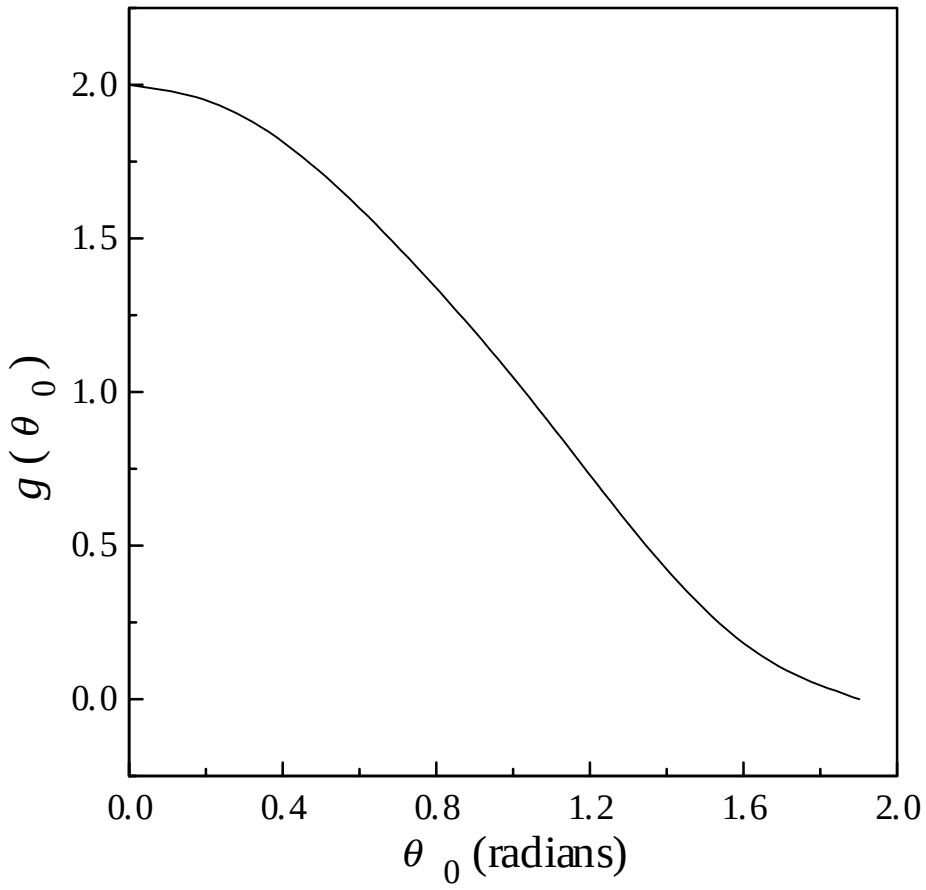

Figure 2.10. Plot of $g(\theta_0)$ versus θ_0 (76).

2.3 Experimental

2.3.1 Sample Preparation

Materials

For flotation experiments, fused-silica beads were obtained from Polysciences, Inc., New York. The sample was screened to obtain a -325+400 mesh fraction, which may be represented as 42.8 μm mean. For ς-potential measurements, a 2-5 μm fraction was obtained from the same company.

For contact angle measurements, polished fused-silica plates were obtained from Heraus-Amersil, New York. They were cleaned in a boiling nitric acid solution for 5 hours, rinsed with Nano-pure distilled water, and then stored in Nano-pure water in a clean Pyrex beaker. Prior to each experiment, the plate was cleaned with Nano-pure water in the ultrasonic bath for 10 minutes and dried with a jet of ultra-pure nitrogen gas.

Methylation

The silica beads and plates were methylated by following a procedure similar to those described by Laskowski and Kitchener (77) and by Blake and Ralston (78). The samples were dried at 100 ^{o}C in an oven for 24 hours and, then, contacted with a trimethylchlorosiliane (TMCS)-in-cyclohexane solution of a desired concentration. Approximately 2 grams of silica beads (-325+400 mesh flotation feed) and a silica plate were contacted with 500 ml of a TMCS solution in a beaker. The beaker was placed in an ultrasonic bath for 10 minutes to facilitate even distribution of TMCS on the silica surfaces. The samples were left in solution for 24 hours to complete the methylation, after which they were filtered while being washed repeatedly with pure cyclohexane. The samples methylated in this manner were dried in an oven at 80 ^{o}C for 24 hours. For ς-potential

measurements, the 2-5 μm glass beads were methylated in the same manner as the flotation feed.

2.3.2 Single Bubble Flotation Tests

Figure 2.11 shows the single-bubble flotation apparatus used in the present work, which was essentially the same as used by Schimmoler *et al.* (14). The apparatus was designed to provide a laminar flow condition so that the kinetic energies for bubble-particle attachment (E_k) and detachment (E_k') could be calculated using Eqs. [2.38] and [2.45], respectively.

Gas bubbles were formed by sparging high-purity nitrogen by means of a syringe pump (***1***) through a capillary tubing (hypodermic needle) (***2***) located at the bottom section of the flotation column (***3***). The column was made of a glass tubing with an inner diameter of 1 cm. The top end of the glass tubing was open to a reservoir (***4***), which was designed to keep the level of the particle suspension constant so that its downward velocity through the column could be is kept constant in a given experiment. The downward velocity was controlled by means of a stopcock (***5***) near the end of the column. The particle suspension exiting the column was collected in a beaker (***6***) located below the column, and was recycled by means of a peristaltic pump (***7***). As a bubble rises through the column, it picked-up hydrophobic particles and entered the Hallimond tube (***8***). The top end of the tube was closed so that the clear water in the tube does not flow out. The bottom end of the tube, whose I.D. (=1.5 cm) was larger than that of the column, was positioned close to the top end of the flotation column so that the bubble-particle aggregate could enter the Hallimond tube containing clear water. The bubble-particle aggregate entering the tube broke as it touches the air/water interface, thereby releasing the particles adhering on the bubble surface. The particles released from the bubble were collected in the collection tubing and weighed (***9***). In order to be able to collect enough samples to weigh, the single-

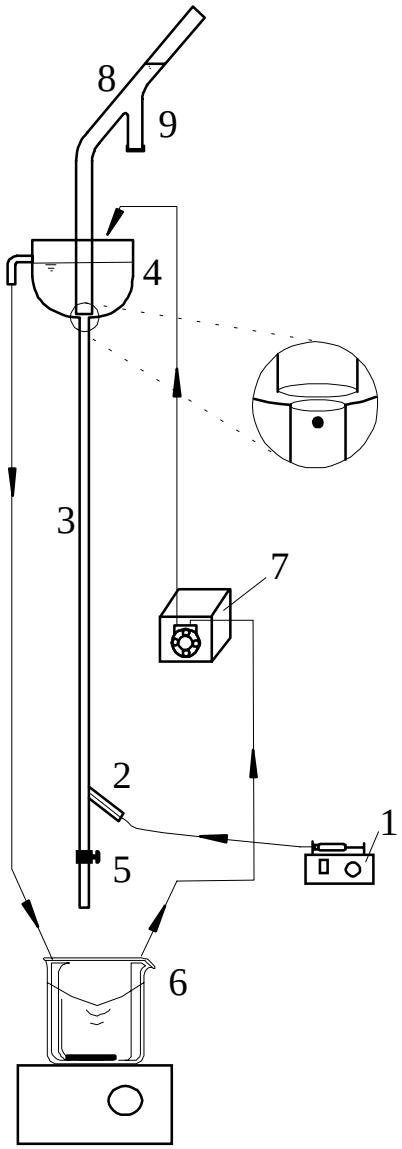

Figure 2.11. A schematic representation of the single-bubble flotation apparatus used in the present work. As shown in the inset, the bottom of the Hallimond tube is brought close to the top end of a flotation column so that bubble-particle aggregates can readily enter the tube.

bubble flotation experiment was conducted for an extended period of time, typically 1-2 hours, while single bubbles were released sequentially. All the flotation experiments were conducted in 10^{-3} M KCl solutions.

In a given experiment, the mean bubble size (R_2) was determined from the bubble rise velocity (u_2) using the relationship given by McCabe and Smith (79):

$$u_2 = \frac{0.153 g^{0.71} (2R_2)^{1.14} (\rho_3 - \rho_2)^{0.71}}{\rho_3^{0.29} \mu^{0.43}} \ , \qquad [2.59]$$

where g is the gravitational acceleration, ρ_2 and ρ_3 are bubble and fluid densities, respectively, and μ is the fluid viscosity. For the conditions employed in the present work, i.e., ρ_2=0, ρ_3=1 g/cm^3 and μ=0.01 poise at 20°*C*, Eq. [2.59] becomes:

$$u_2 = 325\, R_2^{1.14} \ , \qquad [2.60]$$

where u_2 is in cm/sec and R_2 is in cm.

Once the bubble size was measured, a downward flow of particle suspension was introduced into the column. When the system reached a steady state, the time, *t*, taken for a bubble to travel from the tip of the capillary to the bottom of the Hallimond tube was measured. The effective length of the recovery zone (ℓ), which is defined as the height of the particle suspension where bubble-particle interaction takes place, was then calculated using the following relationship:

$$\ell = u_2 t \ , \qquad [2.61]$$

where u_2 is the same as obtained using Eq. [2.60] with a stationary electrolyte solution in the flotation column. At least ten measurements were taken and averaged to determine *t*.

Flotation experiments commenced when the Hallimond tube filled with a clear electrolyte solution was placed near the bottom of the reservoir as shown in Figure 2.11. When a sufficient number of particles were collected in the collection tube, the flotation experiment was stopped and the particles removed. The collected particles were then filtered, dried and weighed to determine the number of particles collected (n_c) during the flotation time employed. The weight-to-number conversion was made using the values of the average diameter ($2R_1$=42.7 μm) and the density (ρ_1=2.65 g/cm^3) of the silica beads. By dividing n_c with the total number of the particles in the paths of all the bubbles used in the flotation experiment, one can determine the probability of collection (P) as follows (13):

$$P = \frac{n_c}{\pi R_2^{\,2} \ell n n_b} \ , \qquad [2.62]$$

where n is the number concentration of particles in the flotation column and n_b is the total number of bubble used in the flotation experiment. The experimental P value can be substituted into Eq. [2.7] to determine the flotation rate constant k.

2.3.3 Contact Angle Measurements

Water contact angles (θ) were measured using the sessile drop technique by means of a Rame-Hart goniometer. The sizes of the water droplets ranged from 2-4 mm. At least 10 separate measurements were taken on different spots of a plate and averaged. The θ values of the glass beads were assumed to be the same as those of the silica plates which had been methylated in the same batch. These values were used to make an initial estimation of K_{131} of Eq. [2.35] in the iteration process, as will be further discussed in the next section. It has been shown that K_{131} varies linearly with $\cos\theta$ at θ<90°C (17).

2.3.4 ς-Potential Measurements

A Rank-Brothers particle electrophoresis apparatus was used to measure the ς-potentials of methylated silica particles and nitrogen bubbles. The methylated silica was dispersed in a 10^{-3} M KCl solution with desired pH adjusted by adding aliquots of HCl and NaOH solutions. After conditioning for about 10 minutes, a small amount of sample was removed for potential measurement.

Microbubbles were generated using the apparatus shown in Figure 2.12, this is similar to those used by other investigators (80, 81). Nitrogen gas was introduced into a stainless steel container filled with desired solution to a level of 75% of its volume and kept at 0.5 MPa internal pressure for 24 hours to assure the solution being saturated by the dissolved nitrogen gas. Just before each potential measurement, about 100 ml solution was withdrawn through the needle valve to a beaker, and a bubble swarm was formed due to the decreasing of pressure from 0.5 Mpa to atmospheric pressure and moved to the surface of the solution. After the solution became clear in a few minutes, about 20 ml solution was introduced into the cell of the electrophoresis apparatus in which small bubbles of size 2-4 μm were observed under microscope, the bubbles stayed in the solution for a few minute, allowing the potential measurement to be completed.

At a given experimental condition, at least five ζ-potential readings of different runs were taken and averaged.

2.4 Results and Discussion

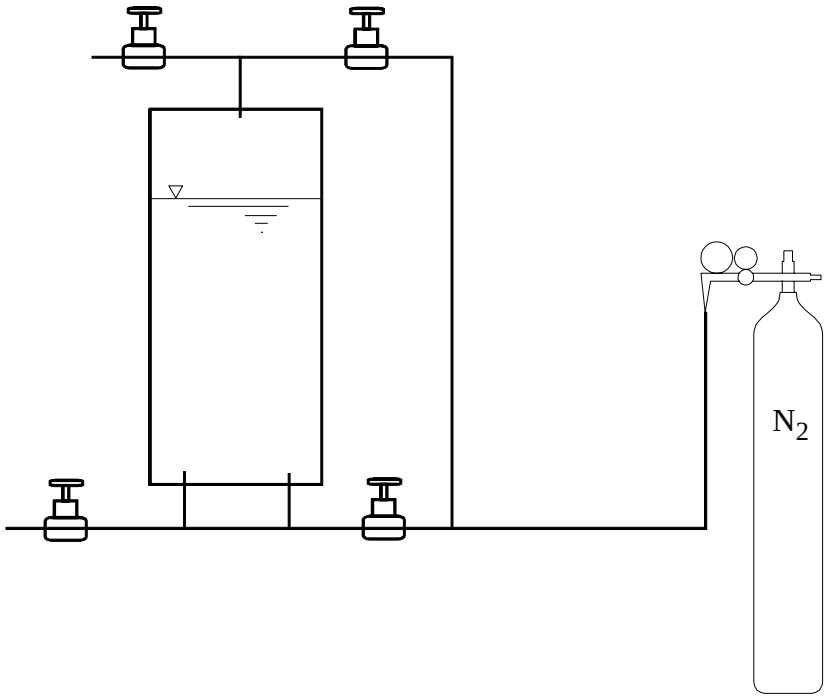

Figure 2.12. Experimental setup used for generating micro nitrogen bubbles.

One can predict the first-order flotation rate constant k using Eq. [2.34], if all of the parameters are known. Some of the parameters affect hydrodynamic forces involved in bubble-particle interaction, while others affect surface forces. Those affecting hydrodynamic forces include: particle size (R_1), bubble size (R_2), which in turn affect the kinetic energies for bubble-particle attachment (E_k) and detachment (E_k') under quiescent conditions. The surface force parameters include the energy barrier (E_1) for bubble-particle interaction, surface tension (γ_v), and water contact angle (θ) of the particles colliding with the bubble. E_1 may be determined using the extended DLVO theory incorporating the electrostatic (V_e), dispersion (V_d) and hydrophobic (V_h) interaction energies (Eq. [2.19]). In the present work, V_e is determined using Eq. [2.21] with the Stern potentials of the particle (ψ_1) and bubble (ψ_2) substituted by the respective Zeta-potentials (ς_1 and ς_2) as an approximation. V_d, on the other hand, can be determined using Eq. [2.22], provided that an appropriate Hamaker constant (A_{132}) is known. It is difficult, however, to determine V_h as there are no theories to predict the hydrophobic force parameters (K_{132}) for bubble-particle interactions. One might consider using the force data obtained using SFA and AFM. It is not certain, however, as to whether the force data obtained for solid-solid interactions can be used for bubble-particle interactions or not. Furthermore, most of the data reported in the literature are for symmetric interactions, i.e., between solid surfaces of equal hydrophobicity. In flotation, bubble and particle may have significantly different hydrophobicities, and it is not known how the force constants obtained for symmetric interactions can be combined for asymmetric interactions. Therefore, the approach taken in the present work was to back-calculate V_h from the experimental value of k and the parameters of Eq. [2.34] that could be determined experimentally or predicted from known theories.

Table 2.1 shows the values of probability of collection (P) obtained using Eq. [2.62] and those of k obtained using Eq. [2.7] from the experimental values of P and S_b. The values of S_b were obtained using Eq. [2.8] from the values of V_g and R_2 employed in the

Table 2.1 Test Conditions and Results of the Single-Bubble Flotation Experiments Conducted with Methylated Glass Spheres.

TMCS (M)	ψ_1 (mv)	θ (°)	$2R_2$ (mm)	S_b (min^{-1})	P ($\times 10^3$)	k_{exp} ($\times 10^3\ min^{-1}$)
10^{-6}	-63.9	35.2	1.02	1.40	7.46	2.60
10^{-5}	-62.9	39.3	1.01	2.18	9.02	4.91
10^{-4}	-61.1	49.9	0.98	1.90	13.1	6.21
10^{-3}	-60.75	52.2	1.13	1.85	14.37	6.65

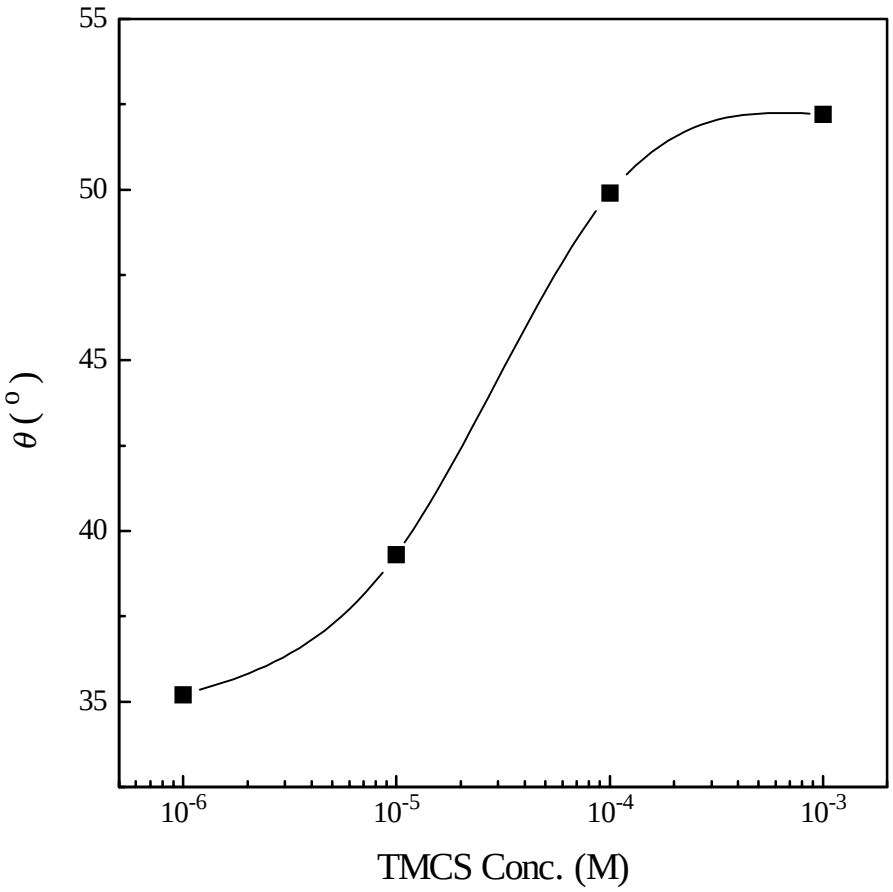

Figure 2.13. Contact angle of the methylated silica as a function of the TMCS concentration.

flotation experiments. The corresponding values of water contact angle are shown in Figure 2.13.

It is shown that the contact angle θ increases with TMCS concentration, indicating that the silica surface becomes increasingly hydrophobic, as the result, the flotation rate constant k is increased, which is consistent with industrial practice. Various surfactants, known as collectors, are used to selectively increase the hydrophobicity of the particles to be floated, while keeping unwanted particles remaining hydrophilic. Thus, the essence of flotation technology is to control the hydrophobicity of minerals to be separated, which is achieved by using collectors that adsorb selectively only on desired mineral(s).

Figure 2.14 shows the ζ potentials of the particles methylated at different TMCS concentration. With increasing TMCS concentration, ψ_1 decreases, but this change is not significant and may be considered in the range of the experimental error. However, the values reported in present work are considerably more negative than those reported by Laskowski and Kitchener (21) and Xu and Yoon (10, 11), which may be attributed to the differences in the sample sources and the methods of preparation.

The ζ potential of bubble (ψ_2) obtained in present work is -32.78 mv, which is less negative than that measured by Jordan (82) despite the fact that the electrolyte (KCl) concentration used by the latter investigator is higher (0.5 M) than used in the present work (10^{-3} M), which may be attributed to the methods of bubble generation. Yordan used a porous sparger, which produced significantly larger bubbles than used in the present work.

Using the experimental data shown in Table 2.1, Figure 2.13 and 2.14, contributions from the hydrophobic force (V_h) to the total interaction energy (V_t) of bubble-particle interactions were back-calculated using the algorithm given in Figure 2.15. The Hamaker constant used in the calculation is -1.0×10^{-20} J (83). In the present work, V_h is represented

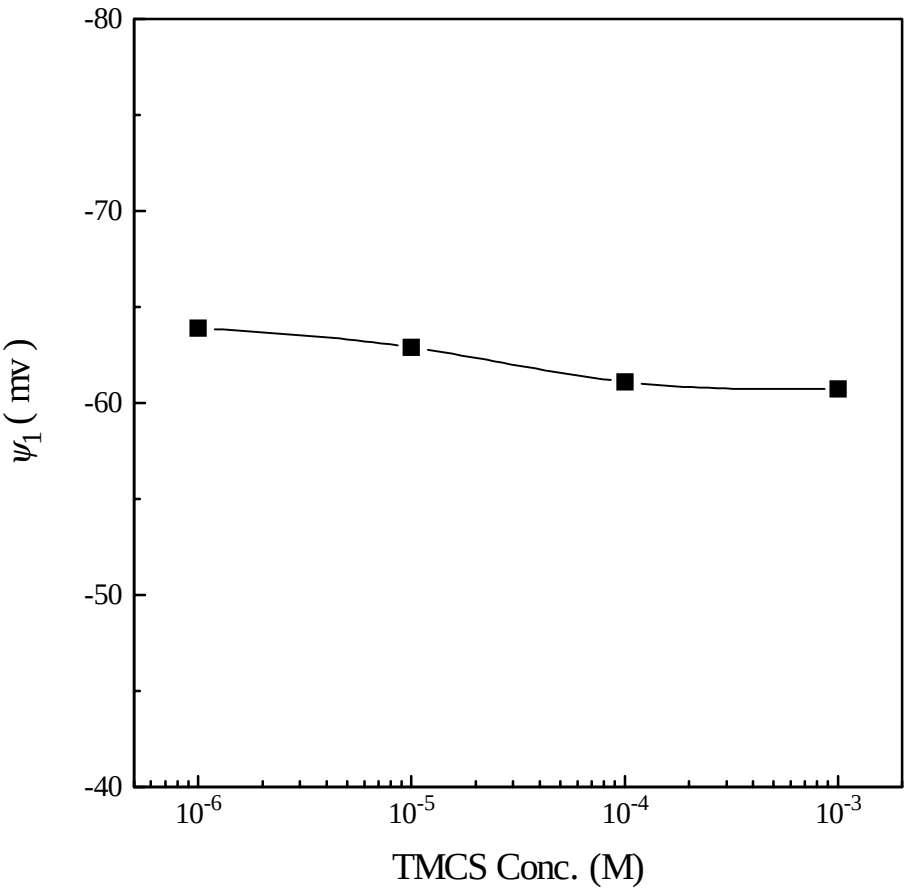

Figure 2.14. Zeta-potential of methylated silica as a function of TMCS concentration.

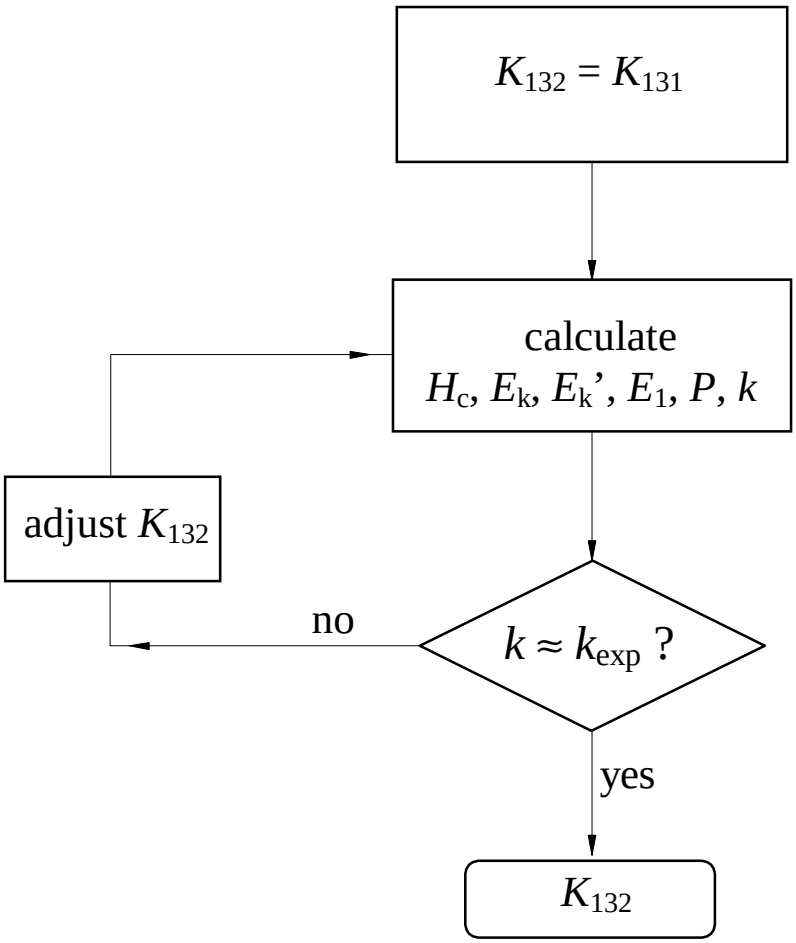

Figure 2.15. An algorithm for back-calculating K_{132} using Eq. [2.34] from the experimental k values and the values of other parameters of the equation that can be determined experimentally or calculated from theory. The initial estimation of K_{132} was K_{131}.

by the power law (Eq. [2.25]) rather than the exponential law (Eq. [2.24]) for convenience, so that the magnitude of the hydrophobic force is represented by a single parameter K_{132}. Initially, the values of K_{132} were estimated using Eq. [2.35] by assuming that K_{132}=K_{131}. The values of K_{131}, in turn, were estimated from the values of θ of the silica samples used for the flotation experiments using a K_{131} *vs.* θ plot reported by Yoon *et al.* (17). This plot was obtained from the direct force measurements conducted with mica surfaces in equilibrium with dodecylammonium hydrochloride and neutral surfactants (octanol or dodecanol). From the initial estimates of K_{132} obtained as such, the values of E_1 and H_1 were obtained using the extended DLVO theory (Eq. [2.19]). E_1 is an important parameter of Eq. [2.34] representing the net effect of the three surface forces, namely, electrostatic, dispersion and hydrophobic forces. Although H_1 is not a parameter of Eq. [2.34], its value is needed in calculating E_k. Recall that E_k is the weighted mean of the maximum kinetic energies of the particles that can be used for thinning the film between the particles and a bubble under consideration at a distance of H_1. Those particles traveling along the north-south pole of the bubble, i.e., α=0, give the maximum kinetic energies, while those traveling along the grazing streamline have zero kinetic energies (because u_r=0 at the equator of the bubble). One can also calculate the values of the kinetic energies for detachment (E_k') using Eq. [2.45]. In the present work, these values were used for calculating k using Eq. [2.34]. If the calculated k values were different from the experimental values, then the value of K_{132} was changed and the calculation was repeated until there was a good agreement between the calculated and experimental k values.

The calculation results are shown in Figure 2.16 to 2.20. Figure 2.16 shows the values of H_1 and E_1 as a function of TMCS concentration. H_1 increases with increasing TMCS concentration, indicating that the thin film between bubble and particle ruptures at increasingly long distance. This is obviously related to better hydrophobicity of the particle achieved at higher concentration of TMCS which produces stronger attractive

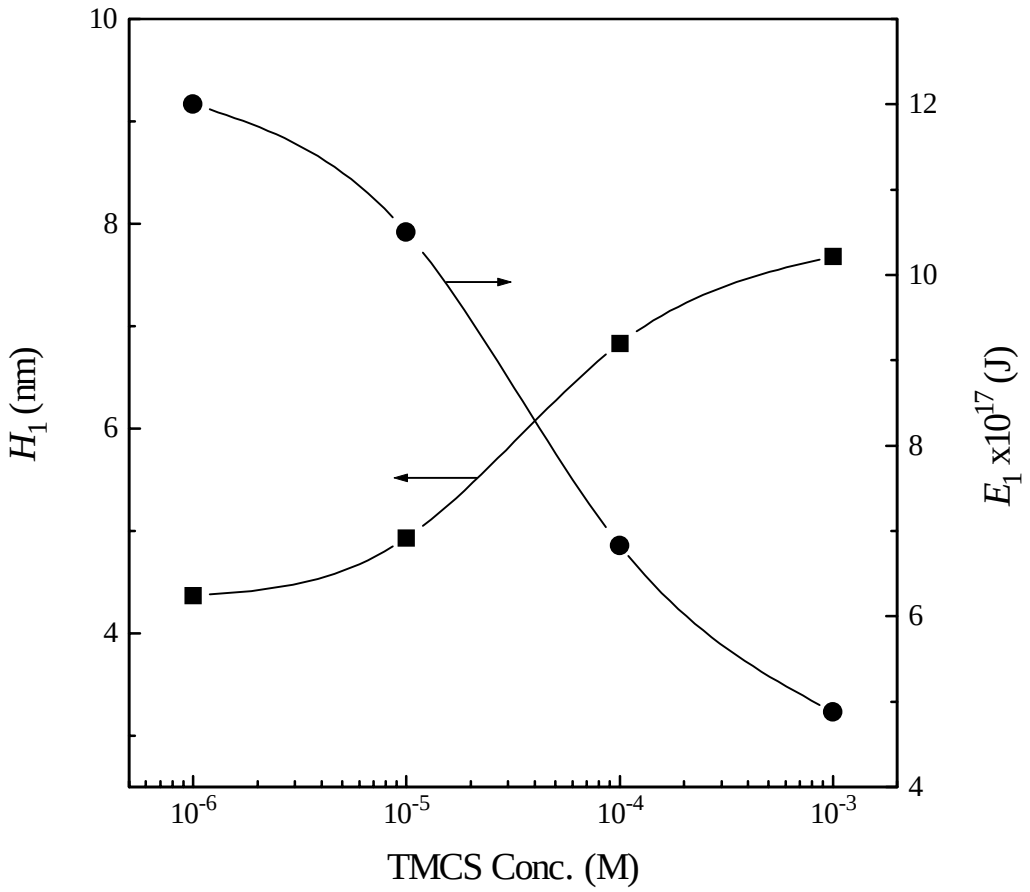

Figure 2.16. The values of H_1 and E_1 as a function of TMCS concentration.

hydrophobic force for bubble-particle attachment. This enhanced attractive force can easily overcome the repulsive double layer and dispersion force, and thus the activation energy E_1 is reduced.

Figure 2.17 shows the values of E_k and E_k' as a function of TMCS concentration. E_k obviously increases with increasing TMCS concentration, which is attributed to the increasing of the critical thickness H_1. As shown in Figure 2.5, the value of β is obviously increased with decreasing distance between bubble and particle, especially when the particle is very close to the bubble surface, in this case, a small increasing of H can result in significant decreasing of β, and thus the resistance force (F_r) is greatly reduced. That means, the kinetic energy of the particles which is used to overcome the energy barrier is required much less or the kinetic energy of the particle is significantly higher at a little bit longer distance. E_k' also increases with TMCS concentration, this is mainly due to the fact that, with the increasing of the hydrophobicity of the particles, E_1 is decreased and P_a is increased, the number of the particles collected by each bubble is increased, thus θ_0 is increased (see Figure 2.6), resulting in increasing of E_k' (see Equation 2.45).

The values of the hydrophobic force parameter K_{132} is considerably increased with increasing of TMCS concentration, as shown in Figure 2.18. K_{132} is the quantitative representation of the hydrophobic force, the increasing of its values clearly related to the improvement of the hydrophobicity of particles.

The calculation results of K_{132} values for different interfaces are summarized in Table 2.2. It turned out that K_{132} was much larger than K_{131}, suggesting that the air bubbles used in the flotation experiment were substantially more hydrophobic than the silica particles. Based on the equilibrium film thickness measurements conducted on free films, Aksoy (36) showed that air bubbles are hydrophobic and the hydrophobicity

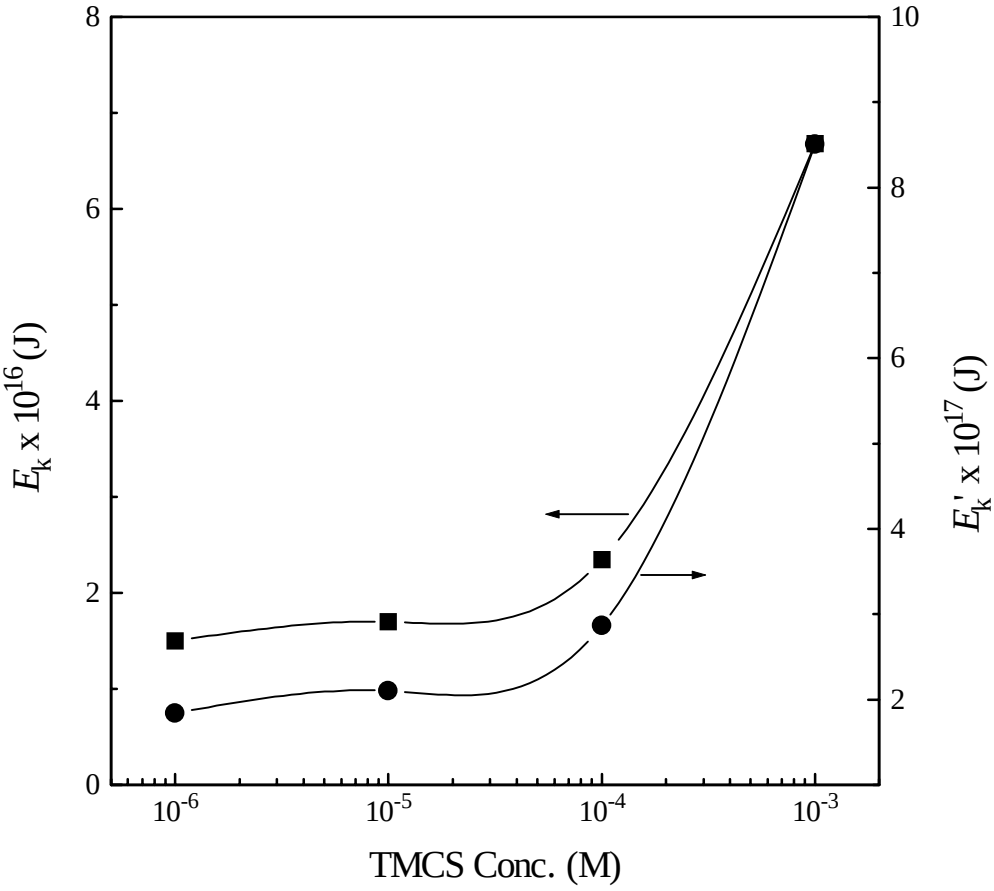

Figure 2.17. The values of E_k and E_k' as a function of TMCS concentration.

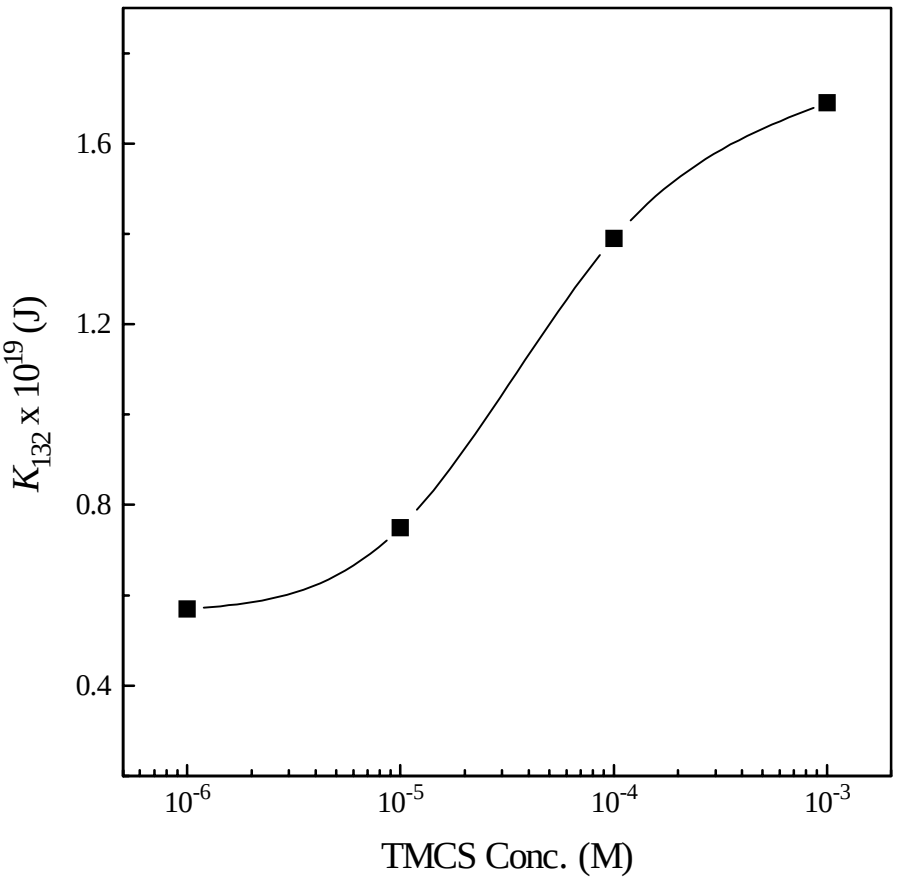

Figure 2.18. Relationship between K_{132} and TMCS concentration.

Table 2.2. Computation of K_{132} Using Eq. [2.34] from the Data Given in Table 2.1 by following the Algorithm Shown in Figure 2.15

TMCS (M)	K_{131} [a] ($\times 10^{21}$ J)	K_{232} [b] ($\times 10^{17}$ J)	$\sqrt{K_{131} \cdot K_{232}}$ ($\times 10^{19}$ J)	K_{132} ($\times 10^{19}$ J)
10^{-6}	1.45	0.4-3.0	0.76-2.08	0.57
10^{-5}	1.99	0.4-3.0	0.89-2.44	0.75
10^{-4}	5.15	0.4-3.0	1.44-3.93	1.39
10^{-3}	6.51	0.4-3.0	1.61-4.42	1.69

[a] form Yoon *et al* (17).

[b] from Aksoy (36)

increases with decreasing surfactant concentration. By extrapolating the data to very low surfactant concentrations (<10^{-5} M), he estimated the hydrophobic force constant (K_{232}) of air bubbles to be approximately 10^{-17} J in the absence of surfactants as shown in Table 2.2. This value is larger than those (K_{131}) of many hydrophobic surfaces whose θ's are in excess of 90^{o}.

It is interesting to note that the K_{132} values obtained in the present work are close to the geometric means of K_{131} and K_{232}, i.e.,

$$K_{132} = \sqrt{K_{131} \cdot K_{232}} \ , \qquad [2.63]$$

rather than the arithmetic and harmonic means of the two. This is the first time to find the relationship (named "Combining Rule") among the hydrophobic force parameters for different interfaces based on the experimental results, it is consistent with those reported later by Flinn (84) based on the direct force measurements conducted with symmetric and asymmetric solid surfaces using an AFM. Eq. [2.63] shows that hydrophobic forces are additive and can be combined just like the Hamaker constants.

If two of three hydrophobic force parameters in Eq. [2.63] are known, the third one can be calculated using the combining rule. Especially, when one of the K parameters is very difficult or even impossible to be determined experimentally, using combining rule is the only way to obtain its value. For example, it has been shown that, the K_{132} value for bubble-particle interaction is very difficult to be measured, but the K_{131} for solid-solid interaction can be determined using SFA or AFM, and K_{232} for bubble-bubble interaction can be determined using Thin-Film-Balance (TFB) technique, thus K_{132} can be calculated using Eq. [2.63]. However, when the hydrophobicity of the solid surface is very high, it's very difficult or impossible to accurately measure such a strong hydrophobic force between two symmetric solid surfaces (K_{131}) using AFM. One may determine the hydrophobic force between two solid surfaces with less hydrophobicity

(K_{232}), and then measure the hydrophobic force between surface with same hydrophobicity as solid 1 and one with same hydrophobicity as solid 2. These are possible because the hydrophobic forces are much weaker in the latter two cases, and both K_{132} and K_{232} are substantially lower than K_{131}, thus the value of K_{131} can be calculated from K_{132} and K_{232} using combining rule.

Based on the K_{132} values back-calculated from the experimental rate constants for the single-bubble flotation experiments, it is now possible to construct the potential energy *vs.* distance diagrams for bubble-particle interactions. Figures 2.19 and 2.20 show the diagrams for the silica particles methylated at 10^{-6} and 10^{-4} M TMCS. In either case, both electrical and dispersion energies are repulsive, while the hydrophobic forces represent the only attractive force for bubble-particle interaction. Note that K_{132} increased from 0.57×10^{-19} J to 1.39×10^{-19} J due to the increase in TMCS concentration. This increase is largely responsible for the decrease in E_1 from 12.0×10^{-17} J to 6.83×10^{-17} J and, hence, the increase in k from 2.60×10^{-3} to 6.21×10^{-3} min^{-1}. Although the decrease in the repulsive electrical and dispersion energies also contributes to the decrease in E_1, the hydrophobic force plays the most decisive role.

It is interesting to note that the value of K_{232} is four-orders of magnitudes larger than those of K_{131}, indicating that air bubbles is substantially more hydrophobic than the particles used in the flotation experiments conducted in the present work. On the other hand, the values of K_{132} are approximately two orders of magnitudes larger than those of K_{131}. These results suggest that control of bubble hydrophobicity is important in flotation.

Since the net surface force between bubble and particle becomes attractive at H_1 (see Figure 2.2), it may be reasonable to expect that the intervening film should rupture at distances below H_1. However, the values of H_1 given in Table 2.2 are in the range of 4-8 nm, which are substantially smaller than the critical rupture thickness measured with wetting films. Derjaguin *et al.* (85) reported values in the range of 200-300 nm, while those

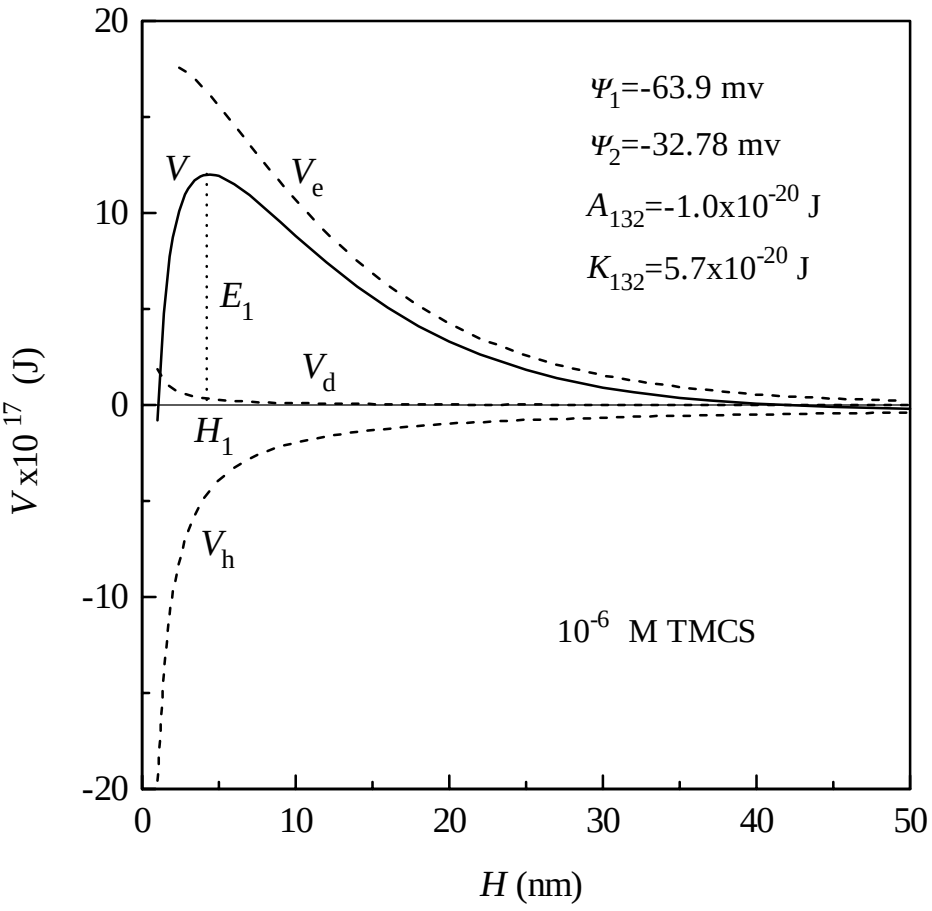

Figure 2.19. Potential energy *vs.* distance diagrams for the interaction between methylated silica particles of radius 42.8 μm and air bubbles of radius 0.51 mm. The silica particles were methylated in a 10^{-6} M TMCS solution. The value of K_{132} was back-calculated using Eq. [2.34] from the experimental k value using the algorithms shown in Figure 2.15.

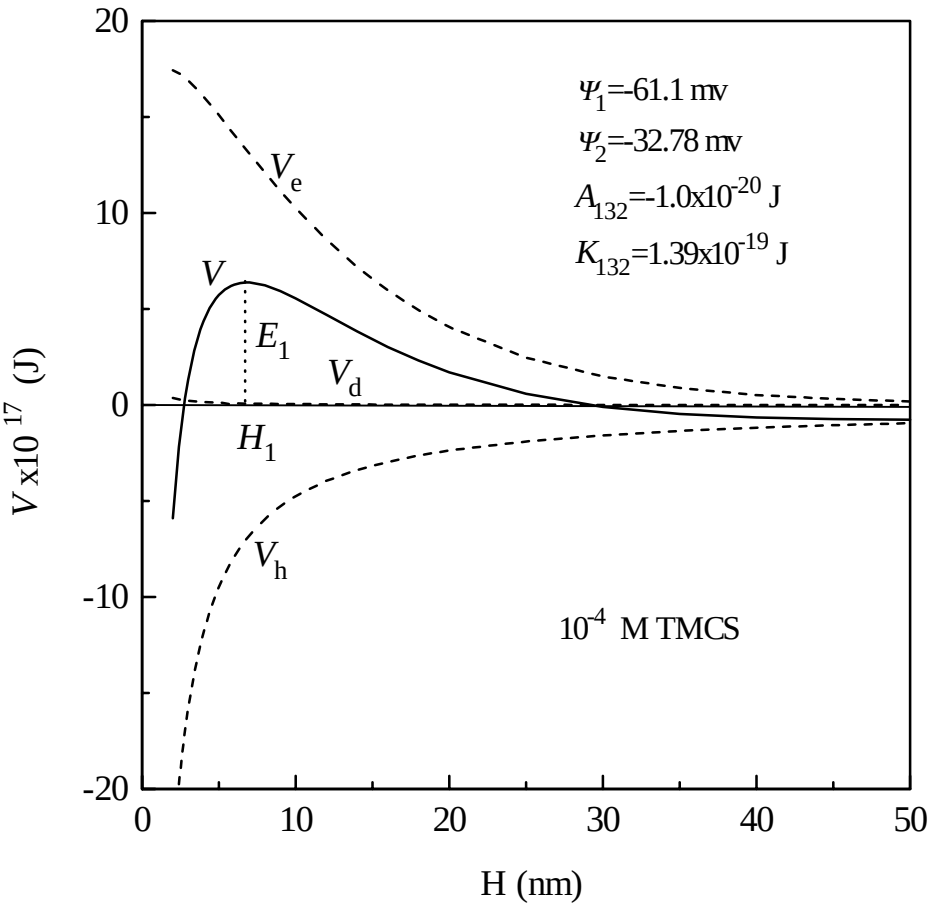

Figure 2.20. Potential energy *vs.* distance diagrams for the interaction between methylated silica particles of radius 42.8 μm and air bubbles of radius 0.47 mm. The silica particles were methylated in a 10^{-4} M TMCS solution. The value of K_{132} was back-calculated using Eq. [2.34] from the experimental k value using the algorithms shown in Figure 2.15.

reported by Blake and Kitchener (22) are in the range of 60-220 nm. Both of these reports were for methylated silica in water. Although smaller rupture thicknesses were measured with silica surfaces equilibrated in dodecylammonium chloride solutions (28), all of these values are substantially larger than those of H_1 calculated in the present work. That the TMCS concentrations used in the present work were much lower than those used by Derjaguin *et al.* and Blake and Kitchener may be a reason. It is also possible that wetting films rupture due to other mechanisms such as local fluctuation (86) and nucleation (87, 88) at thickness significantly larger than predicted by the extended DLVO theory. Further investigation is needed to more fully explain the discrepancy.

Although froth flotation is widely used in the minerals industry, it is effective over a relatively narrow particle size range, i.e., $5<R_1<50$ μm (89). Eq. [2.34] suggests methods of expanding both the upper and lower particle size ranges for flotation. It shows that the flotation rate varies as $(R_1/R_2)^2$, suggesting that for fine particle flotation smaller bubbles must be used. It also shows that the flotation rate varies as S_b, which in turn varies as R_2^{-1}; therefore, the flotation rate should vary approximately as R_2^{-3} at low Re, which has been shown to be the case in experiment (90). Most of the new generation flotation machines developed in recent years are based on using small air bubbles, which is often referred to as microbubble flotation. Eq. [2.34] suggests also that the difficulty in floating coarse particles is due to the high probability of detachment, which in turn is a function of detachment kinetic energy (E_k'). As shown in Eq. [2.45], E_k' varies as R_1^2 and R_2^2. Therefore, the coarse particle flotation should also be improved by using smaller air bubbles. Indeed, recent installation of a microbubble flotation column at the Peak Downs coal preparation plant significantly improved the coarse particle recovery (91). On the other hand, an excessive use of a frothing agent, which may be required to reduce the bubble size, can be detrimental to the coarse particle flotation. According to Eq. [2.34], the detachment probability should decrease with increasing γ_{lv}. Therefore, developing a frothing agent that can decrease bubble size without suppressing γ_{lv} excessively may be important for

improving coarse particle flotation. This suggestion may be consistent with a report which claims that ethoxylated frothing reagents improve coarse particle flotation (92).

With the Combining rule (Eq. 2.63) and the rate equation (Eq. 2.34), the flotation rate can be predicted based on the results of the measurements on the hydrodynamics and surface chemistry of the system. The values obtained can be compared with the experimental results of single bubble flotation to validate the rate equation.

Figure 2.21 and 2.22 show the comparison between the experimental results (k_{exp}) and calculated values (k_{cal}) of the flotation rate constants using the typical value of K_{232} ($=1\times10^{-17}$ J) and the best-fitting value ($=4\times10^{-18}$ J) respectively. A good correlation between k_{cal} and k_{exp} is observed, although more derivation deviation is seen in the Figure 2.21. Clearly, this discrepancy is mainly due to the value of K_{232} used in the computation. Since K_{232} is estimated by extrapolating the experimental data, its exact value in absence of surfactant is still not available. However, in many flotation system, the concentration of the surfactant is high enough to determine the value of K_{232} with similar technique used by Aksoy (36), thus the flotation rate can be predicted with Equation 2.34.

2.5 Summary and Conclusions

A first principle flotation rate model was developed by considering both hydrodynamic and surface forces involved in bubble-particle interactions. A new technique was proposed to determine the kinetic energy for bubble-particle adhesion, and a general expression for bubble-particle detachment was developed. Three surface forces, namely, ion-electrostatic, dispersion and hydrophobic forces, were considered. Since insufficient information is available on the hydrophobic force, its contributions were back calculated from the rate constants determined in single-bubble flotation experiments. The results show that the hydrophobic force constants for bubble-particle interactions (K_{132}) are in the

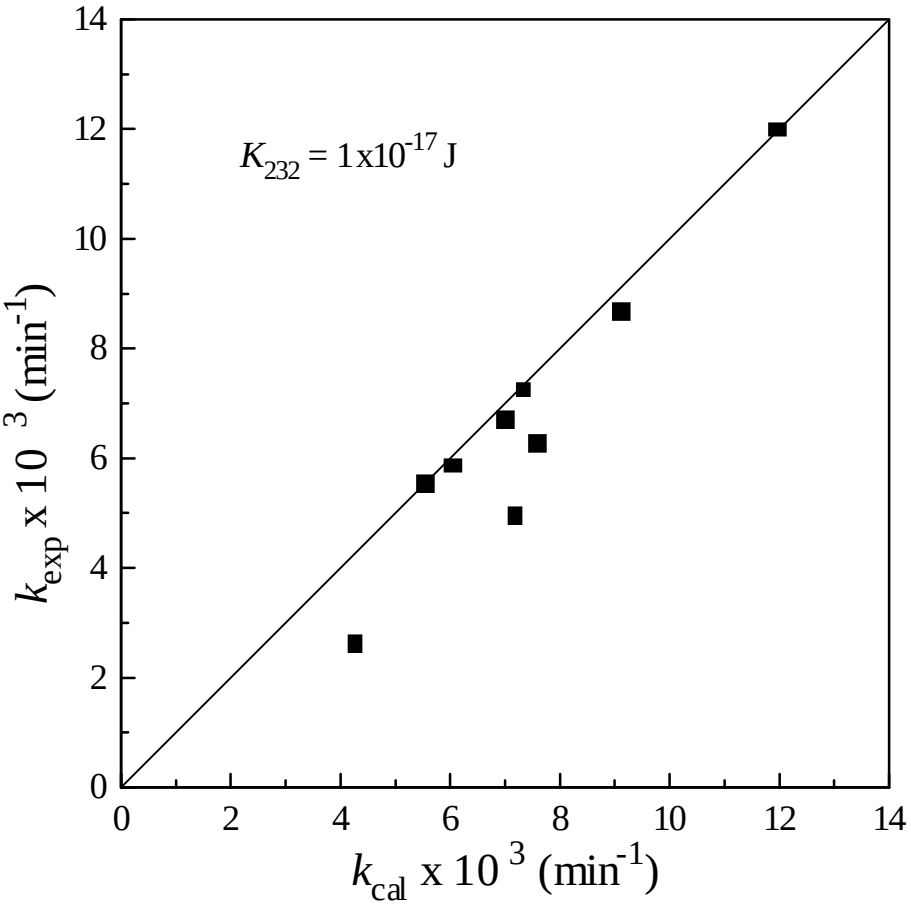

Figure 2.21. The comparison between the experimental data (k_{exp}) and the calculated values (k_{cal}) of flotation rate constant. The value of K_{232} used in the computation is 1×10^{-17} J.

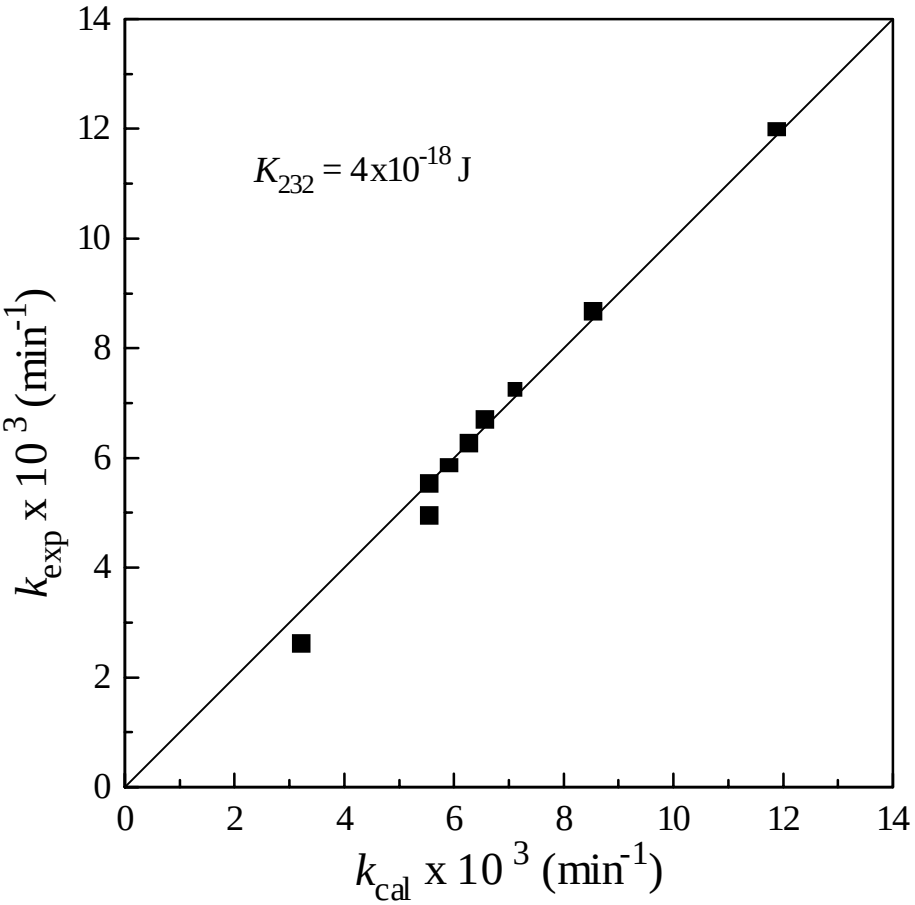

Figure 2.22. The comparison between the experimental data (k_{exp}) and the calculated values (k_{cal}) of flotation rate constant. The value of K_{232} used in the computation is 4×10^{-18} J.

range of 0.6-1.7x10^{-19} J, which are substantially larger than those (K_{131}) for particle-particle interactions but smaller than those (K_{232}) for air bubbles interacting with each other in the absence of surfactants. The K_{132} values obtained in the present work are close to the geometric means of K_{131} and K_{232}, thus a new equation, named "combining rule", was proposed for the first time to express the relationship among the hydrophobic force parameters for different interface. The relationship may have great potential application in determining the hydrophobic force which is otherwise very difficult or impossible to be determined. This finding is consistent with the conclusion derived from direct force measurements conducted later with symmetric and asymmetric solid surfaces. The K_{132} values determined in the present work were used to construct potential energy *vs.* distance diagrams for the interaction between methylated silica and air bubbles during flotation. They show that the hydrophobic force plays the most important role in decreasing the energy barrier for bubble-particle interaction and, hence, increasing the flotation rate. The flotation rate equation derived in the present work suggests various methods of improving the flotation of both fine and coarse particles.

The comparison results between the experimental data and the calculated values of the rate constants demonstrate that, the model proposed in present work can be used to predict the flotation rate constant. The value of K_{232} is important in the computation, which can be determined experimentally for the typical flotation systems.

2.5 References

1. Bushell, C. H., *Trans. A.I.M.E.* **223**, 266 (1962).

2. Lynch, A. J., Johnson, N. W., Manlapig, E. V., and Thorne, C. G., "Mineral and Coal Flotation Circuits"(D. Fuerstenau, Ed.), Vol. 4. Elsevier, New York, 1981

3. Kelsall, D. F., *Trans. Inst. Min. Met*. **70**, 191 (1961).

4. Schubert, H., and Bischofberger, C., *Proceedings 13 Int. Mineral Processing Congr*. Warszawa, **2**, 1261 (1979).

5. Inoue, T., Nonaka, M., and Tmaizumi, T., Advances in Mineral Processing, (P. Somasundaran, Ed.), Chapter 12, Society of Mining Engineers, Inc., 1986.

6. Darcovich, K., *Power Technology* **83**, 211(1995).

7. Darcovich, K., *Power Technology* **83**, 225(1995).

8. Yotsumoto, H., and Yoon, R. H., *J. Colloid Interface Sci.* **157**, 426 (1993).

9. Yotsumoto, H., and Yoon, R. H., *J. Colloid Interface Sci.* **157**, 434 (1993).

10. Xu, Z., and Yoon, R.-H., *J. Colloid Interface Sci.* **132**, 532 (1989).

11. Xu, Z., and Yoon, R.-H., *J. Colloid Interface Sci.* **134**, 427 (1990).

12. Yoon, R. H., *Proceedings of XVII Int. Mineral Processing Congr*. Dresden, Germany, **II**, 17(1991); *LES Techniques*, Dec. 74 (1992).

13. Schimmoller, B. K., Luttrell, G. H., and Yoon, R.-H., *Proceedings of the Engineering Foundation Conference on Dispersion and Aggregation* March, (1992).

14. Schimmoller, B.K., Luttrell, G. H., and Yoon, R.-H., *Proc. VXII Int. Mineral Processing Congr* Sydney, Australia, May 23-28, **3**, 751 (1993).

15. Yoon, R. H., and Ravishankar, S. A. *J. Colloid Interface Sci.* **179**, 403(1996).

16. Yoon, R. H., and Ravishankar, S. A., *J. Colloid Interface Sci.* **179**, 391(1996).

17. Yoon, R. H., and Luttrell, G. H., Development of the Selective Hydrophobic Coagulation Process, Seventh Quarter Technical Progress Report, Contract No. DE-AC22-91PC91164, June, 1993; Ravishankar, S.A. and Yoon, R.H., Langmuir, to be submitted as a letter to the Editor.

18. Rabinovich, Y., and Yoon, R. H., *Langmuir* **10**, 1903 (1994).

19. Derjaguin, B. V., and Duhkin, S. S., *Trans. Inst. Min. Metall*. **70**, 221 (1961).

20. Derjaguin, B. V., and Duhkin, S. S., *Proceedings 13 Int. Mineral Processing Congr*. **2**, 21 (1969).

21. Laskowski, J. S., and Kitchener. J. A., *J. Colloid Interface Sci*. **29**, 670 (1969).

22. Blake, T. D., and Kitchener, J. A., *J. Chem. Soc., Faraday Trans I* **68**, 1435 (1972).

23. Israelachvili, J. N., and Pashley, R., *Nature* **300**, 341 (1982).

24. Pashley, R. M., McGuiggan, P. M., Ninham, B. W., and Evans, D. F., *Science* **229**, 1088 (1985).

25. Claesson, P. M., Blom, C. E. Herder, P. C., and Ninham, B. W., *J. Colloid Interface Sci*. **114**, 234 (1986).

26. Tsao, Y., Yang, S. X., and Evans, D. F., *Langmuir* **7**, 3154 (1991).

27. Rabinovich, Y. I., and Derjaguin, B. V., in "Proceedings, 5th Hungarian Conference on Colloid Chemistry." Loránd Eötvös University, Budapest, Hungary, 1988.

28. Yoon, R. H., and Yordan, J. L., *J Colloid and Interface Sci*. **146**, 565 (1991).

29. Varbanov, R., Forssberg, E., and Hollin, M., *Int. J. Miner. Process*. **37**, 27(1993).

30. Pan, R., Paulsen, F. G., Johnson, D. A., Bousfield, D. W., and Thompson, E. V., *TAPPI J*. **79**, 177(1996).

31. Paulsen, F. G., Pan, R., Bousfield, D. W., and Thompson, E. V., *J. Colloid Interface Sci*. **178**, 400(1996).

32. Wang, L. H., Lee, F. G., and Hayes, P., *ISIJ International* 36, 7(1996).

33. Yoon, R-H., Mao, L., *J. Colloid Interface Sci*. **181**, 613(1996).

34. Pugh, R. J., and Yoon, R. H., *J. Colloid & Interface Sci*. **163**, 169 (1993).

35. Tchaliovska, S., Manev, E., Radoev, B., Eriksson, J. C., and Claesson, P. M., *J Colloid & Interface Sci*. **168**, 190 (1994).

36. Aksoy, B. S., "Hydrophobic Forces in Free Thin Films of Water in the Presence and Absence of Surfactants", Ph. D. Thesis, Dept. of Mining Minerals Eng., Virginia Polytechnic Institute and State University, 1997.

37. Sutherland, K. L., *J. Phys. Chem*. **52**, 394 (1948).

38. Tomlison, H. S. and Fleming, M. G., *Proc. VI Int. Mineral Processing Congr*. 563 (1963).

39. Morris, T. M., *Trans, A.I.M.E*. **193**, 794(1952).

40. Reay, D. and Ratcliff, G. A., *Canada. J. Chem. Engng*. **53**, 481(1975).

41. De Bruyn, H. J. and Modi, H. J., *Trans. A.I.M.E*. **205**, 415(1956).

42. Woodburn, E. T. and Loveday, B. K., *J. South African I.M.M*. **65**, 612(1965).

43. Flint, L. R., *Miner. Sci. Engng.* **5**, 232(1973).

44. Collins, G. L. and Jameson, G. J., *Chemical Engineering Sci*. **31**, 985(1976).

45. Fichera, M. A. and Chudacek, M. W., *Min. Eng*. **5**, 41(1991).

46. Rasemann, W., *Int. J. Miner. Process*. **24**, 247(1988).

47. Kirjavainen, V. M., *Int. J. Miner Process*. **27**, 63(1989).

48. Luttrell, G. H., Hydrodynamic Studies and Mathematical Modeling of Fine Coal Flotation, Ph. D. thesis, Dept. of Mining Eng., Virginia Polytechnic Institute and State University, 1986.

49. Yoon, R.-H, and Luttrell, G. H., *Mineral Processing and Extractive Metallurgy Review*, J. S. Laskowski, ed., Gordon and Breach Science Publishers, Ltd., New York, **5**, 101 (1989).

50. Luttrell, G. H., and Yoon, R.-H., *Journal of Colloid and Interface Sci*. **154**, 129 (1992).

51. Weber, M. E., and Paddock, D., *J. Colloid & Interface Sci*. **94**, 329 (1983).

52. Luttrell, G. H., and Yoon, R.-H., in Proceedings, Engineering Foundation Conference, "Beneficiation of Phosphate: Theory and Practice", Palm coast, FL. Dec., 1993.

53. Yoon, R.-H., and Luttrell, G. H., *Coal Preparation* **2**, 179 (1986).

54. Yoon, R.-H., Adel, G. T., Luttrell, G. H., Mankosa, M. J., and Weber, A. *T.*, in *Interfacial Phenomena in Biotechnology and Materials Processing*, Eds. Attia, Y. A., Moudgil, B. M., and Chander, S., Elsevier, Amsterdam (1988).

55. Weiss, T., and Schubert, H., *Proc. XVI Int. Mineral Processing Congr*. **Part A**, 807 (1988).

56. Derjaguin, B. V., *Trans. IMM* **70**, 569(1960).

57. Fuerstenau, D. W., *Trans. AIME* **208**, 1365(1957).

58. Hogg, R., Healy. T. W., and Fuerstenau, D. W., *Trans. Faraday Soc*. **300**, 1638 (1965).

59. Rabinovich, Y. I., and Churaev, N. V., *Colloid J. USSR* **41**, 1146 (1979).

60. Laskowski. J. S., *Mineral Processing and Extractive Metallurgy Review*, J. S. Laskowski, ed., Gordon and Breach Science Publishers, Ltd., New York, **5**, 25 (1989).

61. Laskowski, J., Xu, Z., and Yoon, R.-H., *LES Techniques* Dec., **95** (1992).

62. Spedden, H. R. and Hannan, W. S., *Tech. Publ. Am. Inst. Min. Engrs.* 2354(1948).

63. Philippoff, W., *Min. Engng*. N.Y., **4**, 386(1952).

64. Brown, D. J., Aerodynamic capture of particles, Pergamon Press, 35(1960).

65. Kirchberg, H. and Töpfer, E., in Proceeding of 7th IMPC, New York, 157(1964).

66. Nutt, C. W., *Chem. Engng Sci*. **12**, 133(1960)

67. Schulze H. J., Wahl, B. and Gottschalk, G., *J. Colloid Interface Sci*. **128**, 57(1989).

68. Nishkov, I. And Pugh, R. J., *Int. J. Mineral Process*. **25**, 275(1989).

69. Schultz, H. J., Physico-chemical elementary processes in flotation, Amsterdam, Elsevier, 384(1984).

70. Holtham P. N. and Cheng, T., *Mineral Processing & Extractive Metallurgy* **100**, 147(1991).

71. Goren, S. L., and O'Neill, M. E., *Chem. Eng. Sci*. **26**, 325 (1971).

72. French, R. H., and Wilson, D. J., *Separ. Sci. Technol*. **15**, 1213 (1980).

73. Schlichting, H., Boundary Layer Theory, McGraw-Hill, New York, (1968).

74. Fair, G. M., Geyer, J. C., and Okun, D. A., Water and Wastewater Engineering, Vol. II. Wastewater Treatment and Disposal, Wiley, New York, (1968).

75. Bird, R. B., Stewart, W. E., and Lightfoot, E. N., Transport Phenomena, Wiley, New York, (1960).

76. Clarke, A. N., and Wilson, D. J., Foam Flotation: Theory and Application, Marcel Dekker, Inc. New Yory and Basel, (1983).

77. Laskowski, J., and Kitchener, J. A., *J. Colloid Interface Sci.* **29**, 1650 (1988).

78. Blake, P., and Ralston, *J. Colloids Surf.* **15**, 108 (1985).

79. McCabe, W. L., and Smith, J. C., Unit Operations of Chemical Engineering, 3rd Edition, McGraw-Hill Book Company, New York, N. Y.

80. Kubota, K., Hayashi, S. and Inaoka, M., *J. Colloid Interface Sci*. **95**, 362(1983).

81. Kubota, K. and Jameson, G. J., *J. Chemical Eng. Of Japan* **26**, 7(1993).

82. Yordan, J., Ph. D. Thesis, Studies on the Stability of Thin Films in Bubble-Particle Adhesion, Dept. of Mining Eng., Virginia Polytechnic Institute and State University, 1989.

83. Israelachvili, J. N., "Intermolecular and Surface Force" Academic Press (1985).

84. Flinn, D., Ph. D Thesis, Modeling Bubble-Particle Interactions in Flotation Using Hydrophobic Solid Surfaces, Dept. of Mining Eng., Virginia Polytechnic Institute and State University, 1996.

85. Derjaguin, B. V., and Kussakov, M., *Acta Physico-Chim. U.R.S.S.* **10**(1), 26 (1939).

86. Vrij, A., *J. Colloid Sci*. **19**, 1(1964).

87. De Vries, A. J., Foams Stability, Rubber Stitching, Delft. Comm. No 326(1957).

88. Kashchiev, D., and Exerowa, D., *J. Colloid Interface Sci*. **77**, 501(1980).

89. Wills, B. A, Mineral Processing Technology 4th Ed., Pergamon Press, New York (1988).

90. Yoon, R. H., *Minerals Engineering* **6**, 619 (1993).

91. Stone, R. G., Brake, I. R., and Eldridge, G., *Proc. 7th Australia Coal Preparation Conference*, Mudgee, Paper **C3**, 145 (1995).

92. Klimpel, P. R., AIME annual Meeting, Las Vegas, Nevada, Preprint 80-34 (1980)

CHAPTER 3: SIMULATION OF FLOTATION PROCESS

3.1 Introduction

In the froth flotation process, hydrophobic particles are separated by floating them to the top of a liquid suspension with air bubbles, while particles that are naturally hydrophilic, or are rendered so by means of suitable treatment, remain in the liquid and are drained out. This techniques has been used in industries for over 100 years to separate a variety of minerals from ore pulps in the production of metals and in the purification of substances such as quartz, mica, phosphates, etc. Traditionally, flotation is also used to recover fine coal, but the emphasis of recent application has been on coal beneficiation in a view of removing pyrite and other minerals from coal. The more and more strict environmental requirements have lent much impetus to the optimization of design and operation of a coal flotation that would make fine coal desulfurization economically feasible on a large scale. An essential requirement for such an optimization is the availability of the mathematical model that can predict the performance based on the parameters in the flotation system.

The fundamental mechanism of flotation is attaching hydrophobic particles to air bubbles. To model this process, it is necessary to understand both hydrodynamic and hydrophobic forces involved. Many of the models developed in the past were successful in incorporating the hydrodynamic forces created both under turbulent and quiescent conditions (1-4). However, it was proved to be more difficult to incorporate the effects of surface forces in the model, mainly due to the lack of information in quantifying the magnitudes of attractive forces.

Derjaguin and Duhkin (5, 6) were the first to use the surface forces to model bubble-particle interactions. However, they only considered the electrostatic and van der Waals forces, which forms the basis of classic DLVO theory (7-10). Neither of these two forces is attractive when both the bubbles and particles are charged negatively, as is often the case in flotation practice. This situation leaves one with a bubble-particle adhesion model without a driving force. It was not until 1982 when Israelachivili and Pashley (11) measured attractive forces between hydrophobized mica surfaces that the possibility of modeling bubble-particle interactions began to emerge (12-20). These authors measured the attractive force, which was appropriately named *hydrophobic force*, that was 10 times larger than the van der Waals force. Many investigators subsequently reported the measurement of stronger hydrophobic forces using the surface force apparatus (SFA) and atomic force microscope (AFM) (21-27). Although its origin is still being debated, there seems to be unequivocal evidence for the existence of hydrophobic forces.

A series of work conducted at Virginia Tech (12, 14) showed promising results for modeling bubble-particle interactions by incorporating hydrophobic forces. The first-order flotation rate equation derived in the previous chapter is the consequence of these researches which for the first time combined both hydrodynamic and surface forces in a single analytical expression. In this chapter, the equation has been used to predict flotation rates as functions of some of the important variables such as contact angle, which is the traditional measurement of the hydrophobicity of minerals, electrical double-layer potentials (or ζ-potentials) of the particles and bubbles, and bubble size. An advantage of the flotation rate model based on first principles is that it can not only predict the results of changing variables but also provides mechanistic interpretations for the results.

3.2 Parameters in Bubble-Particle Interactions

The operating characteristics of a flotation system depend on many independent physical and chemical aspects in a complex manner. Huber-Panu et al stated that (28), a complete model should account for the following factors on which the performance of a flotation process depends: (a) those that are determined by the feed ore, flotation reagents and steps of ore preparation prior to application of flotation, (b) those that are determined by the design of the flotation process, i.e., the mixing and aeration characteristics of the machine, and (c) the pulp transport characteristics. Lynch et al (29) gave a taxonomy of the different variables, and classified the independent variables into two categories: manipulated variables (e.g., air addition, pulp levels, reagent addition, etc.) and disturbance variables (e.g., degree of oxidation, head grade, etc.). They also classified the dependent variables into two categories: performance variables of the final product (e.g., grade, recovery, flow rate, pulp density, etc.) and performance variables of the intermediate product of a similar nature contained in the rougher and scavenger concentrate. Dowling et al (30) considered the flotation system as giving a response that for a given ore is related to three factors: chemical, equipment and operation as shown in Figure 3.1. A change in any one of these factors may result in a change in the overall flotation response. However, these factors are all closely related to the hydrodynamics and surface chemistry properties of the flotation system which are usually included in the fundamental flotation model. For a specific ore, these relationships can be determined empirically based on the experimental results. In present work, the parameters included in the flotation model instead of the factors shown in the Figure 3.1 were considered as the variables in order to obtain more general results of simulation.

The flotation rate equation derived in the previous chapter gives:

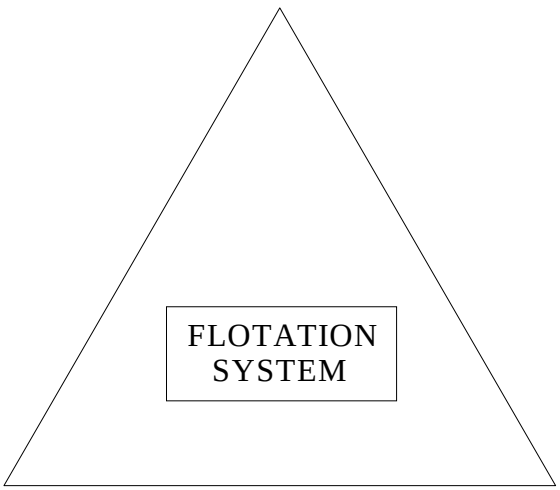

Figure 3.1. Process of flotation illustrated as a three-cornered interactive system (30).

$$k = \frac{1}{4} S_b P_c P_a (1 - P_d)$$
$$= \frac{1}{4} S_b \left[\frac{3}{2} + \frac{4\,\mathrm{Re}^{0.72}}{15} \right] \left(\frac{R_1}{R_2} \right)^2 \exp\left(-\frac{E_1}{E_k} \right) \left\{ 1 - \exp\left[-\frac{\gamma_{lv} \pi R_1^{\,2} (1 - \cos\theta)^2 + E_1}{E_k'} \right] \right\} \quad [3.1]$$

This equation will be used in the simulation to determine the rate constant *k* as a function of different hydrodynamics and surface chemistry parameters involved in the flotation system, which are shown in Figure 3.2. From the detail expressions for the parameters in Eq. [3.1], it can be seen that, the hydrodynamics of the system determines S_b and all three probabilities, while the surface chemistry properties only affect P_a and P_d.

However, some of parameters shown in Figure 3.2, such as densities ρ_1 , ρ_2 , ρ_3, are usually constants, they can not be changed by operation factors. Some of them, such as electrolyte concentration *C*, may affect other parameters, but their relationships, which are necessary for simulation, are not available now, as discussed in following section. Therefore, in present simulation, only several important parameters were examined one by one to determine their influences on the flotation rate constant *k*, while the others are kept constant.

3.3 Simulations with Varying Parameters

3.3.1 Effect of Surface Potential

As mentioned earlier, there are two repulsive forces in bubble-particle interaction, double layer force and van der Waals dispersion force. Usually, the dispersion force is relatively weak when the electrolyte concentration is not very high, thus the repulsive force is primarily dependent on the double layer force which is mainly determined by the

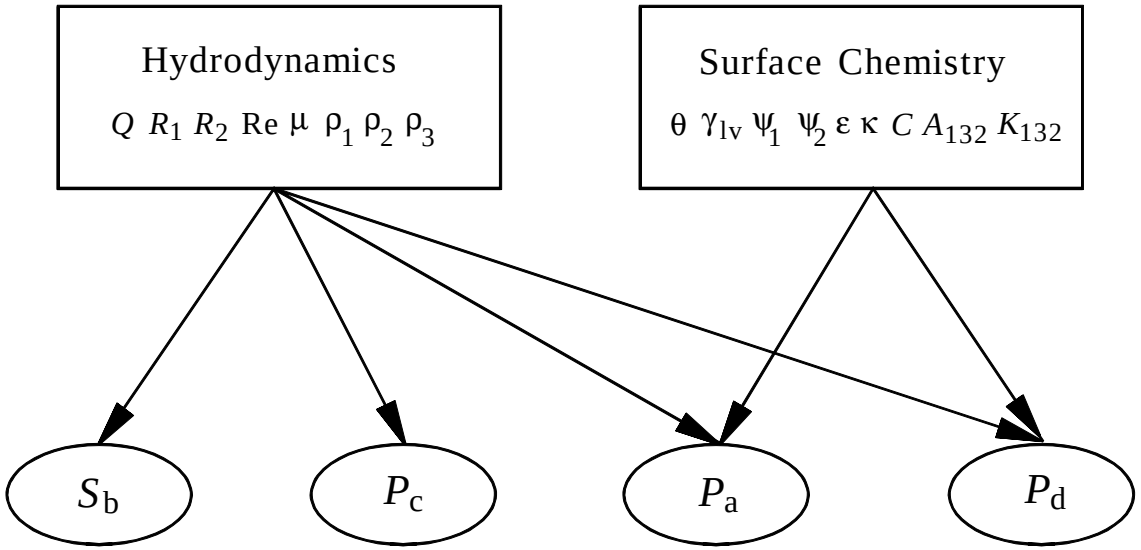

Figure 3.2. Effects of hydrodynamics and surface chemistry parameters on the components of rate constant.

surface potential. Fig 3.3 shows plots of rate constant (k) vs. the surface potential (Ψ_1) of particles at two different K_{132} values, while keeping other parameters of the equation constant as follows: ψ_1=-60 mV, ψ_2=-30 mV, R_1=20 μm, R_2=500 μm, and A_{132}=-1.0x10^{-20} J, where the subscripts **1**, **2** and **3** refer to particle, bubble and water, respectively. The calculation was carried out at S_b=1.53 min^{-1} in order to compare the values of k with the single bubble flotation test, and γ_{lv} is 72.6 dyne·cm.

At K_{132}=1×10^{-19} J, k increases sharply with decreasing magnitudes of Ψ_1. This can be explained by the decrease in repulsive electrostatic energy (V_e). (Note here that the calculations were carried out for the case of both bubbles and particles being negatively charged.) A decrease in V_e results in a decrease in E_1, as shown in Figure 3.4, which in turn increases P_a and, hence, k. The increase in k tapers off significantly when the magnitude of Ψ_1 is less than 20 mV. In this case, the change in Ψ_1 does not affect E_1 significantly, because the contribution from V_e to V is relatively small. The increasing of the rate constant with decreasing magnitude of the surface potential of particles has been recognized in many experiments (31-35), demonstrating that the double layer force plays an important role in flotation.

The results obtained with a more hydrophobic mineral particle, i.e., K_{132}=2×10^{-19} J, show the same trend. However, the k values are substantially higher than those of the less hydrophobic particles. This is consistent with experience, and can be explained by a decrease in E_1 with increasing K_{132}. However, the effect of the surface potential of particles becomes less significant, which is due to the fact that the increasing of the attractive force reduces the relative contribution of the double layer force to the total energy. It may be expected that, if K_{132} is further increased, eventually k will become a constant. Therefore, to achieve better flotation results by controlling the surface potential of both particle and bubble is effective only when K_{132} is relatively low.

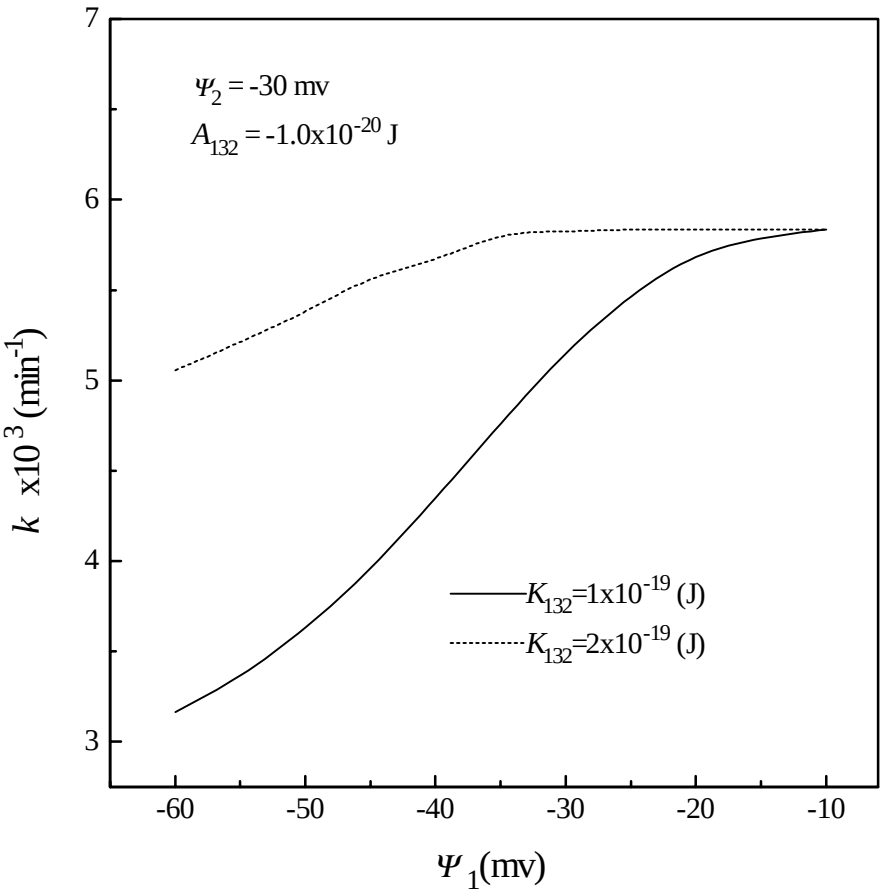

Figure 3.3. Effects of ψ_1 on k at two different K_{132} values, as predicted from Eq. [3.1]. Other parameters used for the calculation were as follows: R_1=20μm, R_2=500 μm, S_b=1.53 min^{-1} and γ_{lv}=72.6 dyne·cm.

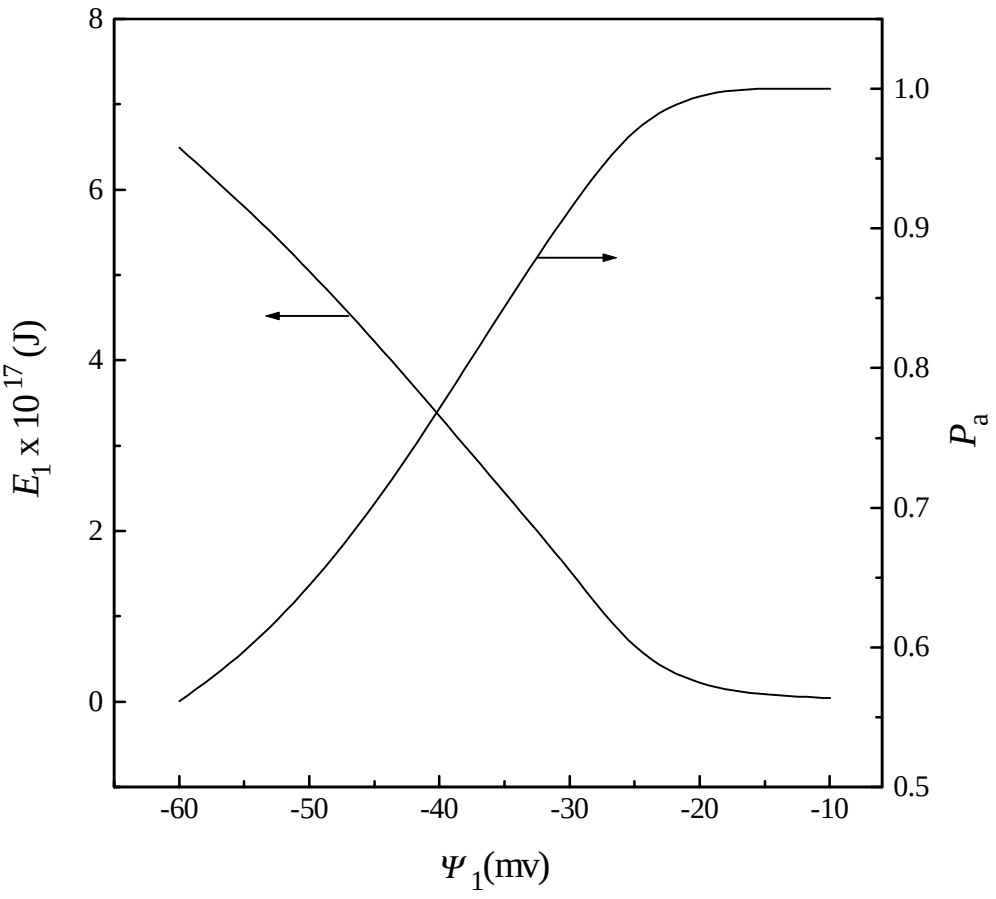

Figure 3.4. Effects of the surface potential on the activation energy E_1 and the probability of attachment P_a.

It is interesting to note that the two minerals with different hydrophobicities show larger differences in k values when the magnitudes of Ψ_1 of the two minerals are large. This finding suggests that the flotation selectivity can be maximized when the magnitudes of Ψ_1 are maximum values. This is probably the reason why many sulfide minerals are floated at alkaline pH. The flotation results of chromite reported by Sysilä et al (36) shows that, when the difference of Zeta-potentials between chromite and gangues decreases, the flotation selectivity is deteriorated. This is consistent with current simulation results.

There is the maximum value of rate constant which is independent on the surface potential and hydrophobic force parameters. In this case, the activation energy $E_1 = 0$, P_a is unity, the hydrodynamic condition may play more important role than surface forces.

3.3.2 Effect of Hydrophobic Force Parameter

The values of K_{132} represent the magnitudes of hydrophobic interactions between particles and air bubbles. Usually, when the surfactant concentration in the solution is not very high and the hydrophobicity of bubble surface is not changed obviously, K_{132} is mainly dependent on the hydrophobicity of the solid surface. Figure 3.5 shows the effect of K_{132} on the rate constants for two particle sizes. Generally, the rate constant of 40 μm particles is larger than that of 10 μm particle, which is consistent with the experimental results reported by Blake and Ralston (37), and clearly attributed to the higher kinetic energy of the larger particles. It can be seen that, with the increasing of the K_{132}, the rate constant (k) is increased slowly first, and then obviously after K_{132} reaches 5×10^{-21} J which is independent on the particle size. When K_{132} is larger than 3×10^{-19} J, k approaches a constant which is clearly a function of particle size.

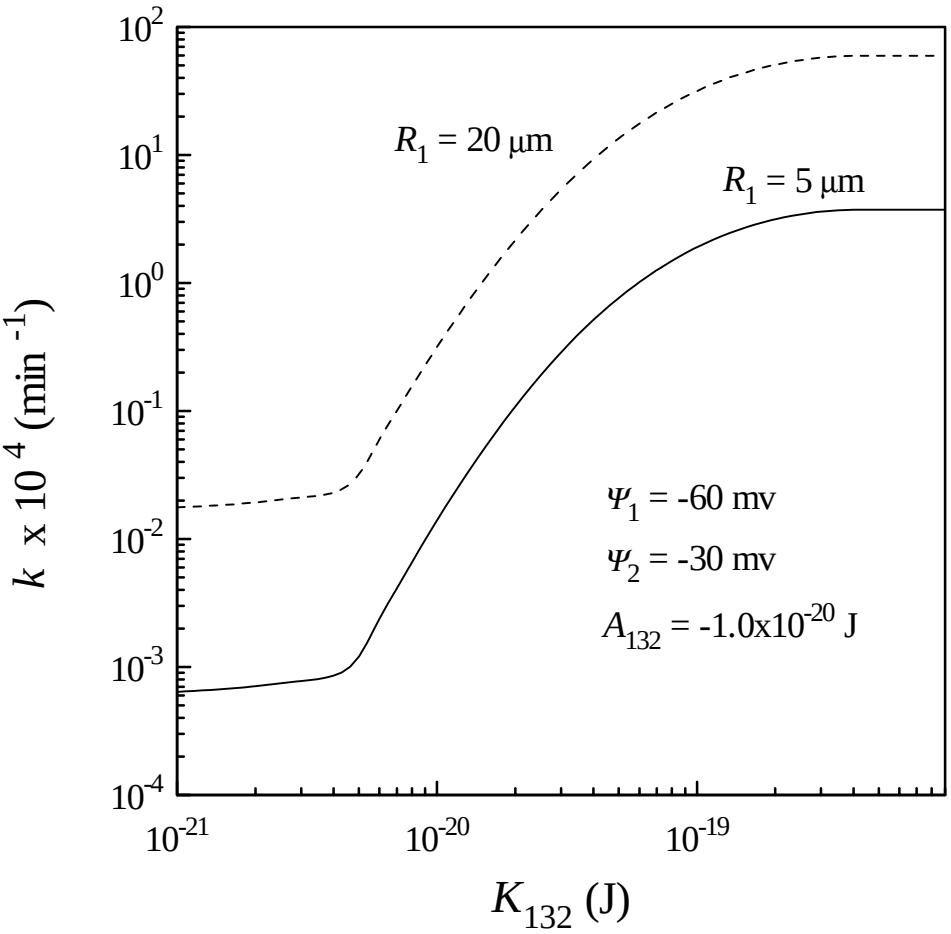

Figure 3.5. Effects of K_{132} on k at two different particle sizes, as predicted from Eq. [3.1]. Other parameters used in the calculations were same as in Figure 3.3.

There is a critical value of K_{132} at which the rate constants of all particles begin to significantly increase. This value is independent on the particle size, when K_{132} is increased beyond this certain value, the flotabilities of all particles are obviously enhanced. Similar "cut-off" values was found in flotation tests performed with methylated quartz particles (37), and now can be explained by the energy changes in the flotation system, as discussed in the following discussion.

Figure 3.6 demonstrates the changing of the total energy curves with increasing K_{132}. Obviously, larger K_{132} means stronger hydrophobic attractive force which decreases the activation energy (E_1). On the other hand, increasing K_{132} results in a larger critical thickness (H_c), and thus the kinetic energy between bubble and particle (E_k) is increased. These two energy changes, as shown in Figure 3.7, enhance the flotation rate. When K_{132} is larger than 3×10^{-19} J, because E_k is much higher than E_1, the probability of adhesion P_a is close to unity, in these cases, the rate constant is determined by hydrodynamics of the flotation system which is clearly related to the particle size.

3.3.3 Effect of Contact Angle

K_{132} indeed represents the hydrophobic force between bubble and particle, however, it is difficult to be determined experimentally. Optical film thickness and ellipsometric measurements are two traditional techniques to examine the interactions between bubble and particle (38-44). Recently, Atomic Force Microscope (AFM) is used to study the wetting film, and considered as one of the most perspective techniques for direct measurement of bubble-particle interaction (45-48), but the difficulties involved still exist in the experiment. Since the surface area of the particle is very small and a bubble must be introduced, it is almost impossible to keep the entirely system

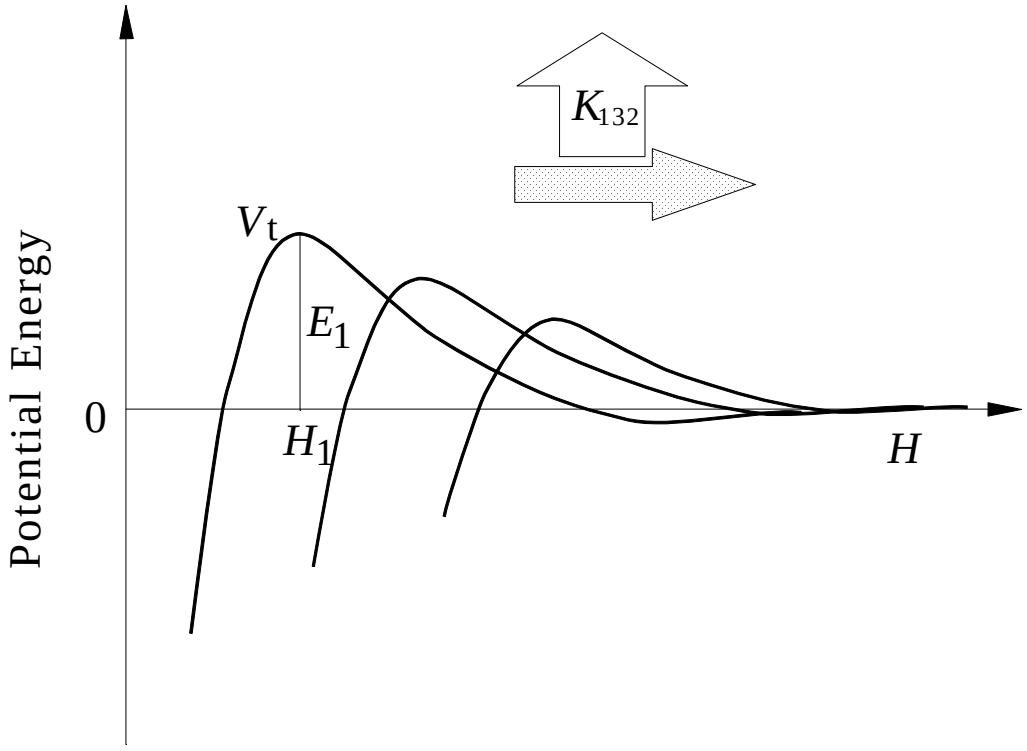

Figure 3.6. Changing of the total interaction energy with increasing of K_{132}.

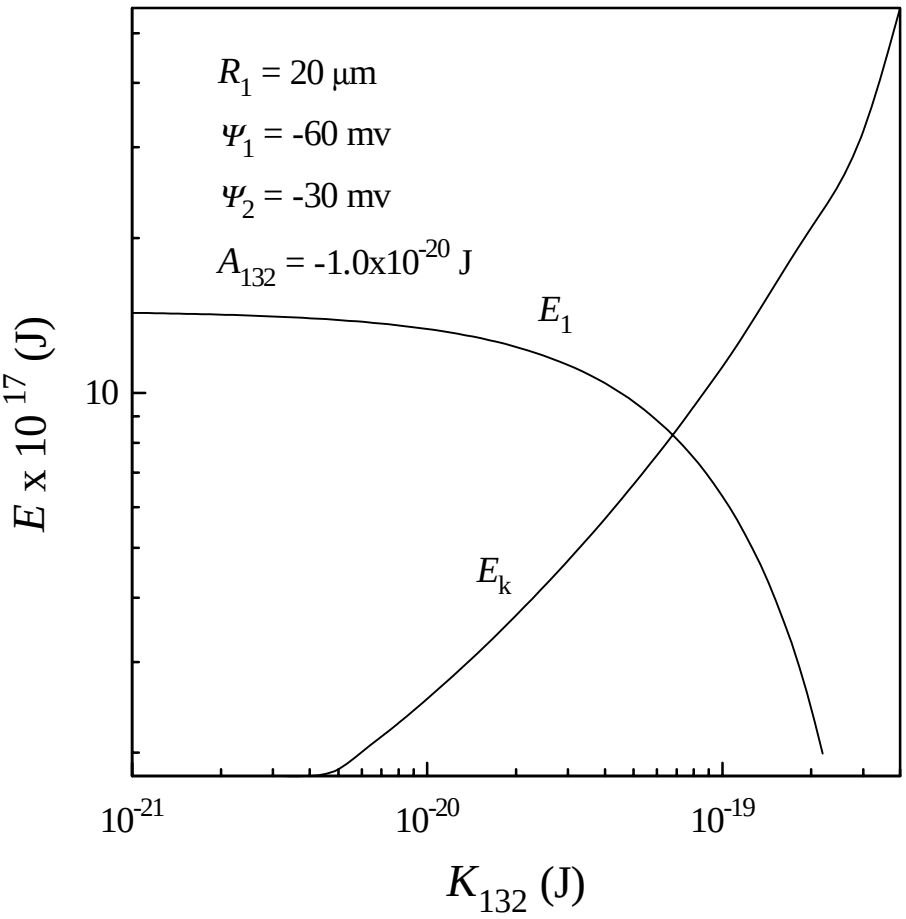

Figure 3.7. Effect of K_{132} on E_1 and E_k.

contaminant free (45, 46), that is one of the weaknesses of the colloid probe techniques, different people may obtain different results even for the same system. In addition, the heterogeneous properties of the particle surface or the deficiencies of the silanation reagents used may cause unexpected interaction between bubble and particle which makes it difficult to analyze the experimental results (47). Also, it has been shown that (45), sometimes not only the particle snapped into the bubble but also part of the cantilever followed, which gives force-versus-distance curves with a variety of shapes. The problem becomes more complicated in the experimental results reported by Fielden *et al* (47), they showed a clear dependence on loading force, which may suggests that the hydrodynamic force is not always ignorable.

The deformation of bubble surface remains a problem to be solved, which makes it very difficult, if not impossible, to determine the absolute distance between bubble and particle (46), therefore the force curves obtained experimentally is hard to be fitted with a DLVO theory. The origin of the hydrophobic force between bubble and particle is still being debated, many experimental results support the "cavitation" mechanism, in these cases, the "jump" distance varies widely, as observed by Ducker *et al*. (46). Since it is almost impossible to get ride of the dissolved gas, the result is dependent on how to prepare solution between bubble and particle (49).

The difficulties involved in the direct force measurement of bubble-particle interaction make it inconvenient to use K_{132} in practice. An alternative of K_{132} is contact angle, which has been traditionally used to represent the hydrophobic force. In most cases, higher water contact angle indicates better hydrophobicity, and thus higher recovery of minerals may be achieved. One important reason to use contact angle in practice is that it is very convenient to be determined experimentally. However, contact angle only reflects the property of mineral surface, while according to Aksoy's investigations, the surface property of bubbles may also play an important role in bubble-particle interaction especially when the concentration of surfactant is high. Nevertheless,

the investigation of the effect of contact angle on the rate constant requires the relationship between K_{132} and contact angle, unfortunately this relationship is not available now.

A indirect way to connect K_{132} to contact angle is based on the combining rule represented by (15, 50):

$$K_{132} = \sqrt{K_{131} \cdot K_{232}}\ , \qquad [3.2]$$

where K_{131} and K_{232} are the hydrophobic force parameters for solid/solid and bubble/bubble interactions respectively. Figure 3.8 shows the relationship between K_{131} and contact angle obtained from the direct force measurements conducted with mica surfaces in equilibrium with DAH and neutral surfactants (51). The values of K_{232} were determined by Aksoy (52) using the thin film balance (TFB) of Sheludko-type as a function of surfactant concentration, as shown in Figure 3.9. At zero surfactant concentrations, the value of K_{232} is approximately 10^{-17} J. The data in these two figures can be used to calculate K_{132} as a function of the contact angle of solid surface with Equation [3.1], the results are shown in Figure 3.10. As expected, K_{132} increases with increasing contact angle due to better hydrophobicity of the solid surface. This relationship can be used in the simulation to investigate the effect of the contact angle on the flotation rate constant.

Fig. 3.11 shows rate constant as a function of θ, other parameters used for the calculation are the same as in Figure 3.3. As expected, k is shown to increase with increasing θ, which is consistent with the conventional wisdom and the experimental results reported in the literature (53). The increase in k with θ can be attributed to the increase in the attractive hydrophobic force, which in turn contributes to the decrease in the energy barrier (E_1) for bubble-particle adhesion, as shown in Figure 3.12. A decrease in E_1 results in an exponential increase in the probability of adhesion (P_a), and thus the

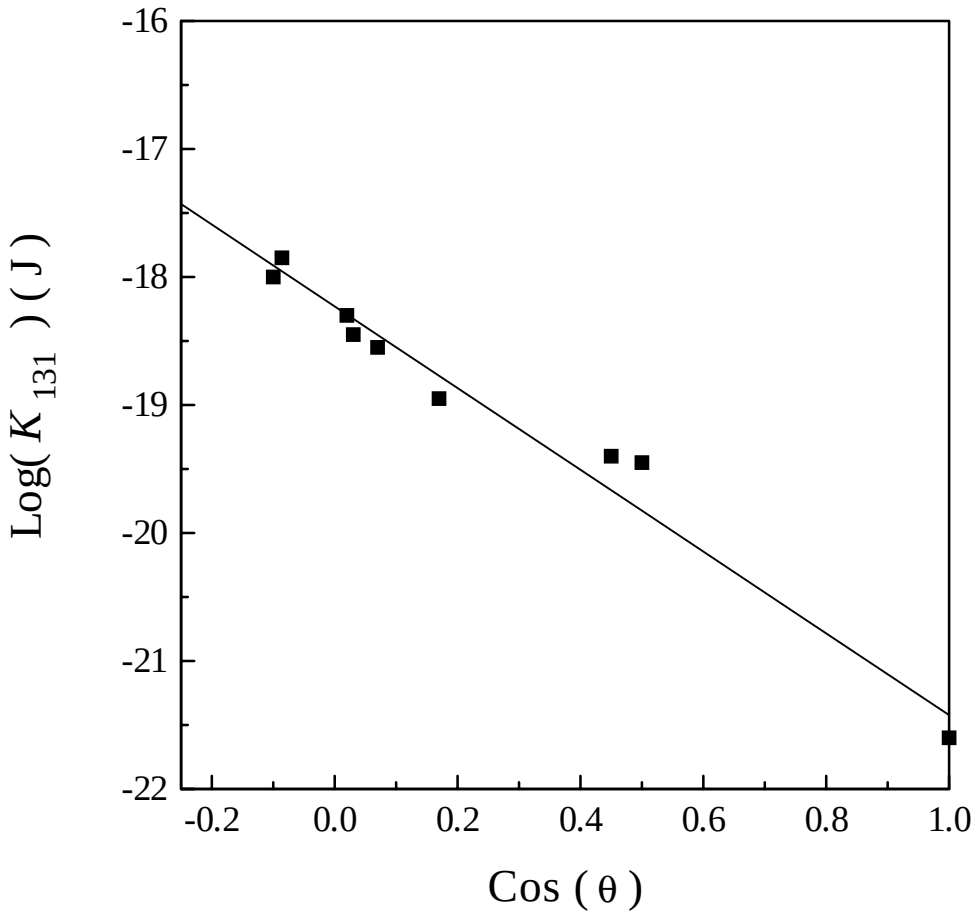

Figure 3.8. Hydrophobic force parameter as a function of contact angle. From reference (51).

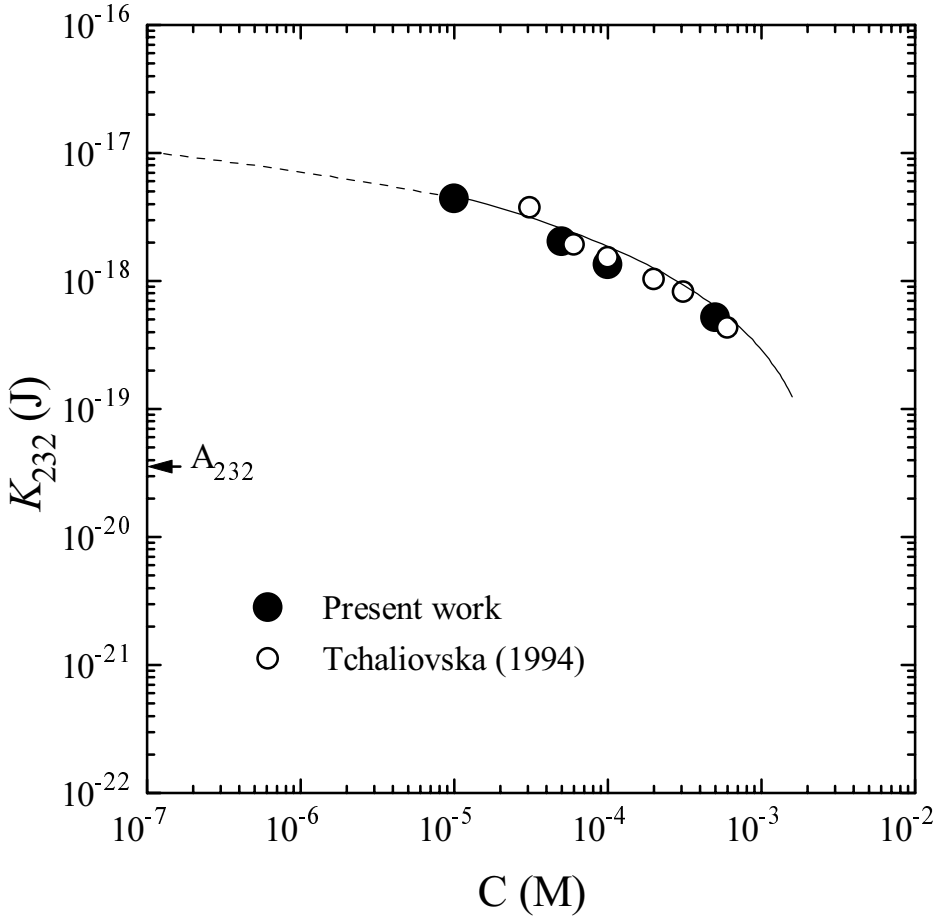

Figure 3.9. The values of K_{232} for free film in the presence of DAH as calculated using the extended DLVO theory. From reference (52).

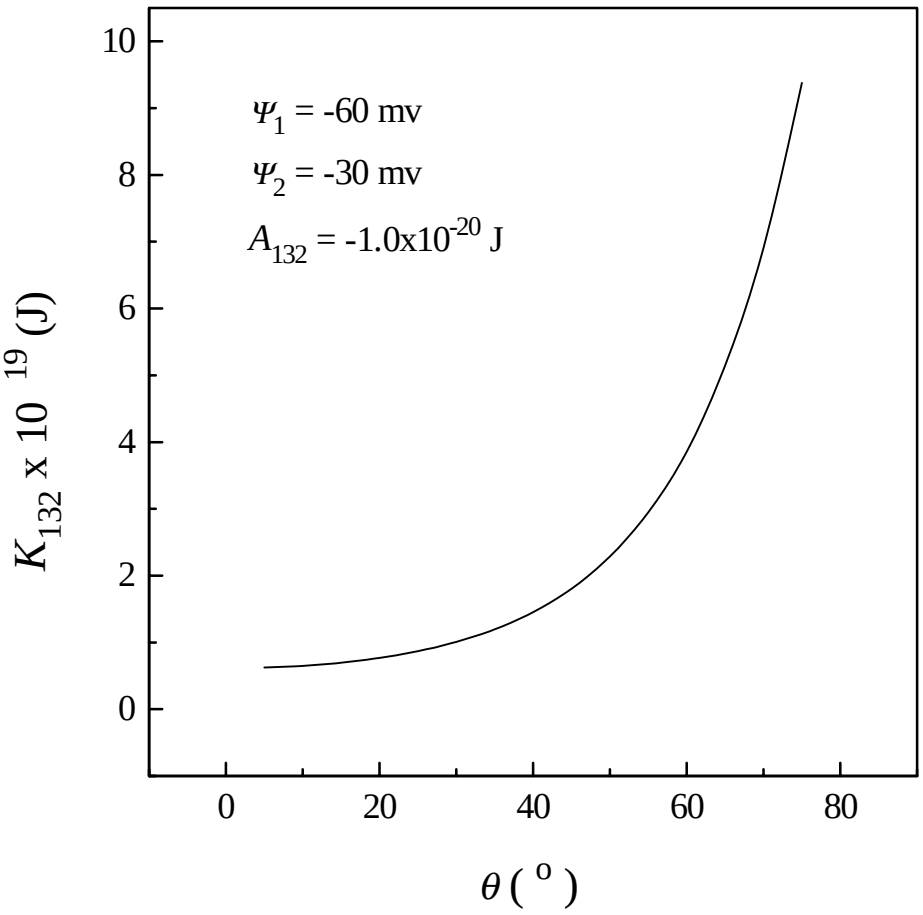

Figure 3.10. Effect of contact angle on K_{132}.

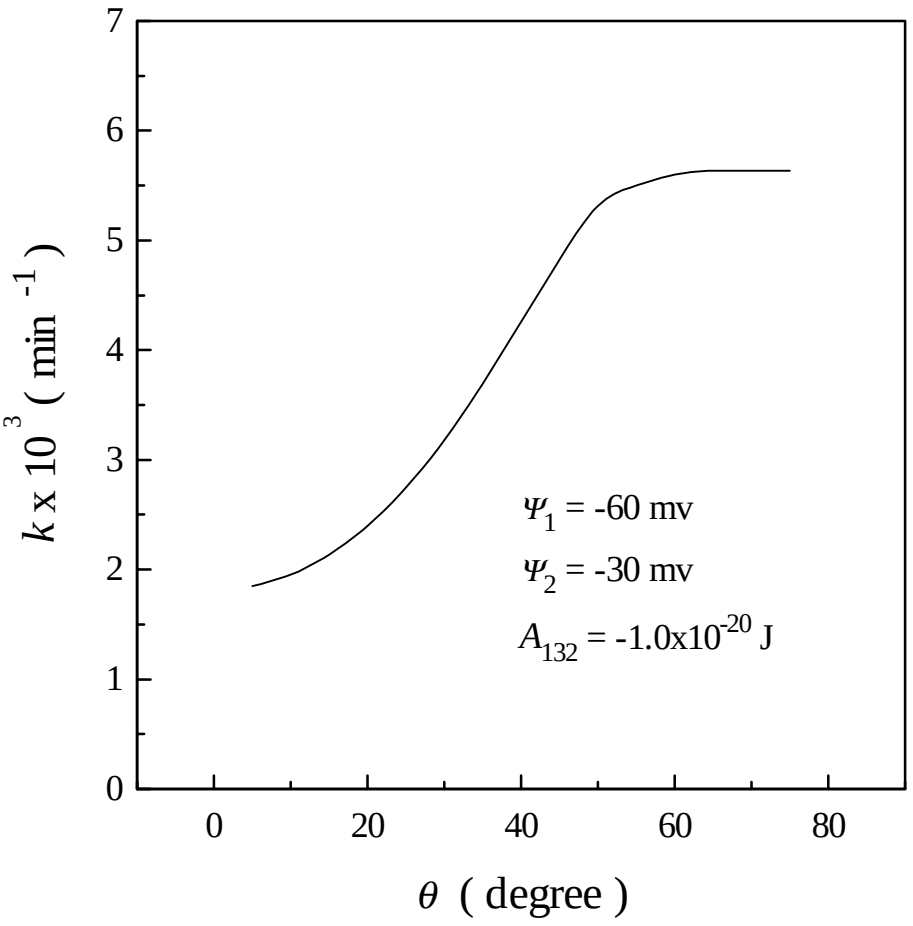

Figure 3.11. A k vs. θ plot obtained using Eq. [3.1]. Other parameters used for the calculation were same as in Figure 3.3. At a given θ, a value of K_{132} was obtained from the values of K_{131} and K_{232} (=10^{-17} J) using the combining rule (Eq. [3.2]).

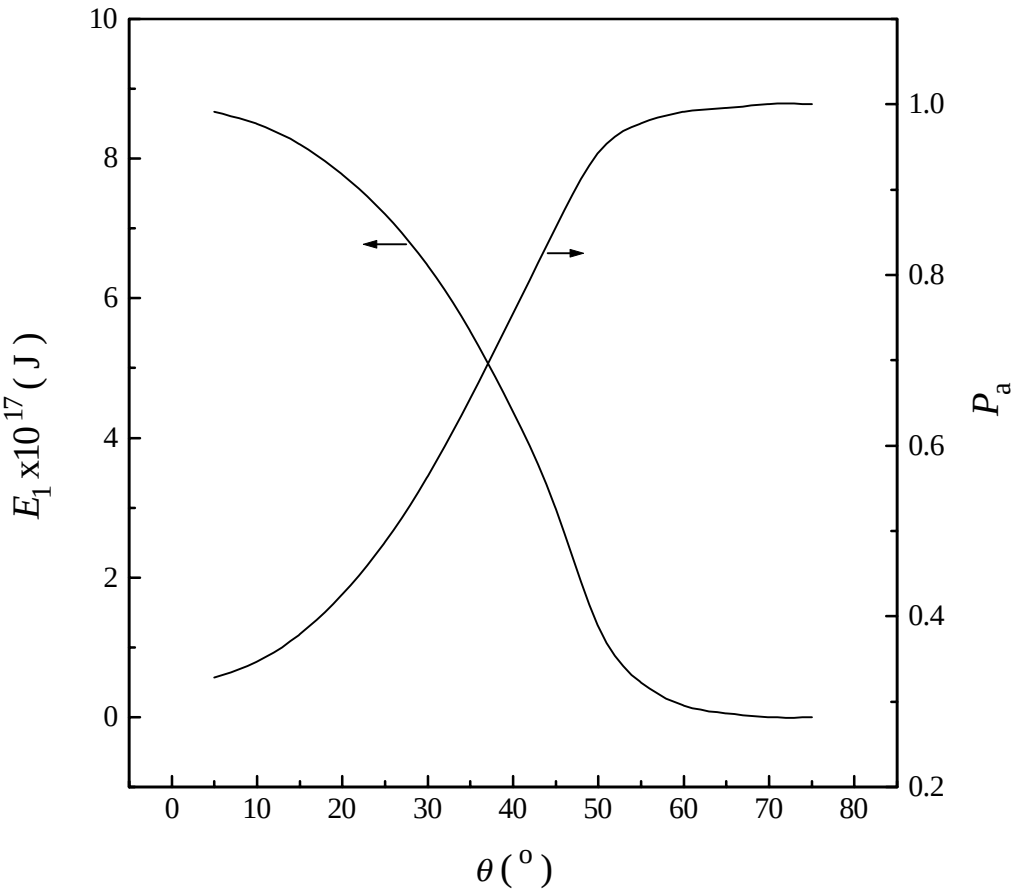

Figure 3.12. The values of E_1 and P_a as a function of contact angle θ.

rate constant is sharply increased as θ increases from approximately 20 to 50^o. After θ increases above 50^o, the increase in k tapers off significantly. In these cases, E_1 approaches zero and P_a does not increase any further.

It was shown that an increase in θ causes an increase in work of adhesion (W_a), which in turn results in a decrease in the probability of detachment (P_d) (see Eq. [3.1]). Therefore, the increase in k with θ should also be ascribed to the decrease in W_a and, hence, in P_d. However, the increase in k due to the decrease in P_d is relatively small for the particles of 20 μm radius considered in the present calculation. Nevertheless, the effect of decreasing P_d with increasing θ becomes significant at θ>50^o, where E_1 approaches zero. Thus, the small increase in k at θ>50^o can be attributed to the decrease in P_d with increasing θ. For larger particles, k should increase more significantly with increasing θ, as W_a varies as R_1^2. This is consistent with the industrial practice, in which coarse particle flotation is aided by the addition of mineral oils, whose role is to increase the particle hydrophobicity and, hence, increase the work of adhesion.

Figure 3.11 shows that k has a finite value, as θ approaches zero. This may seem contradictory to conventional wisdom, because it is generally viewed that flotation is not possible when θ is zero. The fact that Eq. [3.1] gives finite values of k at low values of θ may be explained as following. According to Eq. [3.2], K_{132} is given as a geometric mean of K_{131} and K_{232}. In the present work, the value of K_{232} is taken to be 10^{-17} J based on the thin film balance work reported by Aksoy (52). The value of K_{131} decreases with decreasing θ (51), but it is not likely that K_{131} becomes zero at low values of θ. In this case, K_{132} will have small but finite values, which will in turn result in large but finite values of E_1. This will give rise to finite values of P_a, according to Eq. [3.1], and hence small values of k.

3.3.4 Effect of Electrolyte Concentration

Figure 3.13 shows the effect of the electrolyte concentration on k at various surface potentials of particles (ψ_p). Other parameters used in the calculation are the same as in Figure 3.3. The results show that, with the increasing of the electrolyte concentration, the rate is decreased first and then increased, demonstrating a minimum value of k. This can be explained by the changes of E_1 and E_k. As shown in Figure 3.14, the presence of the electrolyte in the solution compresses the electrical double layer and reduces the double layer repulsive force, as the results, the critical thickness (H_c) is decreased, and both kinetic energy (E_k) and activation energy (E_1) are decreased. However, the magnitudes of these two energy decreasing are different, when the electrolyte concentration is relative lower, E_k reduces much more significantly than E_1, resulting in a decreasing of the rate constant. After the electrolyte concentration reaches a certain value, the decreasing of E_1 becomes dominative, which increases the rate constant.

Figure 3.13 also shows that, the effect of the electrolyte concentration is more significant when the surface potential of particles (ψ_p) is higher, which is clearly related to the more obvious reduction of the double layer force. In addition, the minimum value of k shifts to right with increasing ψ_1, which is due to the fact that, when ψ_p is higher, the stronger double layer force slows down the decreasing of E_1, thus higher electrolyte concentration is needed for the change of E_1 to be dominative.

Figure 3.15 shows the experimental results of the flotation of the silica particles with DAH as a collector. The results shows that, when DAH concentration is $1x10^{-5}$ M, there is a minimal value of rate constant, but when the concentration of DAH is $1x10^{-4}$ M, the minimal rate constant disappears. This is due to the fact that, the simulations were carried out based on a necessary assumption of a constant K_{132} at different electrolyte concentration. However, increasing the electrolyte concentration may also change the

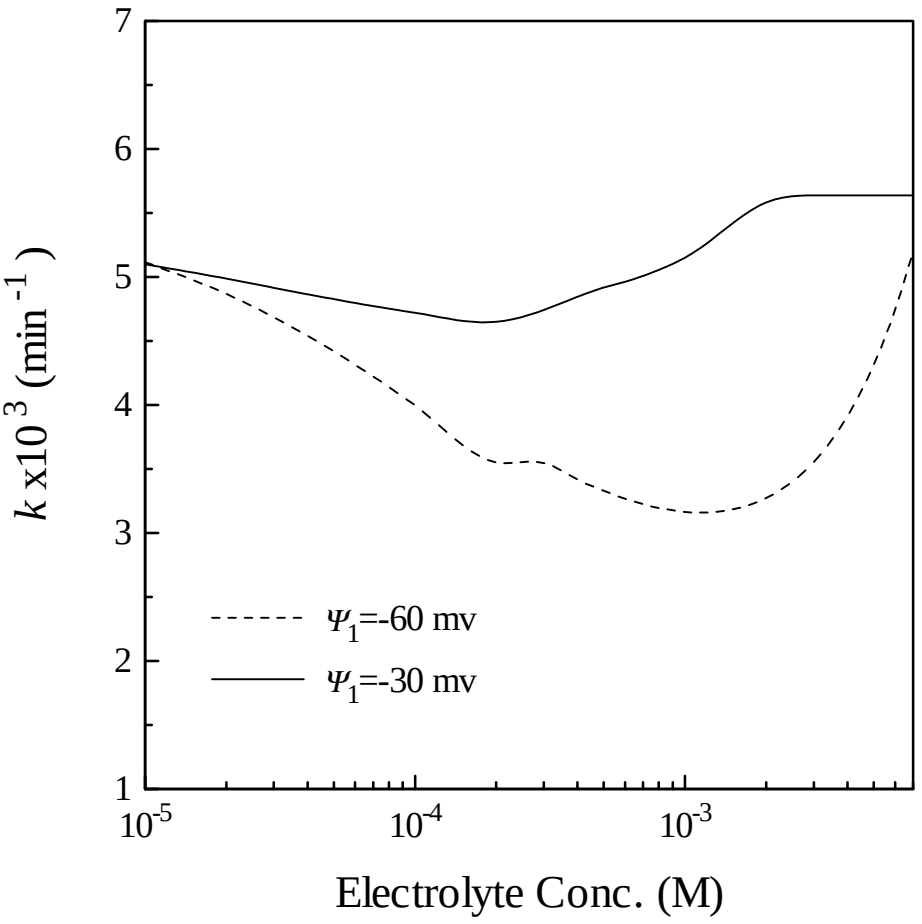

Figure 3.13. Flotation rate constant as a function of electrolyte concentration at two different potentials of particle. Other parameters used in the calculation were same as in Figure 3.3.

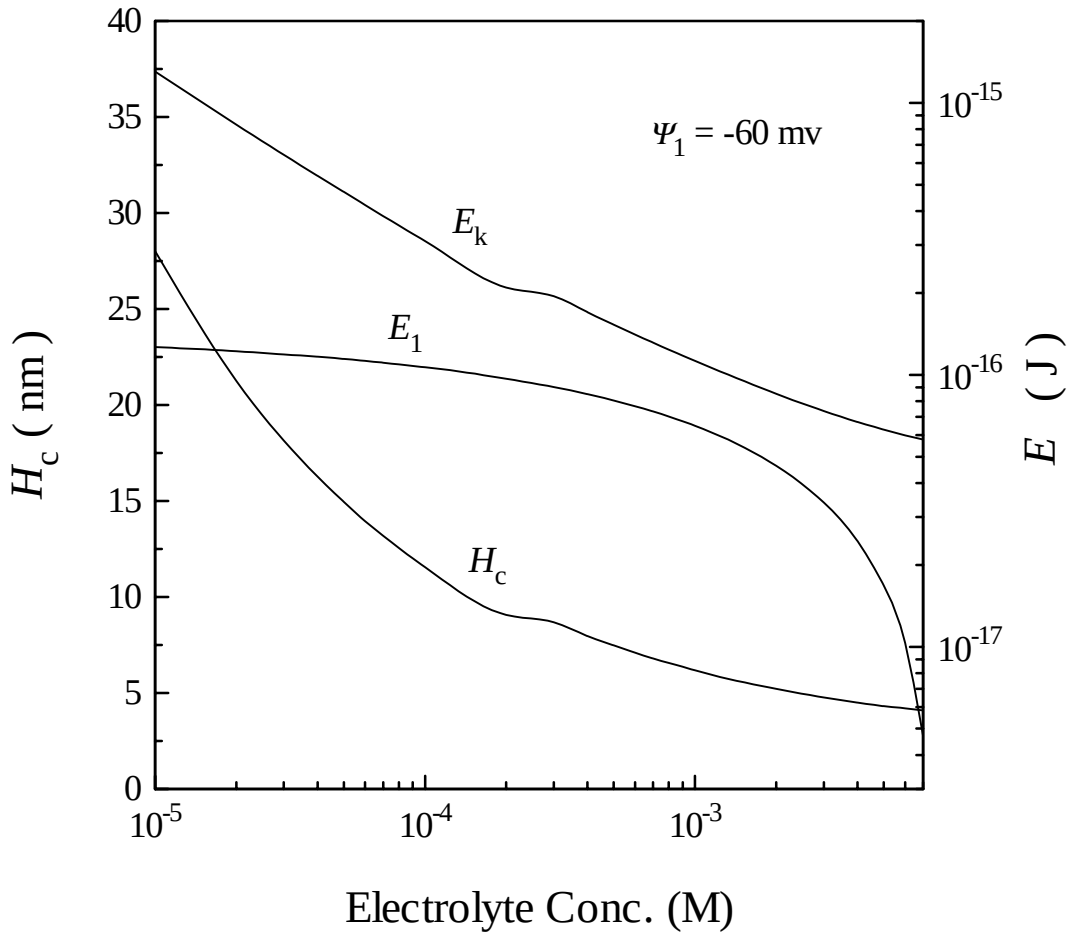

Figure 3.14. Effect of electrolyte concentration on the critical thickness H_c, activation energy E_1 and kinetic energy E_k.

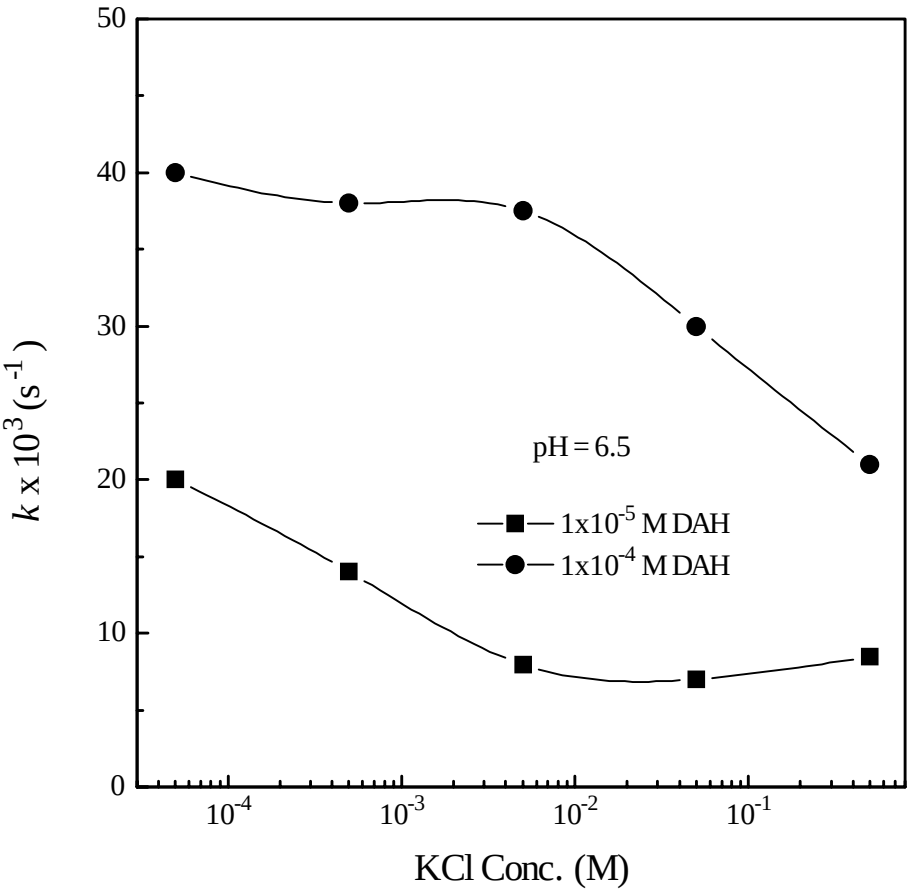

Figure 3.15. Experimental results of rate constant as a function of electrolyte concentration.

hydrophobic force parameter (54-57), which can not be simulated without the relationship between K_{132} and the electrolyte concentration. Usually, increasing the electrolyte concentration may reduce the hydrophobic force, resulting in decreasing of the rate constant, this occurs especially in the flotation of minerals with good hydrophobicity.

An increasing flotation rate with increasing electrolyte concentration were also apparent in the work of other investigators (37, 53, 58-60) which is conventionally related to a reduction in double layer repulsion between bubble and particle (61, 62). This observation indicates that, the hydrophobicity of particles required to flotation is less strict in higher concentration of electrolyte, which is obviously advantageous in recovering weakly hydrophobic minerals.

3.4.5 Effect of Particle Size

Particle size has been recognized as an important parameter which may obviously affect the flotation rate, earlier theoretical analysis (63,64) suggest that:

$$k \propto d_p{}^n, \qquad [3.3]$$

where d_p is the particle diameter and n is a constant. Eq. [3.3] can be written as:

$$\log(k) \propto n \log(d_p). \qquad [3.4]$$

Eq. [3.4] indicates a linear relationship between log(k) and log(d_p) which was observed in many experiments, and the constant n is dependent on the flotation system (53, 63-69). The data from a large number of batch flotation tests (53, 65, 66) shows that n is a unity, some flotation experiments performed with spherical particles support a value for n falling between 1.5 and 2 (67, 68, 70), whereas for oil droplets n is reported as 1-1.8 (69).

The effects of other parameters were considered to attribute the difference in n (37, 53, 60).

Figure 3.16 shows the rate constant as a function of particle size at two different K_{132} values. Other parameters are the same as those in Figure 3.3. As expected, k is shown to increase with increasing particle size, and there is a linear relationship between $\log(k)$ and $\log(d_p)$ which is consistent with the experimental observations described in the previous paragraph. Note that simulation results at different K_{132} values give different slopes of lines, indicating that the value of n does depend on other parameters in flotation system.

The increasing of k with particle size can be explained by the changes of E_1, E_k and E_k', as shown in Figure 3.17. With increasing particle size, all three energies are obviously increased. However, the increasing of E_k is much more significant than those of E_1 and E_k', which results in increasing of P_a and thus k. Although P_d is also increased due to the increasing of E_k', the change is too small to compensate the increase of P_a.

3.4.6 Effect of Bubble Size

Bubble size has long been recognized as one of the most important parameters in flotation. Earlier work on the hydrodynamics of bubble-particle adhesion suggested that the probability of collision increase with decreasing bubble size. As the result, the flotation rate and hence recovery should increase with the decreasing bubble size. Figure 3.18 shows the effect of bubble size on k at various K_{132} values. Other parameters, except S_b, used in the calculation are the same as those given in Figure 3.3. The results show that at a given K_{132} there exists an optimum bubble size (R_2) for the maximum k.

The increase in k with decreasing R_2 is clearly attributed to the increase in P_c (71). Figure 3.19 shows the changes in P_c with R_2 under conditions employed in the present

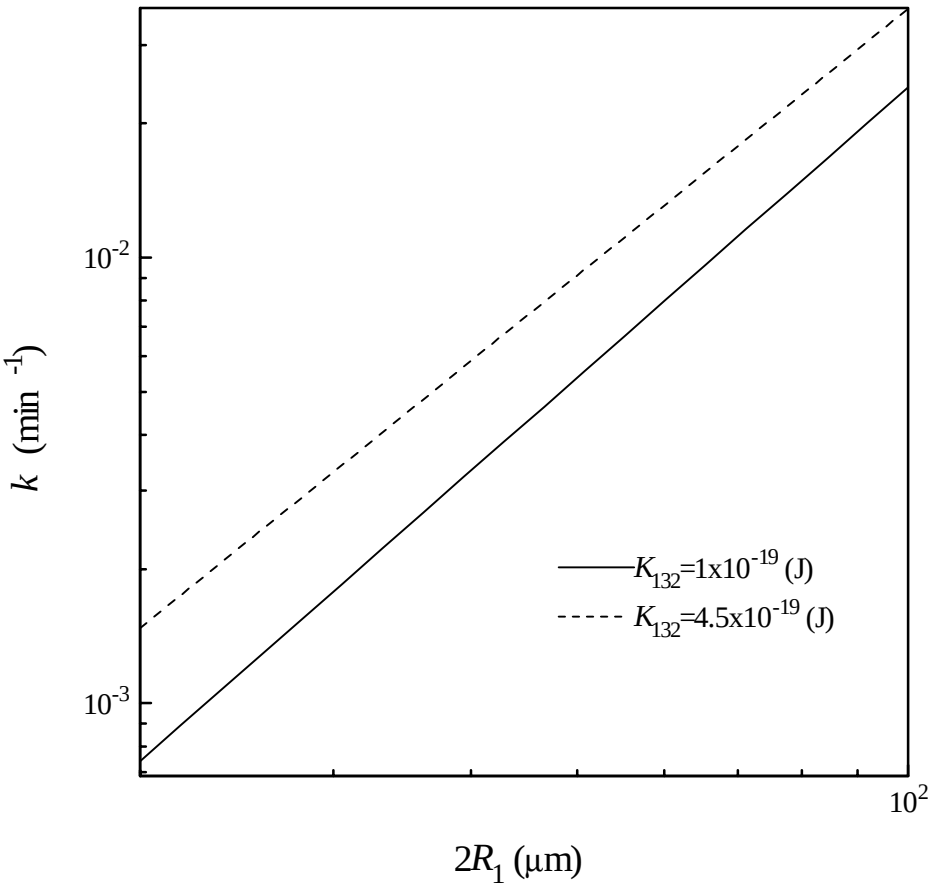

Figure 3.16. Effects of particle size on rate constant at different K_{132} values. Other parameters used in the calculation were same as in Figure 3.3.

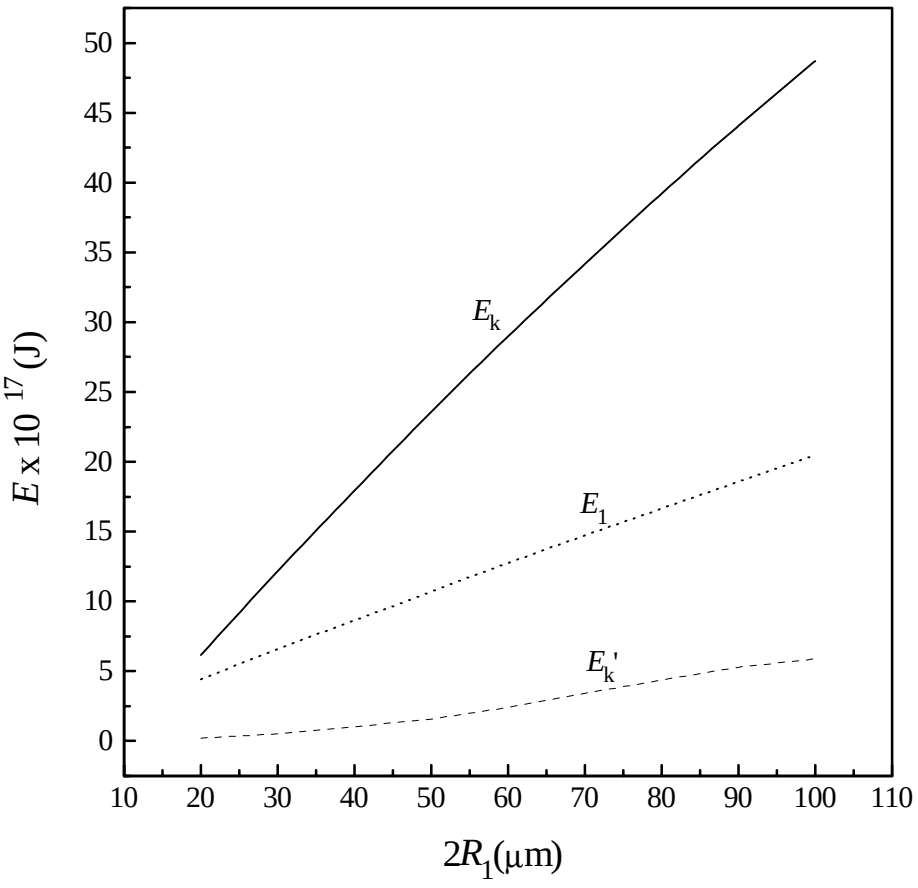

Figure 3.17. The values of E_1, E_k and E_k' as a function of particle size at $K_{132}=1\times10^{-19}$ J.

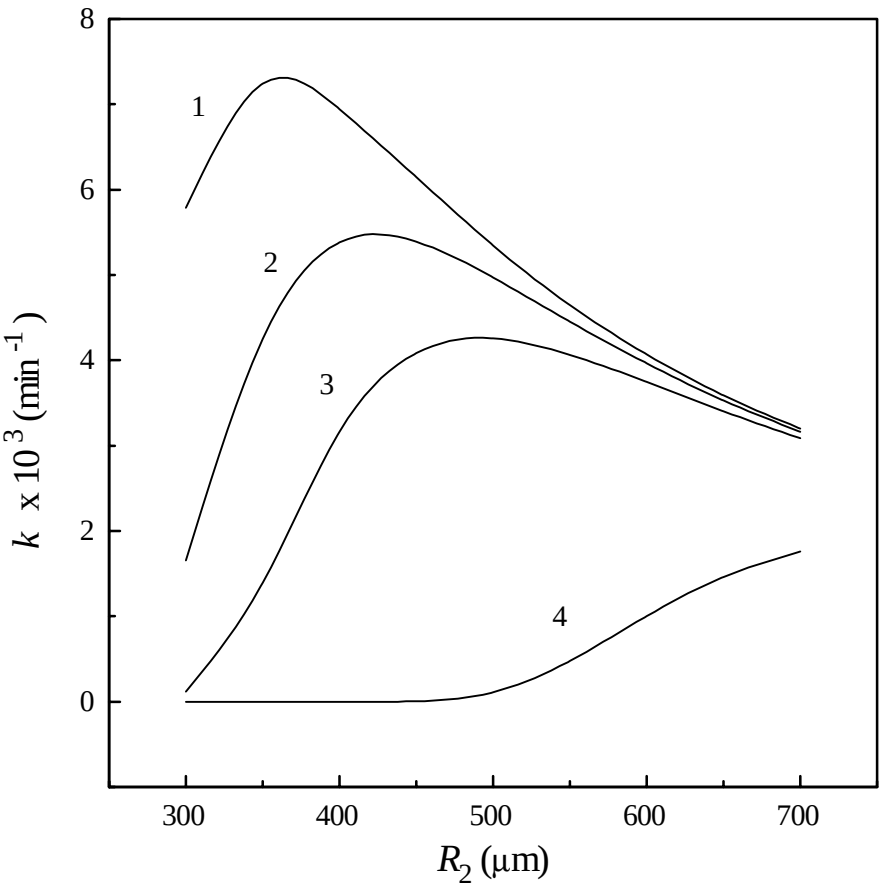

Figure 3.18. k vs. R_2 plots obtained using Eq. [3.1] at the following K_{132} values: 2.0×10^{-19} J (curve 1); 1.5×10^{-19} J (curve 2); 1.0×10^{-19} J (curve 3); 1.0×10^{-21} J (curve 4). Other parameters used in the calculations were same as in Figure 3.3.

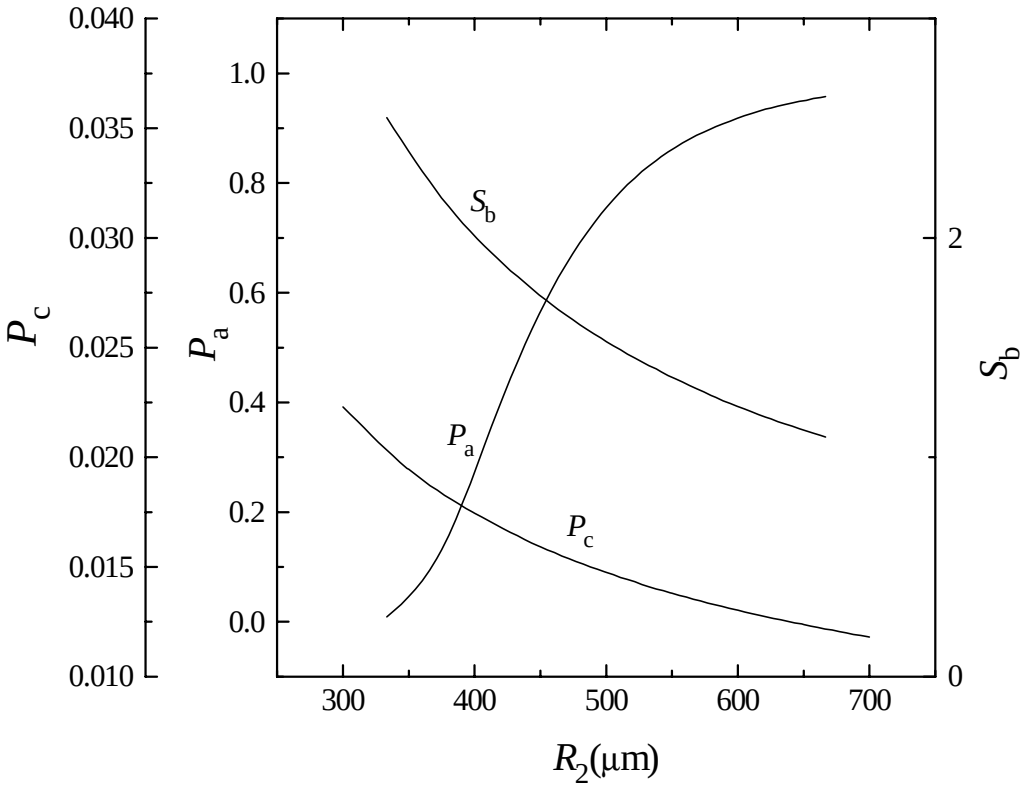

Figure 3.19. Effects of the bubble size (R_2) on the probability of collision (P_c), probability of adhesion (P_a) and superficial surface area rate of bubbles (S_b). The air flow rate (Q) was kept constant at 0.04 ml/min., while the value of K_{132} used for the calculation was 1.0×10^{-19} J. Other parameters used in the calculation were same as in Figure 3.3.

calculation. Also shown in Figure 3.19 is the fact that S_b increases with R_2 at a given aeration rate (0.04 ml/min.), this is another important contribution to the increasing of the rate constant with decreasing of the bubble size which has been ignored before. Therefore, the increase in k with decreasing R_2 can be attributed to the increase in both P_c and S_b. However, a decrease in R_2 also causes a decrease in P_a, providing an explanation for the decrease in k when R_2 is below the optimum bubble size. This is due to the fact that, with the increasing of R_2, both kinetic energy (E_k) and activation energy (E_1) between bubble and particle are increased, however, E_k increases more significantly than E_1 as shown in Figure 3.19, which results in a increasing of k. Obviously, when the bubble size is below the optimum value, the effect of increasing P_a overwhelms that of decreasing S_b and P_c, but the latter effect dominates the rate constant when the bubble is larger than the optimum size. Recently, Wang et al showed that such optimum bubble size is also important for inclusion removal from molten steel by flotation (72).

Figure 3.18 also shows that, k increases with increasing K_{132}, which is obviously due to the increasing of hydrophobic force between bubble and particle. The optimum value of R_2 is also dependent on K_{132}, it shifts to lower R_2 values as shown in Figure 3.18 as mineral particles become more hydrophobic. This can be explained by the fact that the P_a curve shown in Figure 3.19 shifts to smaller R_2 values. At a given R_2, P_a should increase with increasing particle hydrophobicity and, thus, the shift in P_a curve. It can be expected that, if K_{132} is continuously increased, the peak of k curve will shift left further, eventually, for very hydrophobic particles, the peak will be at very small bubble size, in this case, P_a is actually a unity, one may only find the effect of S_b and P_c in the normal range of bubble size (60, 71).

It is interesting to note that, the difference between two curves in Figure 3.18 is also a function of bubble size, that means, bubble size is an important factor to determine the selectivity of separation, and there is a optimum value of bubble size at which the best selectivity can be achieved. Figure 3.20 shows the experimental results reported by

Szatkowski and Freberger (73), it can be seen that there do exist an optimal bubble size for selectivity. In industrial practices, the selectivity is also dependent on the distribution of the bubble size.

3.5 Summary and Conclusions

A flotation rate equation developed in the previous chapter has been used to predict flotation rates as functions of various parameters of characteristics of minerals to be floated and of operating conditions. Although the model predictions need to be validated experimentally in future work, they are consistent with what is expected from experience. The model is capable of not only predicting flotation rates but also explaining the mechanisms involved. The model predicts that flotation rate increases with decreasing magnitudes of the double-layer potentials of the mineral particles. When both the minerals and air bubbles are charged negatively, the model suggests that the maximum selectivity can be achieved when the minerals have large negative potentials. The model also predicts that the rate constant increases with increasing K_{132}, which is attributed to the decreasing of activation energy (E_1) and increasing of the kinetic energy (E_k) for bubble-particle attachment. The flotation rate increases with increasing contact angle, which can be explained by the decrease in energy barrier for bubble-particle adhesion and by the increase in work of adhesion which in turn causes a decrease in probability of detachment. Increasing the electrolyte concentration decreases both E_1 and E_k, which results in a minimum value of k. Unfortunately, the effect of electrolyte concentration on the hydrophobic force can not be simulated due to the lack of the relationship between K_{132} and electrolyte concentration. The rate constant is also a function of the particle size, with increasing of R_1, the increasing of E_k is the dominant effect, which results in increasing of P_a and thus k. Model prediction made as a function of bubble size shows that there exist optimum bubble sizes for floating particles

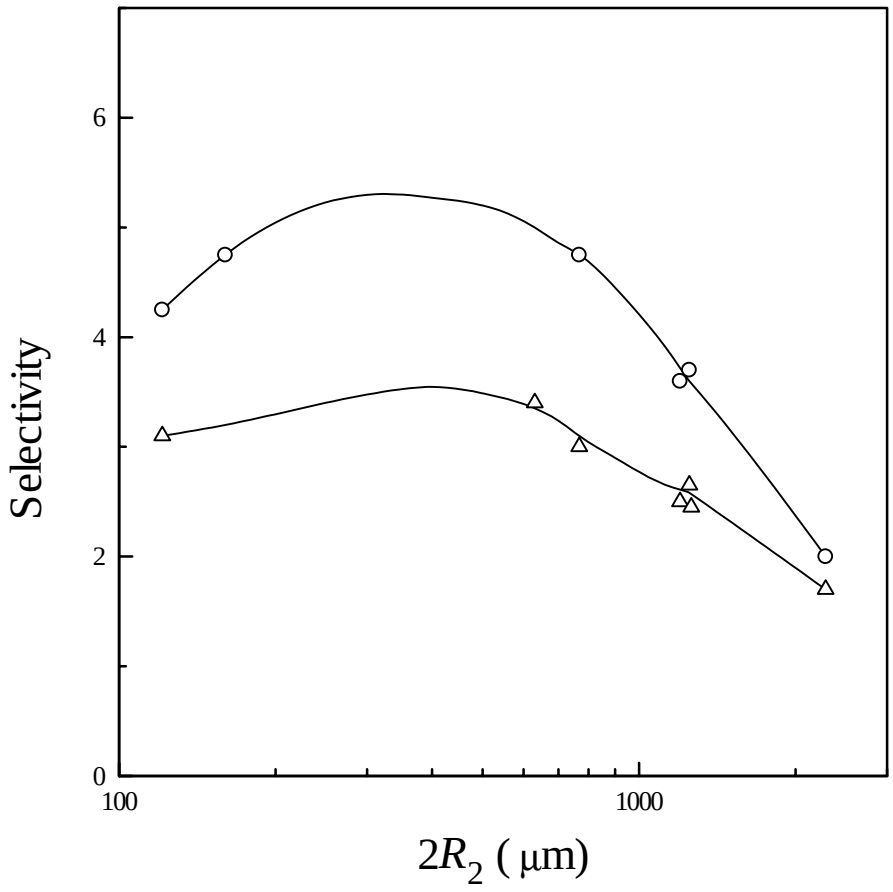

Figure 3.20. The selectivity of flotation as a function of bubble size. From reference (73).

of different hydrophobicities. The optimum shifts toward smaller bubble sizes as the particle hydrophobicity increases. The existence of optimum bubble size can be explained by the increases in probability of collision and in bubble surface area rate with decreasing bubble size (the latter is first recognized in present work) and the corresponding decrease in probability of adhesion.

3.6 Reference

1. Schubert, H., and Bischofberger, C., *Proc. 13th Int. Mineral Process. Congr.*, Warszawa, Vol. 2, pp. 1261(1979).

2. French, R. H. and Wilson, D. J., *Separ. Sci. Technol*. **15**, 1213(1980).

3. Schulze, H. J., Physico-chemical Elementary Processes in Flotation An Analysis from the Point of View of Colloid Science including Process Engineering Considerations, In: Fuerstenau, D. W. Ed. Developments in Mineral Processing, Elsevier, New York, 1984.

4. Inoue, T., Nonaka, M., and Tmaaizumi, T., "Advances in Mineral Processing" (P. Somasundaran, Ed.), Chap. 12 Society of Mining Engineering, 1986.

5. Derjaguin, B. V. and Duhkin, S. S., *Trans. Inst. Min. Metall*. **70,** 221(1961).

6. Derjaguin, B. V. and Duhkin, S. S., *Proc. 13th Int. Mineral Processing Congr*. **2**, 21(1979).

7. Derjaguin, B. V. and Laudau, L., *Acta Physicochim, URSS* **14**, 633(1941).

8. Verwey, E. J. W. and Overbeek, J. Th. G., Theory of the stability of lyophobic colloid. Elsevier, New York (1948).

9. Hogg, R., Healy, T. W. and Fuerstenau, D. W., *Trans. Faraday Soc*. **300**, 1638(1965).

10. Rabinovich, Y. I. and Churaev, N. V., *Colloid J. USSR* **41**, 392(1979).

11. Israelachvili, J. N. and Pashley, R., *Nature* **300**, 341(1982).

12. Schimoller, B. K., Luttrell, G. H. and Yoon, R. H., *Proc. XVIII. Int. Mineral Processing Congr*. pp. 751(1993).

13. Yoon, R. H., *Proc. XVII Int. Mineral Processing Congr*. Dresden, Germany, Vol. II, pp.17(1991).

14. Yoon, R. H. and Yordan, J. L., . *J. Colloid Interface Sci*. **146**, 565(1991).

15. Yoon, R. H. and Mao, L., 1996. *J. Colloid Interface Sci*. **181**, 613(1996).

16. Luttrell, G. H., Hydrodynamic studies and mathematical modeling of fine coal flotation, Ph. D. Thesis, Dept. of Mining and Minerals Eng., Virginia Polytechnic Institute and State University, U.S.A. (1986).

17. Luttrell, G. H. and Yoon, R. H., *J. Colloid Interface Sci*. **154**, 129(1992).

18. Varbanov, R., Forssberg, E. and Hallin, M., *Int J. Miner. Process*. **37**, 27(1993).

19. Pan, R., Paulsen, F. G., Johnson, D. A., Bousfield, D. W. and Thompson, E. V., *TAPPI J*. **79**, 177(1996).

20. Paulsen, F. G., Pan, R., Bousfield, D. W. and Thompson, E. V., *J. Colloid Interface Sci*. **178**, 400(1996).

21. Yoon, R. H. and Ravishankar, S. A., *J. Colloid Interface Sci*. **179**, 391(1996).

22. Yoon, R. H. and Ravishankar, S. A., *J. Colloid Interface Sci*. **179**, 403(1996).

23. Rabinovich, Y. and Yoon, R. H., *Langmuir* **10**, 1903(1994).

24. Rabinovich, Y. and Yoon, R. H., *Colloids and Surfaces* **93**, 263(1994).

25. Claesson, P. M., Blom, C. E., Herder, P. C. and Ninham, B. W., *J. Colloid Interface Sci.* **114,** 234(1986).

26. Churaev, N. V. and Derjaguin, B. V., *J. Colloid Interface Sci*. **103**, 542(1985).

27. Pashley, R. M., McGuiggan, P. M., Ninham, B. W. and Evans, D. F., *Science* **229**, 1088(1985).

28. Huber-Panu, I. Ene-Danalache, E and Cojocariu, D. G., In: M. C. Fuerstenau (Editor), Flotation - A. M. Gaudin Memorial Volume. AIME, New York, NJ. Vol. 2, 675(1976).

29. Lynch, A. J., Johnson, N. W., Maniapig, E. V. and Thorne, C. G., Mineral and coal flotation circuit. In: D. W. Fuerstenau (Editor), Developments in Mineral Processing, Vol. 3, Elsevier, Amsterdam.

30. Dowling, E. C., Klimpel, R. R. and Aplan, F. F., *Miner. Metallurg. Process.* **2**, 87(1985).

31. Derjaguin, B. V. and Shukakidse, N. D., *Trans. I.M.M*. **70**, 569(1961).

32. Jaycock, M. J. and Ottewill, R. H., *Trans. I. M. M*. **72**, 497(1963).

33. DeVivo, D. G. and Karger B. L., *Sep. Sci*. **5**, 145(1970).

34. Spielman, L. A. and Cukor, P. M., *J. Colloid Interface Sci*. **43**, 51(1973).

35. Collins, G. L. and Jameson, G. J., *Chemical Engineering Sci*. **32**, 239(1977).

36. Sysilä, S., Laapas, H ., Heiskanen, K and Ruokonen, E., *Minerals Engineering* **9**, 519(1996).

37. Blake, P. and Ralston, J., *Colloids Surf*. **16**, 41(1985).

38. Derjaguin, B. V. and Kussakov, M., *Acta Physicochim. URSS* **10**, 25(1939).

39. Blake, T. D. and Kitchener, J. A., *J. Chemical Soc. Faraday I* **68**, 1435(1972).

40. Arson, M. P. and Princen, H. M., *J. Colloid Interface Sci*. **52**, 345(1975).

41. Read, A. D., Kitchener, J. A., *J. Colloid Interface Sci*. **30**, 391(1969).

42. Nakamura, M. and Uchida, K., J. *Colloid Interface Sci*. **78**, 479(1980).

43. Pashley, R. M. and Kitchener, J. A., *J. Colloid Interface Sci*. **71**, 491(1979).

44. Gee, M. L., Healy, T. W. and White, L. W., *J. Colloid Interface Sci*. **140**, 450(1990).

45. Butt, H., *J. Colloid Interface Sci*. **166**, 109(1994).

46. Ducker, W. A., Xu, Z. and Israelachvili, J. N., *Langmuir* **10**, 3279(1994).

47. Feilden, M. L., Hayes, R. A. and Ralston, J., *Langmuir* **12**, 3721(1996).

48. Claesson, P. M., Ederth, T., Bergeron, V. and Rutland, M. W., *Advanced in Colloid and Interface Sci*. **67**, 119(1996).

49. Wood, J. and Sharma, R., *Langmuir* **11**, 4797(1995).

50. Yoon, R. H. and Flinn, D. H. and Rabinovich, Y. I., *J. Colloid Interface Sci.* **185**, 363(1996).

51. Yoon, R. H. and Luttrell, G. H., Development of the selective hydrophobic coagulation process, Seventh Quarter Technical Progress Report, Contract No. DE-AC22-91PC91164 (1993).

52. Aksoy, B. S., Hydrophobic Forces in Free Thin Films of Water in the Presence and Absence of Surfactants, Ph. D. Thesis, Dept. of Mining Minerals Eng., Virginia Polytechnic Institute and State University, 1997.

53. Crawford, R and Ralston, J., *Int. J. Miner. Process*. **23**, 1(1988).

54. Claesson, P. M., Blom, C. E., Herder, P. C. and Ninham, B. W., *J Colloid Interface Sci*. **114**, 1(1986).

55. Christensson, H. K., Claesson, P. M. and Parker, L. J., *J Phys. Chem*. **96**, 6725(1992).

56. Tsao, Y. and Evans, D. F., *Langmuir* **9**, 779(1993).

57. Li, C., Preprint 92-110, SME Annual Meeting, Phoenix, Arizona (1992).

58. Laskowski, J. and Iskra, J., *Trans. IMM* sect. C, **79**, C6(1970).

59. Paulson, O. and Pugh, R. J., *Langmuir* **12**, 4808(1996).

60. Anfruns, J. F. and Kitchener, J. A., *Trans. IMM* Sect. C, **86**, C9(1977).

61. Laskowski, J. and Kitchener, J. A., *J. Colloid Interface. Sci*. **29**, 670(1969).

62. Israelachvili, J., Intermolecular and Surface forces, Academic Press, London, (1985).

63. Flint, L. R. and Howarth, W. J., *Chem. Eng. Sci*. **26**, 1155(1971).

64. Reay, D. and Ratcliff, G. A., *Can. J. Chem. Eng*. **51**, 178(1973).

65. Sutherland, K. L., *J. Phys. Chem.* **52**, 394(1948).

66. Trahar, W. J., *Int. J. Miner. Process*. **13**, 167(1981).

67. Reay, D. and Ratcliff, G. A., *Can. J. Chem. Eng*. **53**, 479(1975).

68. Collins, G. L. and Jameson, G.J., *Chem. Eng. Sci*. **31**, 985(1976).

69. Sylvester, N. D. and Byeseda, J. J., *Soc. Pet. Eng. J*. **20**, 579(1980).

70. Tomlinson, H. S. and Fleming, M. G., *Proc. VI Int. Mineral Processing Congr*. pp. 563(1963).

71. Yoon, R. H. and Luttrell, G. H., *Mineral processing and extractive metallurgy review* **5**, 101(1989).

72. Wang, L., Lee, H. G., and Hayes, P., *ISIJ International* **36**, 7(1996).

73. Szatkowski, M. and Freberger, W. L., *Int. J. Miner. Process*. **23**, 213(1988).

CHAPTER 4: HYDROPHOBICITY OF DODECANE

4.1 Introduction

Coalescence of oil droplets in an emulsion plays an important role in many industrial processes and environmental cleanup operations. In all liquid-liquid extraction processes, after contact of the liquid phases and inter-phase mass transfer has been completed, the efficiency of the subsequent phase separation depends on the coalescence of the dispersed liquid droplet (1). Coalescence of the emulsions formed during alkaline flooding operations is necessary to produce a stable oil bank and increase oil recovery (2, 3). In petroleum refineries, porous coalescers, settlers, chemicals, particles and electric field are commonly used to achieve the coalescence of fine oil mist which is directly related to processes such as extraction, distillation and tertiary oil recovery (4-8). In the flotation of hydrocarbons from their emulsions, the coalescence of oil droplets determines the amount of big globules (> 5 μm) which dominates oil-bubble attachment and thus flotation efficiency (9). Coalescence of emulsion droplets is usually very undesirable in food products, coalesced droplets in oil-in-water emulsion merge to become larger spherical droplets and eventually free oil is seen on the top of the sample. Proteins are often used to prevent this coalescence and thus stabilize the emulsion (10, 11).

Like all other dispersed systems, oil droplets dispersed in another phase are usually thermodynamically unstable. The free energy associated with the large interfacial area between the dispersed and continuous phases can be decreased by aggregation or coalescence of the dispersed phase which depends on the physicochemical properties and hydrodynamics of the system. Interfacial tension, interfacial tension gradients, interfacial shear viscosity, size and velocity of the droplets etc., are usually considered as the important parameters which control the overall coalescence rate (12, 13).

Similar to the bubble-particle interaction described in the Chapter 1, the coalescence process may be divided into three stages (14): (i) approach of one droplet toward another in the liquid phase; (ii) formation and thinning of a thin liquid film between two interfaces; and (iii) rupture of the film as the thickness of the film becomes sufficiently small, i.e. there is a critical thickness at which the film becomes unstable and the coalescence spontaneously take place (15-20). Generally, in the first two stages, the hydrodynamics of the system plays a more important role than intermolecular forces, while in the third stage, when the thickness is less than approximately 100 nm, the drainage process is controlled by surface forces. These forces were first described by Derjaguin and Kussakov (21) in terms of "disjoining pressure", the hydrostatic pressure in the interior of the film that opposes the approach and coalescence of two droplets.

The London-van der Waals force and electrostatic double layer force are traditionally considered as two components of the disjoining pressure, which forms the basis of the classical DLVO theory (22, 23). When two symmetric droplets approach each other, the disjoining pressure due to the London-van der Waals force is always attractive, which enhances the thinning process and so as to destabilize the intervening film. On the other hand, the contribution of the double layer force to the disjoining pressure is usually repulsive, which stabilizes the film and retard coalescence of two droplets. The net resultant contribution of these two opposite effects determines whether the intervening film will reach a critical thickness at which it becomes unstable and rupture, and coalescence occurs, or will attain an equilibrium thickness without further drainage.

The classical DLVO theory is commonly used to explain the stability of the thin film with varying degrees of success. Chen (14) showed that the classical DLVO theory can be used to predict the stability and thickness of dimpled film between two spherical droplets. The results of deposition experiments conducted by Sanders *et al* (25) showed that, the behavior of the bitumen droplets dispersed in aqueous solution could be

accurately predicted from the classical DLVO theory. However, asphaltene-stablized mineral oil emulsions did not follow the DLVO theory. Groeneweg *et al* (25) investigated the stability of the W/O emulsions prepared from vegetable oil, and showed that an additional attractive force was necessary to explain the experimental result. Similar conclusions were obtained for microemulsions (droplet size < 0.5 μm) in the presence of surfactant (26, 27). Recently, Deshiikan and Paradopoulos (28, 29) visually observe the coalescence of n-hexadecane oil droplets suspended inside an aqueous phase of varying pH and ionic strength, and explained the results with classical DLVO theory. The decrease of the repulsive double layer force was considered as the mechanism of oil coalescence at very low and very high pH. However, the calculation results of the total interaction energy showed a very high energy barrier, indicating that the oil coalescence is impossible at these pH ranges. They believed that some important characteristics might decide the stability of the thin film interfaces. It is now generally recognized that non-DLVO forces such as steric force, hydration force and hydrophobic force are also important to the stability of thin films (30-34).

Recent advancement in the techniques of direct force measurement provided evidences of hydrophobic forces existing in the thin aqueous film between two macroscopic solid surface and in the free water film (34, 35). Tchaliovska *et al* (36) measured the equilibrium film thickness of dodecylammonium chloride (RNH_3Cl) solutions using the thin film balance (TFB) of the type developed by Scheludko (37, 38). The data were used to calculate the double-layer potentials using classical DLVO theory. The results showed that the potentials were substantially lower than those calculated based on the adsorption densities of the surfactants at the interface, which was attributed to an additional attractive force. Recently, Aksoy (39) conducted similar experiments with dodecylammonium chloride (RNH_3Cl) and Sodium Dodecyl Sulfate (SDS), and used the extended DLVO theory, which included the contribution from hydrophobic force in addition to those from the van der Waals and double layer forces, to determine the hydrophobicity of an air bubble as a function of surfactant concentration. The results

showed that, air bubbles are inherently hydrophobic, the attractive hydrophobic force was usually the main driving force for bubble coalescence in pure water. In presence of surfactant, the hydrophobicity of the bubble decreases with increasing surfactant concentration. The decrease of the hydrophobic force provides an explanation of the stabilization of the bubbles by various surfactants. Recognizing that the oil droplets are usually considered to be inherently hydrophobic, it would not be unreasonable to seek for the evidence of hydrophobic forces between two oil droplets in aqueous solution using the same technique.

It is the purpose of the present investigation to study the role of hydrophobic forces between two oil droplets in aqueous solution using the thin film balance (TFB) technique. For the first time, the hydrophobicity of oil droplets will be quantified, and the results will be compared with those of the free film to investigate the possible relationship between the hydrophobicity and the physicochemical properties of liquids.

4. 2 Experimental

4.2.1 Materials

Research grade dodecylamine hydrochloride supplied by Eastman Kodak Co. was used as surfactant in the present work. Purified grade dodecane and ACS grade sodium chloride were obtained from Fisher Scientific Co. and used as oil and electrolyte respectively. The NaCl was roasted at 600°C before using to remove possible organic contaminants. The pH of the surfactant solution was controlled by ACS grade hydrochloric acid and sodium hydroxide solution. Deionized water (18 mΩ), prepared with a Nanopure II water treatment unit, was used in all of the experiments.

4.2.2 Equilibrium Film Thickness Measurement

The equilibrium thickness of the aqueous dodecylammonium chloride surfactant film in the dodecane was determined with a thin film balance (TFB) technique developed by Scheludko *et al*. (37, 38). Figure 4.1 shows the modified experimental set-up. A flat horizontal film was formed in a film holder, a cylindrical glass tube with a radius of 2 mm, due to capillary pressure. This film was then carefully introduced into a glass container that contains enough dodecane to produce an oil-solution-oil interface. The TFB cell was placed on an inverted Zeiss microscope, which in turn was mounted on a vibration-free stone table. The images of the aqueous thin film, generated using a monochromatic light source, were monitored and captured by an image processing system (Kontron SEM-IPS) to determine the equilibrium thickness of the aqueous film. At least ten measurements were taken at a given experimental condition and averaged.

In a typical test, the aqueous film was thinned by drawing some liquid from the film using a syringe pump until the first interference pattern was formed. This image was digitized with the image processing system after the film is stabilized. The thickness (H) of the film was calculated from the reflectance (R) of the interference pattern (see Appendix 4.1).

For each measurement, RNH_2Cl solution was prepared in Nanopure water. All glassware were cleared by boiling them in the concentrated nitric acid solution for 5-6 hours, followed by rinsing with Nanopure water until the pH of the washing water is 5.8±0.2, and finally drying with pure nitrogen gas.

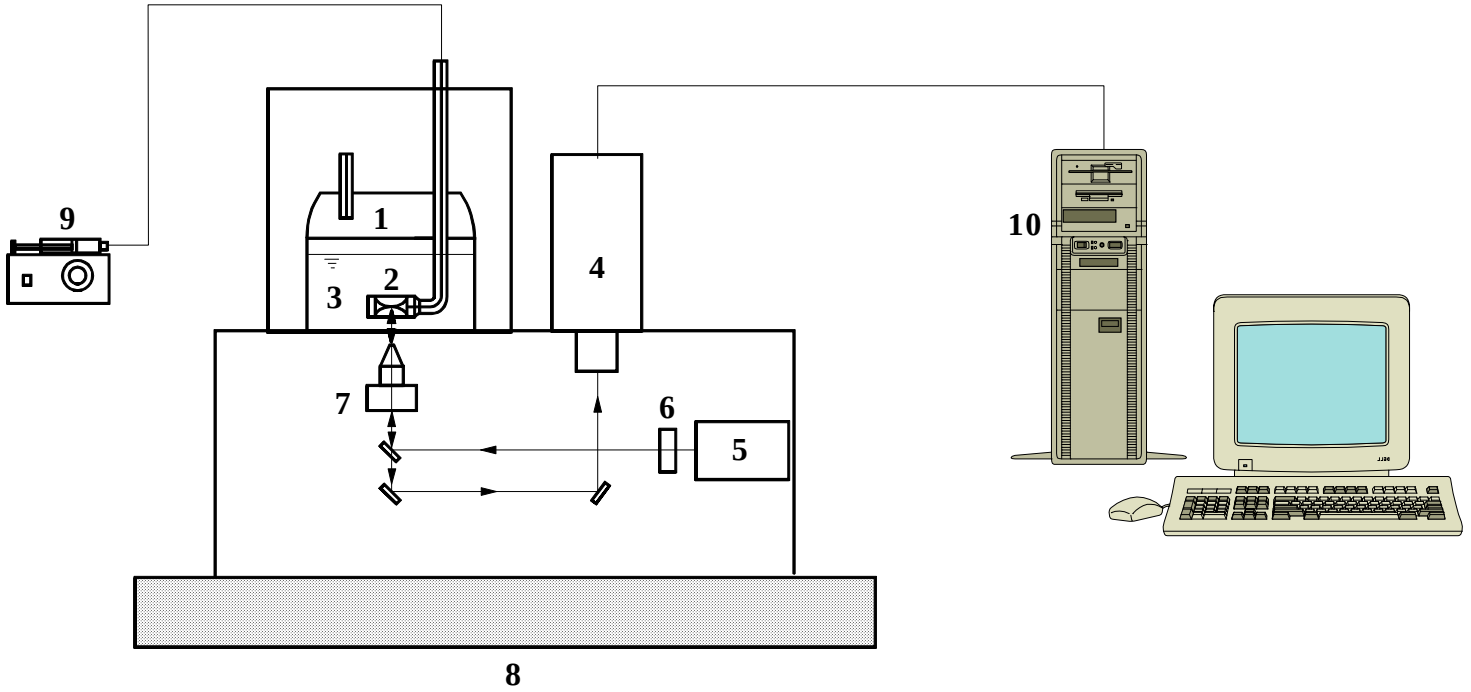

Figure 4.1. The experimental set up used for equilibrium film thickness measurements. **1**. Cell, **2**. Film holder with aqueous film, **3**. Oil, **4**. Video camera, **5**. Light source, **6**. Filter, **7**. Inverted Zeiss microscope, **8**. Vibration-free table, **9**. Syringe pulp, **10**. Image analysis system.

4.2.3 Interfacial Tension Measurement

A block diagram of the experimental set-up for interfacial tension measurement is shown in Figure 4.2. The main components of the pendent drop tensiometer are a Ramé-Hart contact angle goniometer and an image processing system (Kontron SEM-IPS). The optical system consists of the light source **1**, diffuser **2**, microscope and video camera **5**, which provide the image of the pendent drop formed at the tip of the capillary tube **3**. This image is captured and processed by the image processing system to determine the profile of the drop, which in turn is used to calculate the interfacial tension of two liquids (40-42). The cell **4** is made of quartz and has a length of 10 mm. It contains enough dodecane to immerse the capillary tip and whole pendent drop. The capillary tube is connected with a syringe pump to precisely control the size of the aqueous drop.

4. 3 Results and Discussion

4.3.1 Equilibrium Film Thickness

The equilibrium thickness of a flat film is reached when the disjoining pressure between two oil-solution interfaces is balanced by the capillary pressure. Figure 4.3 shows the equilibrium film thickness (H_e) measured using different concentrations of DAH. No supporting electrolyte was used in these experiments, and the pH of the solution was in the range of 5.8±0.2. As shown in the figure 4.3, H_e decreases with increasing DAH concentration, indicating that the aqueous film is stabilized by the surfactant. This is because the increased DAH concentration results in a higher ionic strength which decreases the long-range double-layer repulsive force. The increased stability of the oil film is also attributed to the adsorption of RNH_3^+ ions at the oil/solution interface, which changes the interfacial potential, and the hydrophobic interaction, as discussed below.

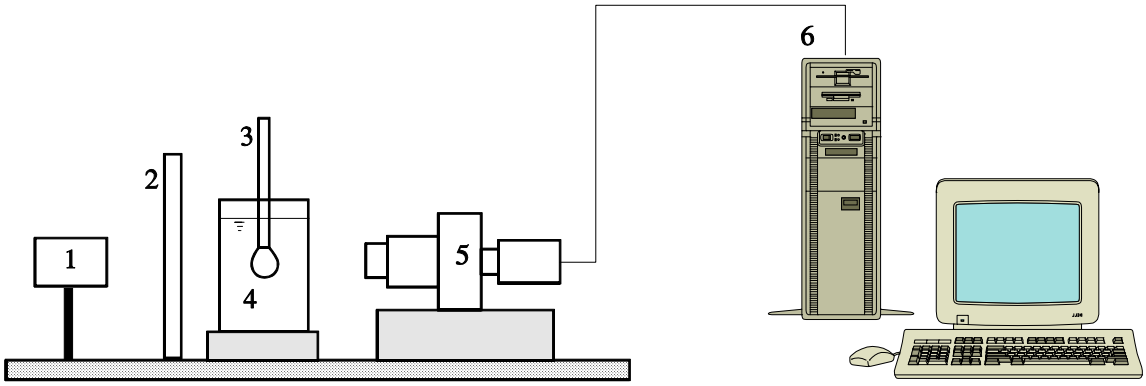

Figure 4.2. A block diagram of the experimental set-up for interfacial tension measurement. **1**. Light source, **2**. Diffuser, **3**. Capillary tube with pendant aqueous drop, **4**. Cell with oil, **5**. Video camera, **6**. Image analysis system.

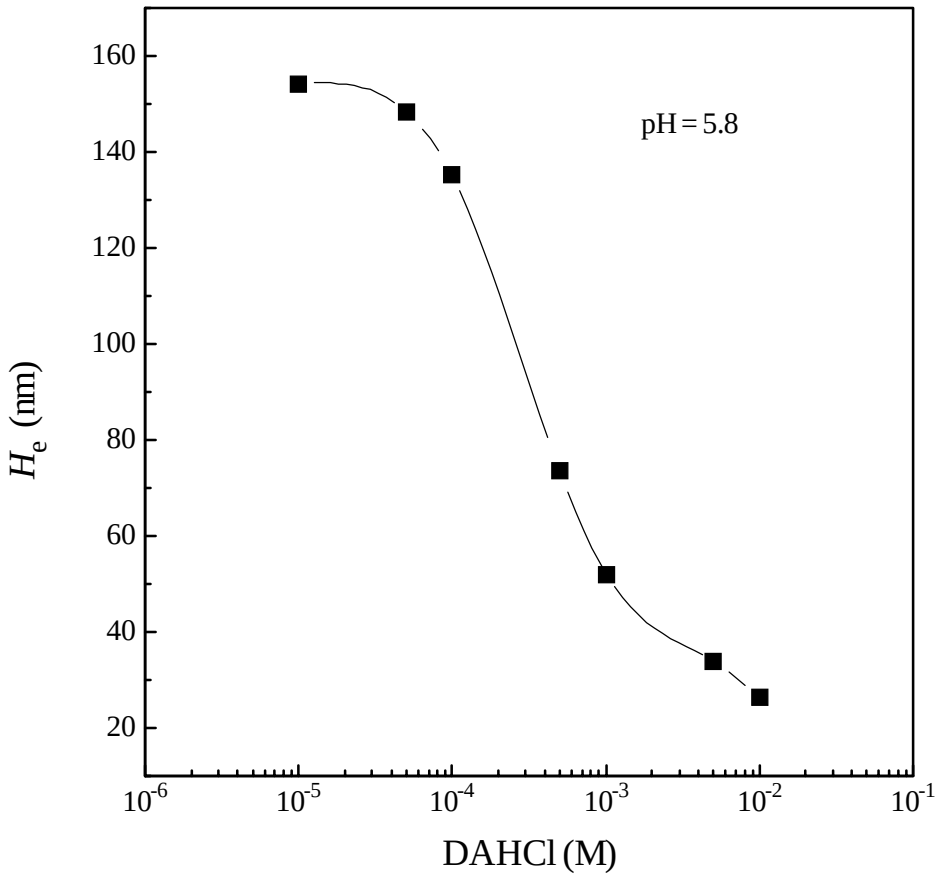

Figure 4.3. Equilibrium film thickness (H_e) as a function of DAH concentration at pH 5.8.

The largest value of the film thickness obtainable in the present work is about 150 nm when the DAH concentration is 10^{-5} M. Below this concentration, the film becomes so unstable that it is very difficult to have metastable films that last long enough time to conduct the measurement.

Figure 4.4 shows the effect of the pH of the solution on the equilibrium film thickness in the absence of the supporting electrolyte when the DAH concentration is 10^{-4} M. H_e slightly increases with increasing pH, indicating that the aqueous film becomes a little bit unstable. It is well known that, with the increasing pH, the hydrolysis of the RNH_3^+ ions is increased, forming more soluble neutral amine RNH_2(aq). These neutral amine may co-adsorb with RNH_3^+ species at the oil/solution interface in the mechanism similar to that proposed for the adsorption of the same species on the quartz (43) and mica (44, 45) and for the adsorption of iono-molecular species $RNH_2 \cdot RNH_3^+$ on quartz and air water interface (46). The presence of more RNH_2(aq) species at oil/solution interface decreases the interfacial charge density and the surface potential which reduces the repulsive double layer interaction between two interfaces, also these neutral species induces better hydrophobicity than RNH_3^+ due to less hydration, therefore the attractive hydrophobic force is increased. Consequently, the stability of the aqueous film is decreased as increasing pH. If the pH of the solution is further increased to 10.0, the aqueous film becomes so unstable that it is very difficult to measure the equilibrium film thickness.

Figure 4.5 shows the equilibrium film thickness as a function of the electrolyte concentration. As expected, the value of H_e dramatically decreases with increasing KCl concentration. This is due to the fact that the addition of the electrolyte compresses the electrical double layer at oil/solution interface, the repulsive double layer force is decreased, and thus the capillary pressure is balanced by disjoining pressure at a shorter distance. Unlike the increasing of the interfacial potential upon the addition of surfactant

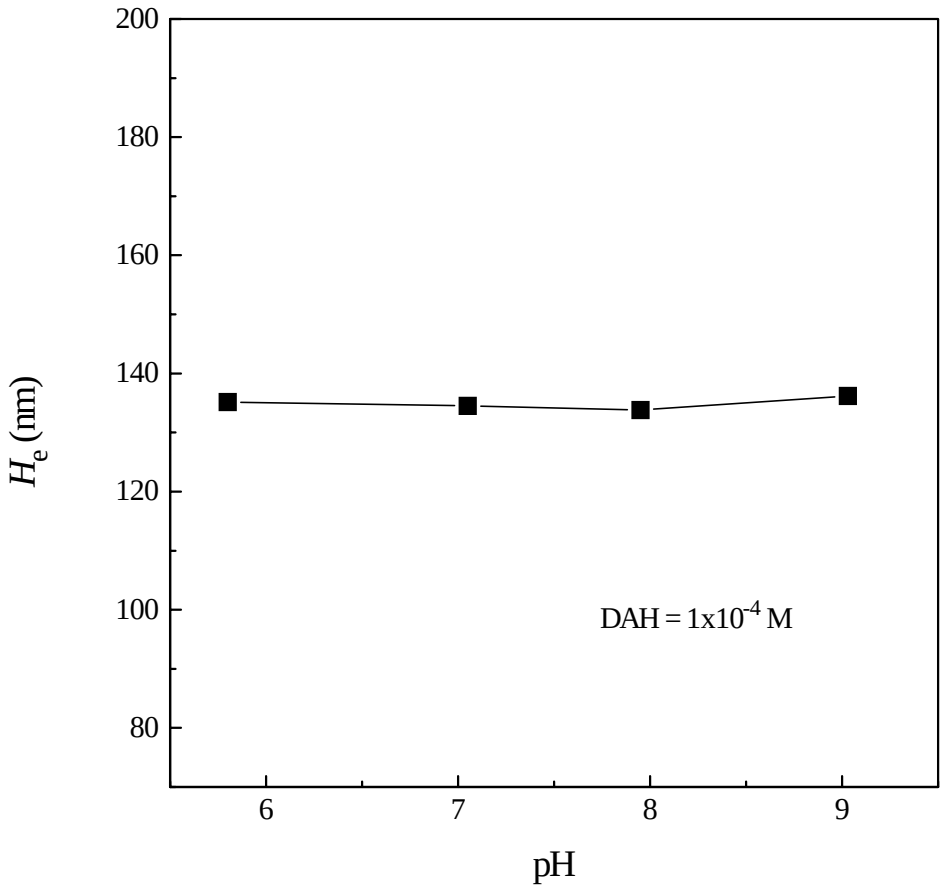

Figure 4.4. Equilibrium film thickness (H_e) as a function of pH in 10^{-4} M DAH solution.

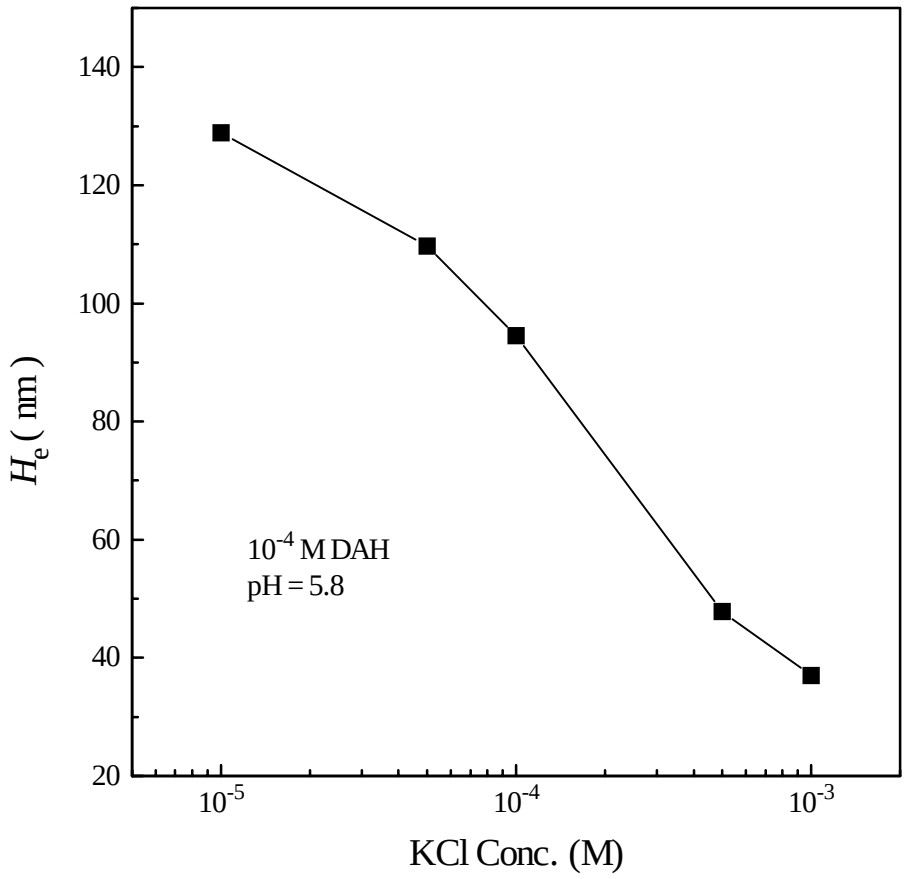

Figure 4.5. Equilibrium film thickness (H_e) as a function of KCl concentration in 10^{-4} M DAH solution.

which partly compensates the decreasing of the double layer force due to the double layer compression, the increasing of the electrolyte concentration does not increases the interfacial potential because the K^+ and Cl^- ions of the electrolyte are not specifically adsorbed at the oil/solution interface, and therefore the effect of the double layer compression is more significant.

4. 3. 2 Interfacial Tension

Figure 4.6 shows the interfacial tension of the oil/solution interface as a function of DAH concentration at pH 5.8±0.2 in the absence of a supporting electrolyte. As expected, the interfacial tension obviously decreases with increasing surfactant concentration. This is simply attributed to the adsorption of RNH_3^+ and RNH_2 at the oil/solution interface. Figure 4.7 shows the effect of pH of the solution on the interfacial tension, the interfacial tension decreases with increasing pH from 5.8 to 9.0, this is obviously related to the increasing concentration of soluble neutral amine RNH_2(aq) in the solution. The change of the interfacial tension was also observed at the air/solution interface (39, 47). The interfacial tension is slightly increased with the increasing electrolyte (NaCl) concentration at pH 5.8 when the DAH concentration is 10^{-4} M, as shown in Figure 4.8. This is due to the fact that KCl is not surface active, their presence causes the increasing of the interfacial tension.

4. 3. 3 Double-Layer Potentials

When a horizontal film reaches equilibrium in a TFB, the attractive capillary pressure (P_c) is balanced by the repulsive disjoining pressure (Π) as follows:

$$\Pi - P_c = 0 . \qquad [4.1]$$

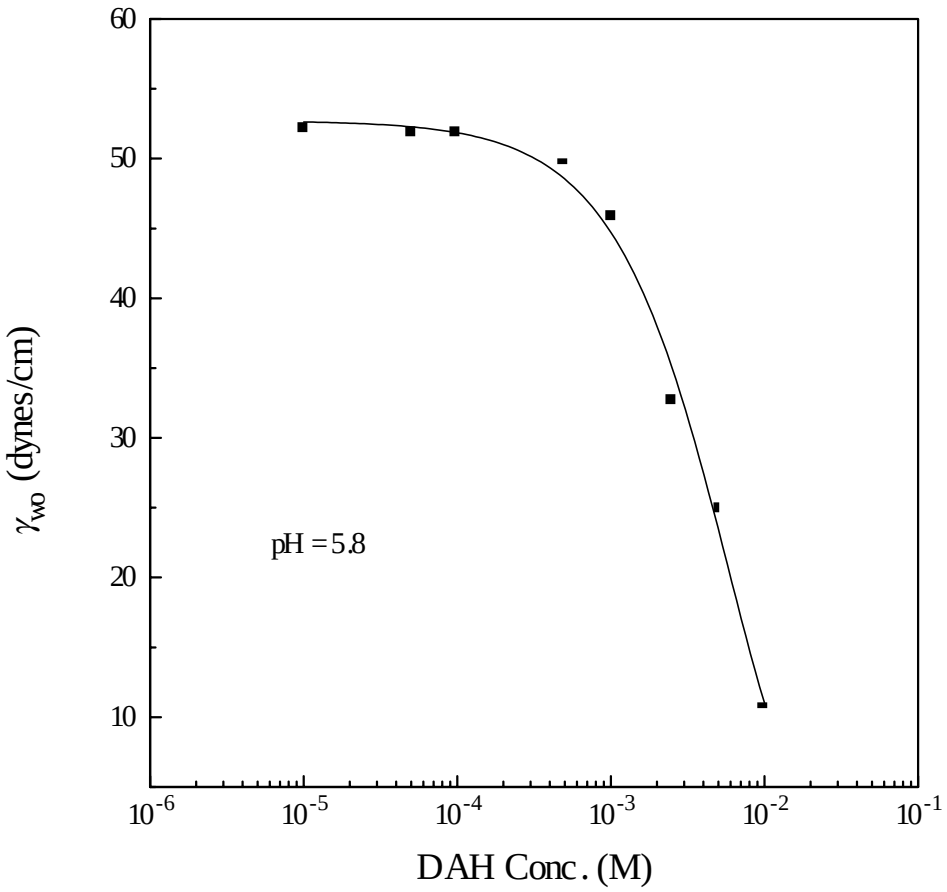

Figure 4.6. The interfacial tension of the oil/solution interface as a function of DAH concentration at pH 5.8±0.2 in the absence of a supporting electrolyte.

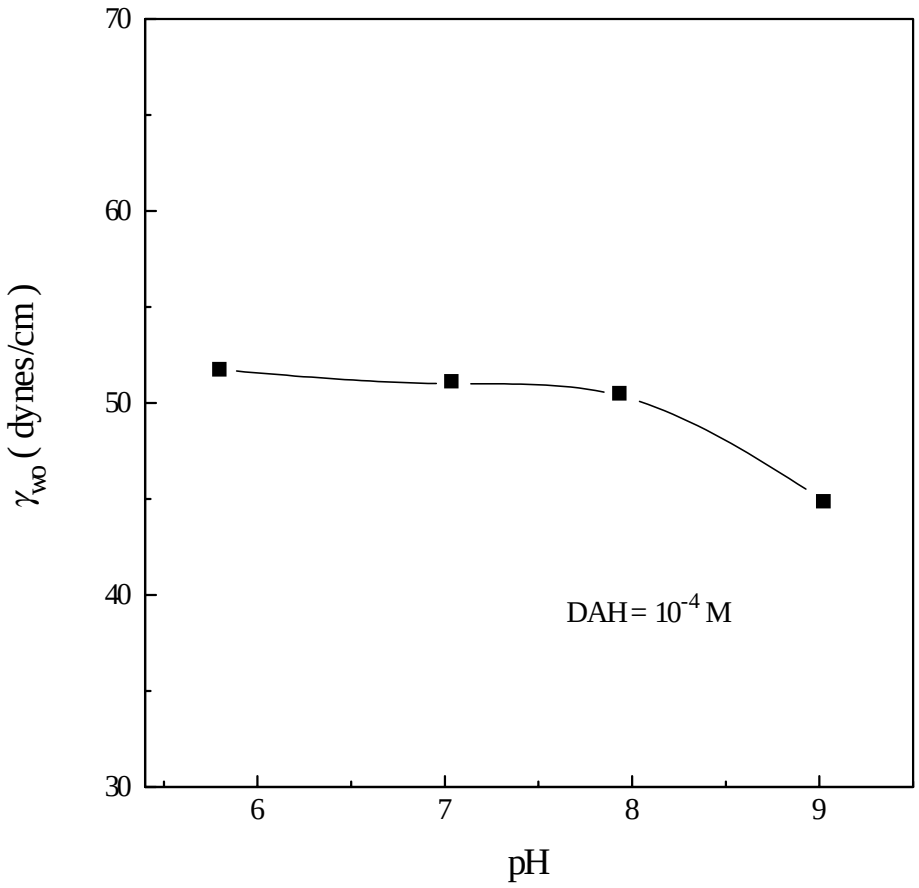

Figure 4.7. The interfacial tension of the oil/solution interface as a function of pH in 1×10^{-4} M DAH solution.

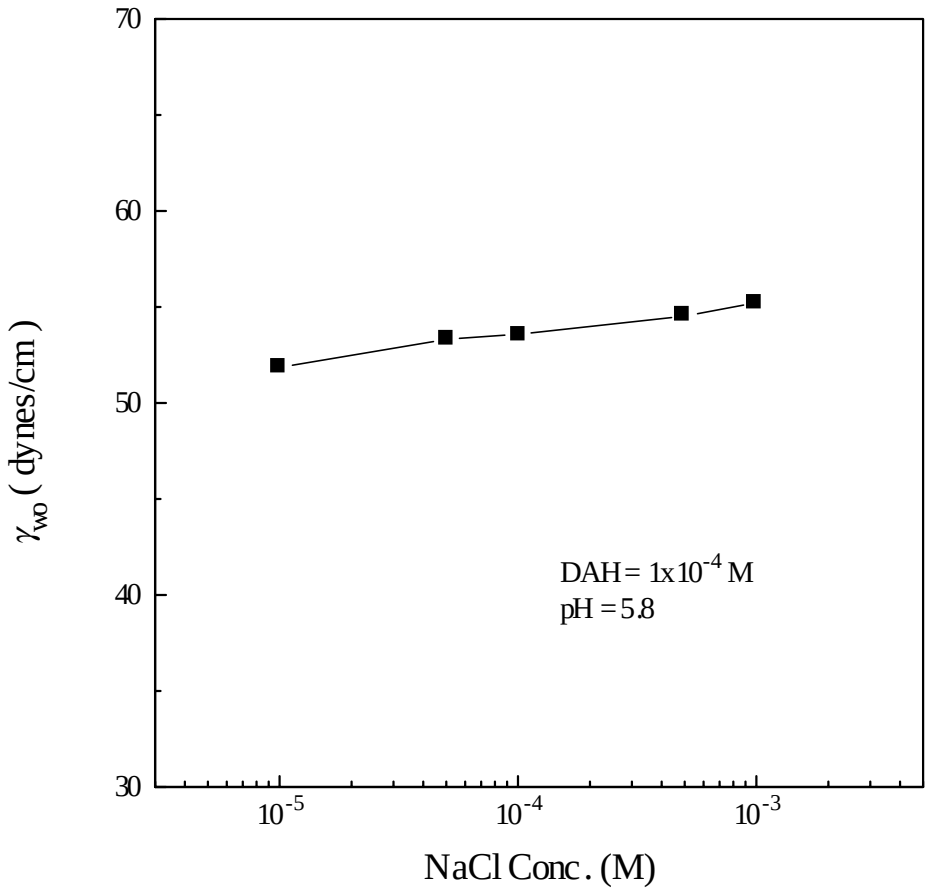

Figure 4.8. The interfacial tension of the oil/solution interface as a function of electrolyte concentration at pH 5.7-6.0 in the presence of 1×10^{-4} M DAH.

The capillary pressure is given by (38)

$$P_c = 2\gamma_{wo}\left[\frac{r_c \cos\theta_R - r\sin\theta_r}{r_c^{\,2} - r^2}\right], \qquad [4.2]$$

where γ_{wo} is the interfacial tension of the oil/solution interface, r_c is the radius of curvature of the liquid meniscus, r is the radius of the flat circular film, θ_R is the contact angle between the liquid meniscus and the inner surface of the film holder, and θ_r is the angle between the flat film and the adjacent meniscus, which is negligible except for very thin black film (30, 48). In current work, the inner surface of the film holder was made rough by sand-blasting to enhance the wetting so that θ_R is close to zero, thus Equation 4.2 can be approximated as:

$$P_c = \frac{2\gamma_{wo}}{r_c}. \qquad [4.3]$$

In classical DLVO theory, the disjoining pressure (Π) consists of two components

$$\Pi = \Pi_e + \Pi_{d,} \qquad [4.4]$$

in which Π_d is due to the double-layer force and Π_e the van der Waals force. When the distance between two interfaces is significantly larger than the Debye length (κ^{-1}), as in the current work, the repulsive double-layer force is expressed as:

$$\Pi_e = 64CRT\tanh^2\left(\frac{ze\psi}{4kT}\right)\exp(-\kappa H), \qquad [4.5]$$

where C is the electrolyte concentration, R the gas constant, T the absolute temperature, z the valence of the ions in the solution, e the electronic charge, ψ the double-layer potential, k the Boltzmann constant, κ^{-1} the Debye length and H is the distance between two interfaces, or film thickness. The expression of Π_d is given by,

$$\Pi_d = -\frac{A_{232}}{6\pi H^3}, \qquad [4.6]$$

in which A_{232} is the Hamaker constant for two oil surfaces interacting across the solution.

At equilibrium, Eqs. 4.3-4.6 can be used to calculate the double-layer potential ψ from the values of H_e shown in Figure 4.3 and interfacial tension value shown in Figure 4.6, with the value of $A_{232} = 5.0\times10^{-21}$ J (49). The calculation results are shown in Figure 4.9. As expected, the double layer potential increases with increasing surfactant concentration due to increasing adsorption of DAH at the oil/solution interface. Higher potential produces larger repulsive double-layer force which increases the stability of the films. Also increasing the surfactant concentration compresses the double layer, resulting in decreasing of the equilibrium thickness H_e, as shown in Figure 4.3. When the surfactant concentration is 2×10^{-4} M, a closed-packed monolayer may be formed, as the concentration is further increased, due to the compression of the double layer and the increasing concentration of the counter-ion at the interface, ψ is decreased.

The calculation of the double-layer potential with classical DLVO theory assumes that there are only double-layer force and van der Waals force interacting between two oil/solution interfaces. To verify this assumption, one may calculate the potential from the interfacial tension isotherm. Gibbs' equation for ionic surfactant gives:

$$\Gamma = -\frac{1}{2RT}\frac{d\gamma}{d\ln C}, \qquad [4.7]$$

where Γ is the surface excess. It can be used to determine the surface charge density σ_0 with the relationship (36, 39):

$$\sigma_0 = e\,N_0\,\Gamma, \qquad [4.8]$$

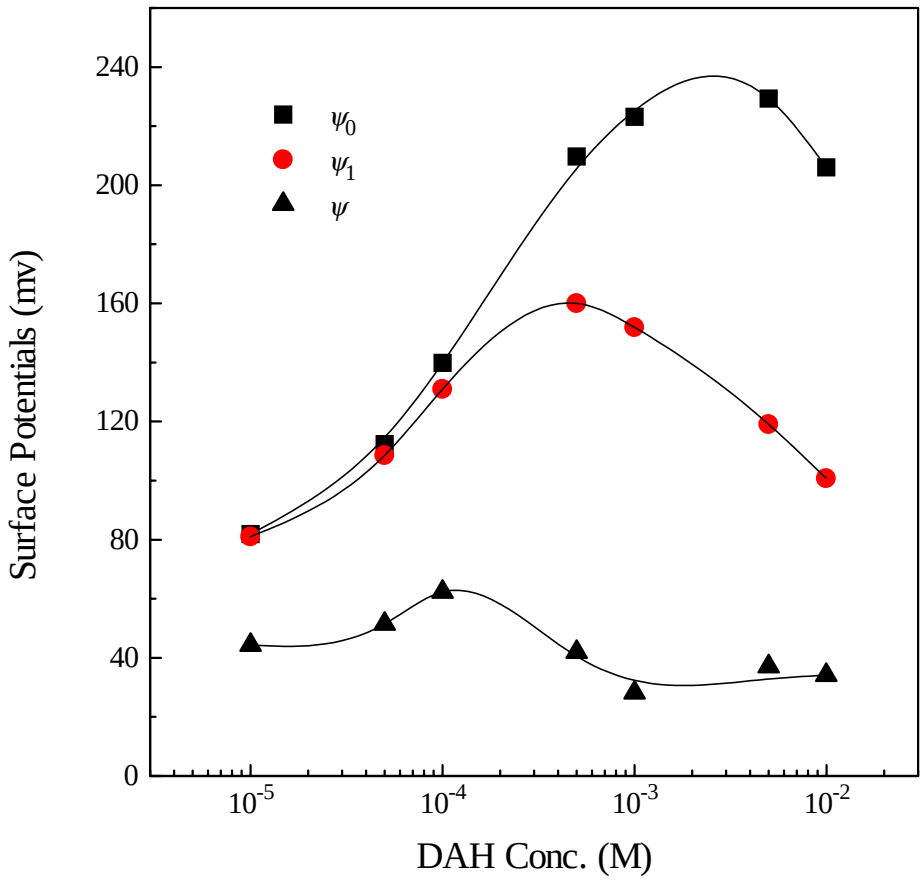

Figure 4.9. The double-layer potentials at oil/solution interface as calculated from classical DLVO theory, Gibbs' adsorption isotherm and at the Outer Helmholtz Plane (OHP).

where *e* is the electronic charge and N_0 Avogadro's constant. Using the Poisson-Boltzmann approximation, the interfacial potential (ψ_0) can be obtained from σ_0 with the following relationship (50):

$$\sigma_0 = \sqrt{8RT\varepsilon_0\varepsilon C}\sinh\left(\frac{e\psi_0}{2kT}\right), \qquad [4.9]$$

where ε_0 and ε are the permittivity of vacuum and the dielectric constant of water, respectively. The calculation results of ψ_0 are also shown in Figure 4.9. Clearly, the calculation based on the Gibbs' adsorption equation gives much higher interfacial potential than those using classical DLVO theory, and this discrepancy increases with increasing surfactant concentration.

Figure 4.9 also shows the potential at the Outer Helmholtz Plane (OHP) which is obtained by considering the hydrated counter ion (Cl^-) near the polar head of the RNH_3^+ ions adsorbed at the oil/solution interface. Figure 4.10 is the schematic representation of the model, it shows that the maximum distance (*h*) between the OHP and the center of the RNH_3^+ ions is the sum of the radius of RNH_3^+ ($r_{RNH_3^+}$), diameter of the water ($2r_{H_2O}$) molecule and the radius of the counter ion Cl^- (r_{Cl^-}), i.e.

$$h = r_{RNH_3^+} + 2r_{H_2O} + r_{Cl^-}$$

$r_{RNH_3^+}$, r_{H_2O} and r_{Cl^-} are 2.8 Å, 1.4 Å and 1.81 Å respectively (44, 51), thus

$$h = 2.8 + 2 \times 1.4 + 1.81 = 7.41 \text{ Å}. \qquad [4.10]$$

For the symmetrical electrolyte, Poisson-Boltzmann equation gives (52, 53):

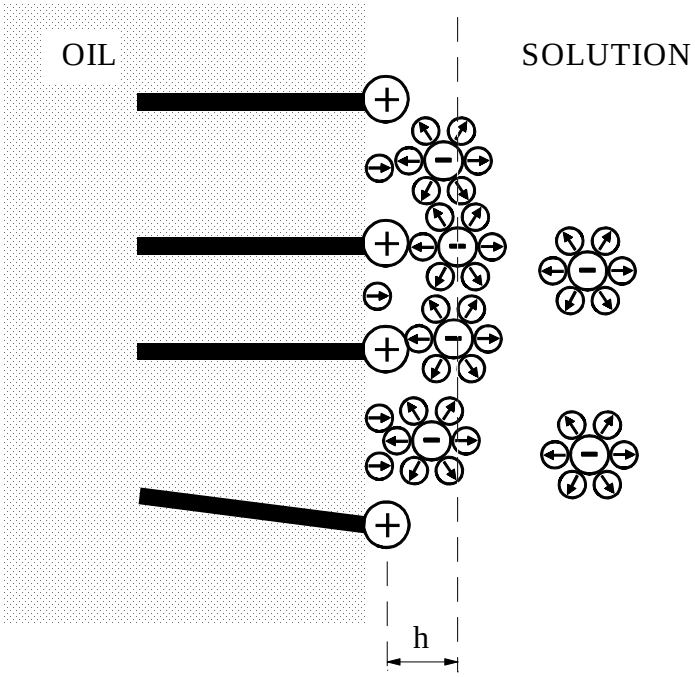

Figure 4.10. Schematic representation of the electrical double-layer at the oil/solution interface in the presence of DAH. *h* is the maximum distance between Outer Helmholtz Plane (OHP) and the center of the RNH_3^+ ions adsorbed on the oil/solution interface.

$$\frac{\partial^2 \psi}{\partial x^2} = \frac{8\pi z e n_0}{\varepsilon} \sinh\left(\frac{ze\psi}{kT}\right), \qquad [4.11]$$

where n_0 is the number concentration of ion in the bulk solution, x is the distance from the interface. Integrating Equation [4.11] with boundary conditions

$$\text{x} = 0, \qquad \psi = \psi_0$$
$$\text{x} = \infty, \qquad \psi = 0$$
$$\frac{d\psi}{dx} = 0$$

gives:

$$\psi = \frac{2kT}{ze} \ln\left[\frac{1+\gamma \exp(-\kappa x)}{1-\gamma \exp(-\kappa x)}\right], \qquad [4.12]$$

where

$$\gamma = \frac{\exp\left(\frac{ze\psi_0}{2kT}\right)-1}{\exp\left(\frac{ze\psi_0}{2kT}\right)+1} \qquad [4.13]$$

and

$$\kappa = \sqrt{\frac{8\pi n_0 z^2 e^2}{\varepsilon kT}}\,. \qquad [4.14]$$

$1/\kappa$ is called the Debye length. Substituting *h* in the Equation [4.10] to the Equation [4.12], the potential at OHP (ψ_1) can be easily obtained.

As shown in Figure 4.9, the values of ψ_1 is obviously lower than ψ_0, but still considerably higher than the values of potential calculated using the classical DLVO

theory. Parts of the reasons may be the variance of the pK_a of DAH solution and ignorance of the ion-ion correlation in the Poisson-Boltzmann equation (54-56), but the most possible contribution might be from the hydrophobic force, which was first suggested by Pugh and Yoon (57) and recently validated in the investigation of the stability of the free film (39).

4. 3. 4 Hydrophobic Force

When the contribution from the hydrophobic force is important in the interaction between two oil/solution interfaces, the classical DLVO theory may be modified as follows:

$$\Pi = \Pi_e + \Pi_d + \Pi_{h,} \qquad [4.15]$$

where Π_h is the hydrophobic force component of the disjoining pressure, it may be expressed as a single exponential law (58) or a double exponential law(59-61), but most conveniently it is represented by a power law (35, 62)

$$\Pi_h = -\frac{K_{232}}{6\pi H^3}, \qquad [4.16]$$

where H is the distance between two oil/solution interfaces and K_{232} is a constant. The advantages of using Equation [4.16] are that it is of the same form as Equation [4.6] and has only one parameter. Therefore K_{232} can be directly compare with the Hamaker constant A_{232}.

Substitute Equations [4.5] [4.6] and [4.16] into [4.1] and [4.15], there is

$$64CRT\tanh^2\left(\frac{ze\psi}{4kT}\right)\exp(-\kappa H_e) - \frac{A_{232}}{6\pi H_e^{\ 3}} - \frac{K_{232}}{6\pi H_e^{\ 3}} - \frac{2\gamma}{r_c} = 0, \qquad [4.17]$$

in which H_e is the equilibrium film thickness, as shown in Figure 4.3. A_{232} is 5×10^{-21} J, r_c is 2 mm, the values of ψ_0 or ψ_1 can be used for approximation of ψ, thus the only unknown parameter K_{232} can be determined using Equation [4.17].

Figure 4.11 shows the results of K_{232} at different DAH concentrations when ψ_0 and ψ_1 are used in the calculation. Although the difference between ψ_0 and ψ_1 is obvious when the DAH concentration is high, the values of K_{232} obtained using these two different potentials are very close to each other. This is due to the fact that the double layer is more compressed at higher ionic strength, the contribution of the double-layer force is less important to the total disjoining pressure at a given distance, therefore K_{232} is less sensitive to the surface potential at higher DAH concentration.

Figure 4.11 shows that the oil surface is inherently hydrophobic, and its hydrophobicity or K_{232} decreases with increasing surfactant concentration, indicating that the oil/solution interface becomes less hydrophobic. This is clearly related to the increasing adsorption of RNH_3^+ ions at the oil/solution interface. Because the polar heads of the RNH_3^+ are strongly hydrated, the presence of these ions reduces the hydrophobicity of the interface.

As mentioned earlier, when the DAH concentration is lower than 1×10^{-5} M, the aqueous film is so unstable that it is very difficult to measure the film thickness. However, if the K_{232} versus concentration curve shown in Figure 4.11 is extrapolated, the value of K_{232} in the absence of surfactant is about 6×10^{-18} J, which is 1200 times larger than the Hamaker constant. Therefore the stability of the aqueous film between two oil surfaces or the coalescence of two oil droplets is dominated by the hydrophobic force. This force may be dampened by the hydrated polar heads of the surfactant

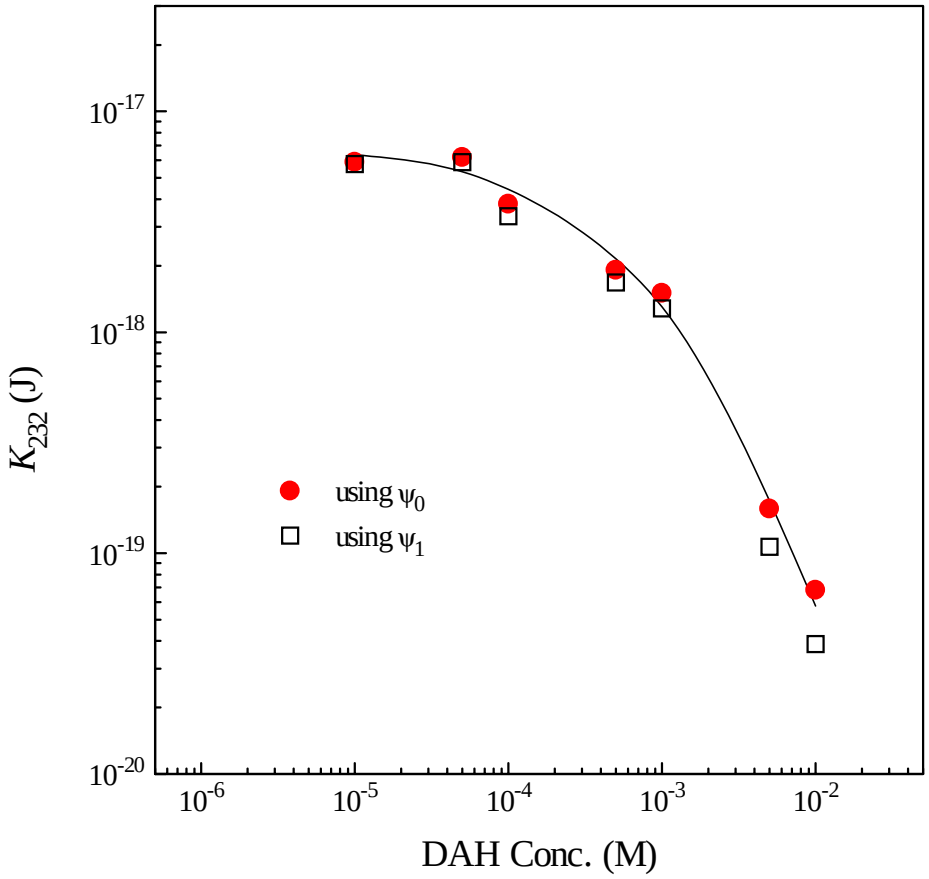

Figure 4.11. The values of K_{232} for the interaction between two oil/solution interfaces in the presence of DAH as calculated using Equation [4.17].

molecules brought to the oil/solution interface as parts of surfactant molecules.

Figure 4.12 shows the values of K_{232} as a function of pH in the presence of 1×10^{-4} M DAH. K_{232} increases with the increasing of pH from 5.8 to 9.0, although the change is not significant. This is attributed to the increasing concentration of the neutral amine $RNH_2(aq)$ in the solution. These species are less hydrated, their adsorption at the oil/solution interface diminishes the effect of the highly hydrated polar heads of the RNH_3^+ ions, and thus the hydrophobicity of the interface is improved.

The presence of supporting electrolyte changes the values of K_{232}, as shown in Figure 4.13. When the electrolyte concentration is higher than 1×10^{-4} M, the decreasing of K_{232} with increasing concentration is considerable, indicating that there are some electrostatic contributions, directly or indirectly, to the hydrophobic force. Similar dependence of the hydrophobic force on the electrolyte concentration was also found in other system (60, 63, 64). If the double exponential function is used to represent the hydrophobic force, the effect of the electrolyte is mainly to decrease the amplitude but not the decay length of the force. However, no simple relation is found between the decay length of the hydrophobic force and the Debye screening length κ^{-1}, suggesting that the decreasing in the long-range hydrophobic force upon addition of the electrolyte does not arise from the generation of the double layer interaction. Obviously, with the increasing of electrolyte concentration, the number of the electrolyte ions near the oil/solution interface is increased. These ions are strongly hydrated which may decreases the hydrophobicity of the interface. However, these ions can not be specially adsorbed at the oil/solution interface as found for surfactant, their presence can not obviously change the interfacial potential, and thus the effect of the electrolyte concentration on the interfacial hydrophobicity is not as significant as that of surfactant.

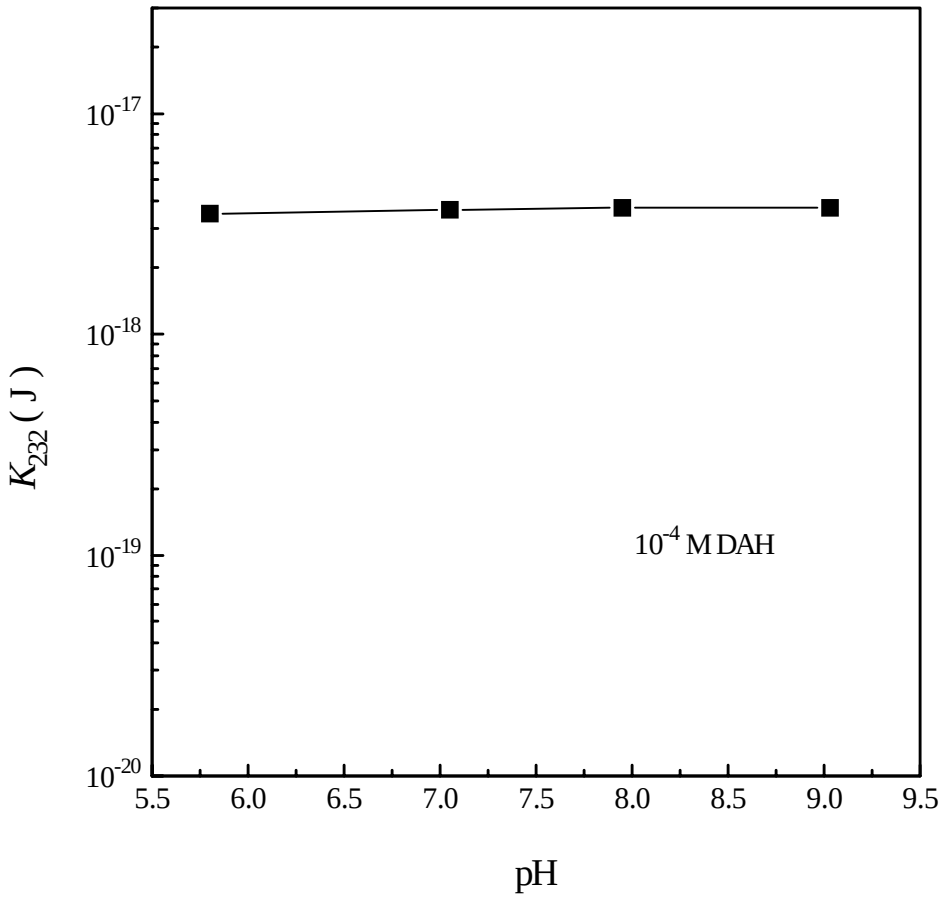

Figure 4.12. The values of K_{232} as a function of pH in the presence of 1×10^{-4} M DAH.

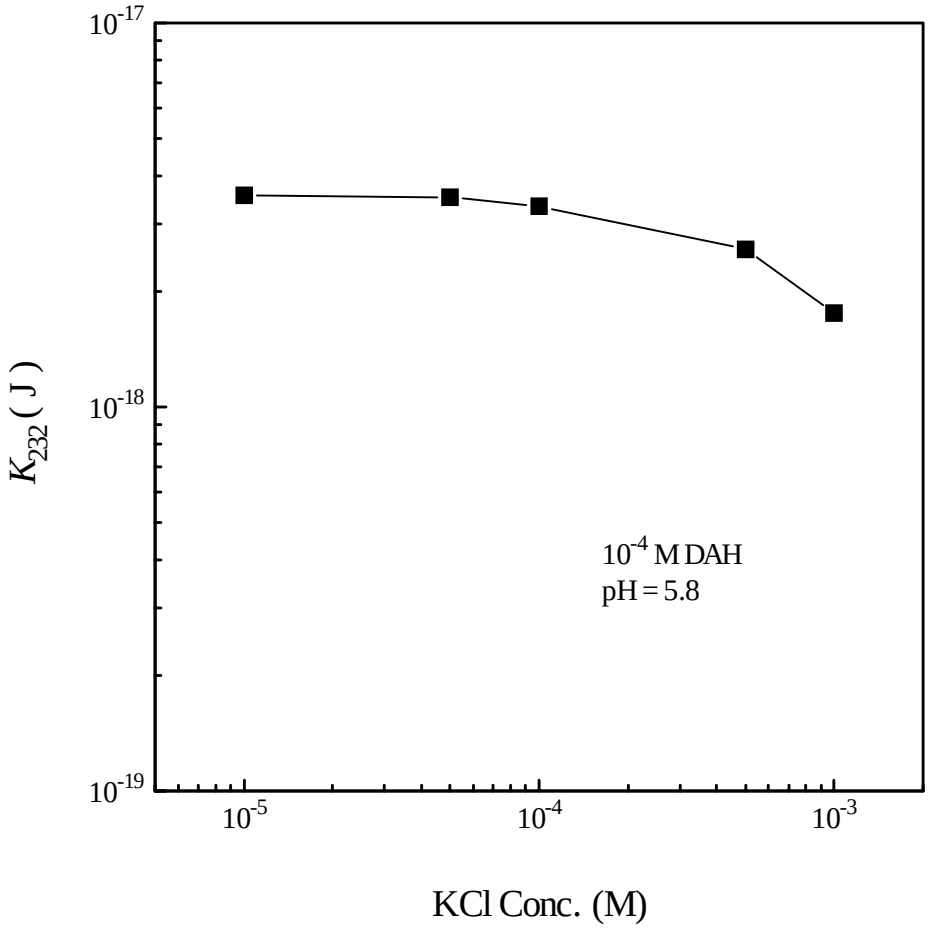

Figure 4.13. The value of K_{232} as a function of electrolyte concentration in the presence of 1×10^{-4} M DAH.

4.3.5 Adsorption Model of DAH at Oil/Solution Interface

At the oil/solution interface, when the DAH concentration is high enough, the RNH_3^+ may form a uniform monolayer, as shown in Figure 4.14(a). In this case, the area occupied by each RNH_3^+ ion at oil/solution interface should be close to the cross-sectional area (25 $Å^2$) (44) of RNH_3^+ ion. However, due to the repulsive electrostatic force among the polar head groups of DAH, this layer is difficult to be closely packed, thus the dodecane molecules may present between two RNH_3^+ ions, as shown in Figure 4.14(b). In this case, the area occupied by each RNH_3^+ ion will be much larger than 25 $Å^2$.

From the interfacial tension isotherm shown in Figure 4.6, the area occupied by each RNH_3^+ ion at oil/solution interface can be obtained using Gibbs' equation, as shown in Figure 4.15. The area decreases with increasing DAH concentration, indicating that more RNH_3^+ ions are adsorbed at the oil/solution interface. When the DAH concentration is higher than 5×10^{-3} M, the area is close to a constant 48 $Å^2$. This area is much larger than the cross-sectional area of RNH_3^+ ion, in fact, it's approximately two times of hydrocarbon cross area, therefore the adsorption model shown in Figure 4.14(b) is more reasonable.

4.3.6 Comparison Between Oil/Solution and Air/Solution Interfaces

The value of K_{232} for air/solution system was calculated based on the experimental results obtained by Aksoy (39), and shown together with the data of oil/solution system in Figure 4.16 for comparison. In the absence of surfactant, the value of K_{232} for air/solution interface is about 1×10^{-17} J which is larger than that for oil/solution interface (about 6×10^{-18} J), thus the inherent hydrophobicity of air/water interface is better than that of oil/water interface. This may be related to the fact that the interfacial tension at the air/water

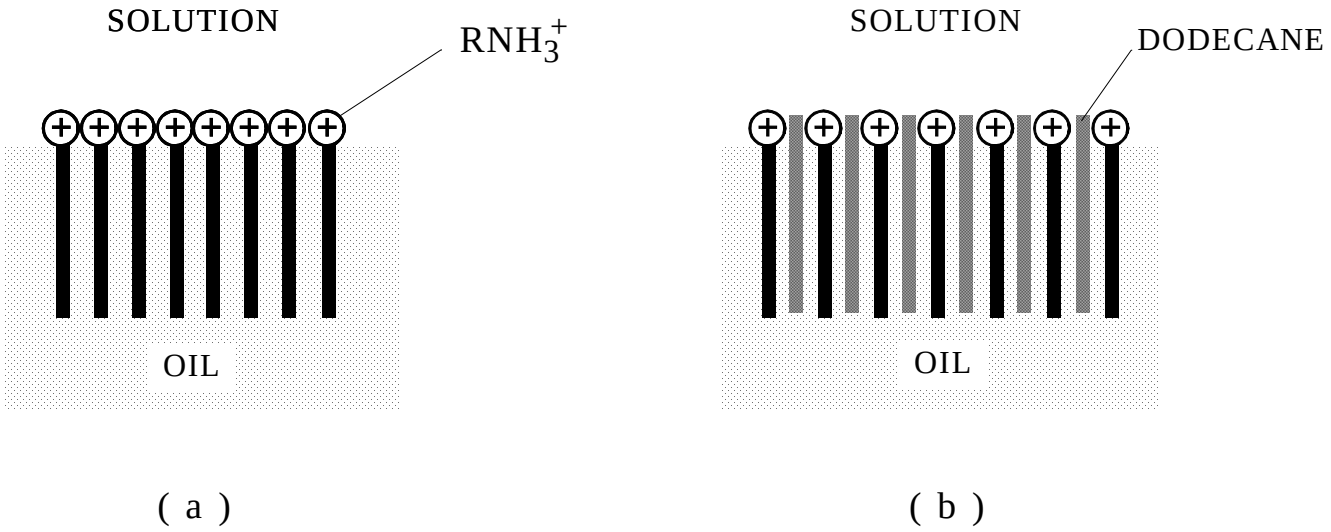

Figure 4.14. Schematic representation for the adsorption of RNH_3^+ at oil/solution interface.

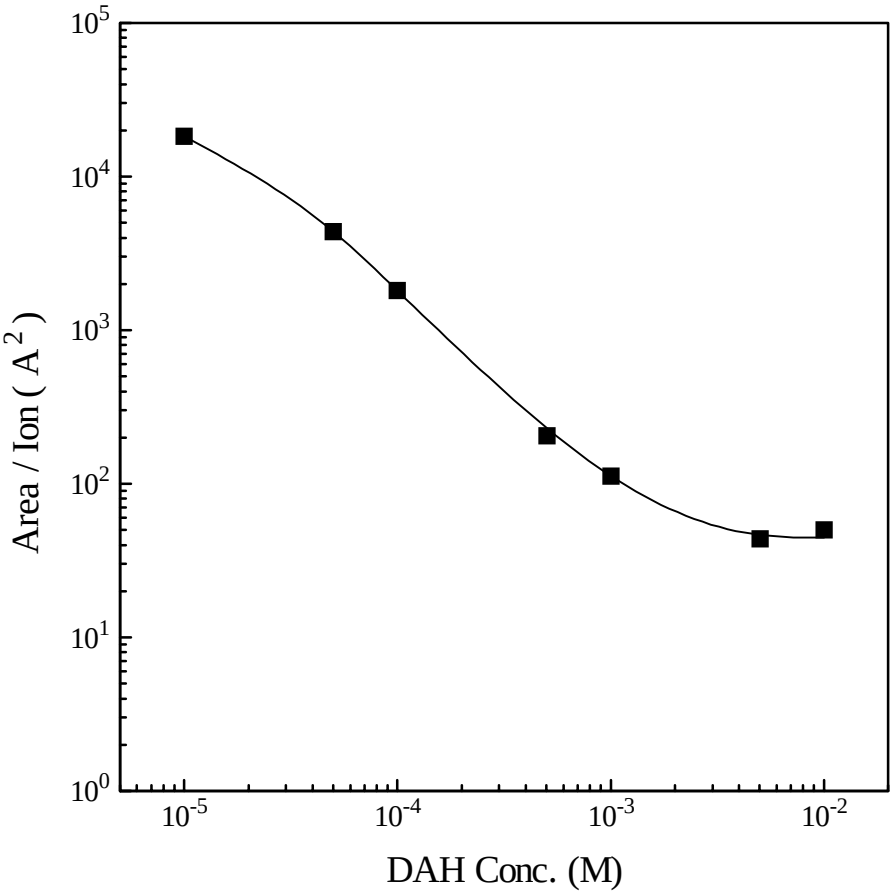

Figure 4.15. The area occupied by each RNH_3^+ ion at oil/solution interface as a function of DAH concentration.

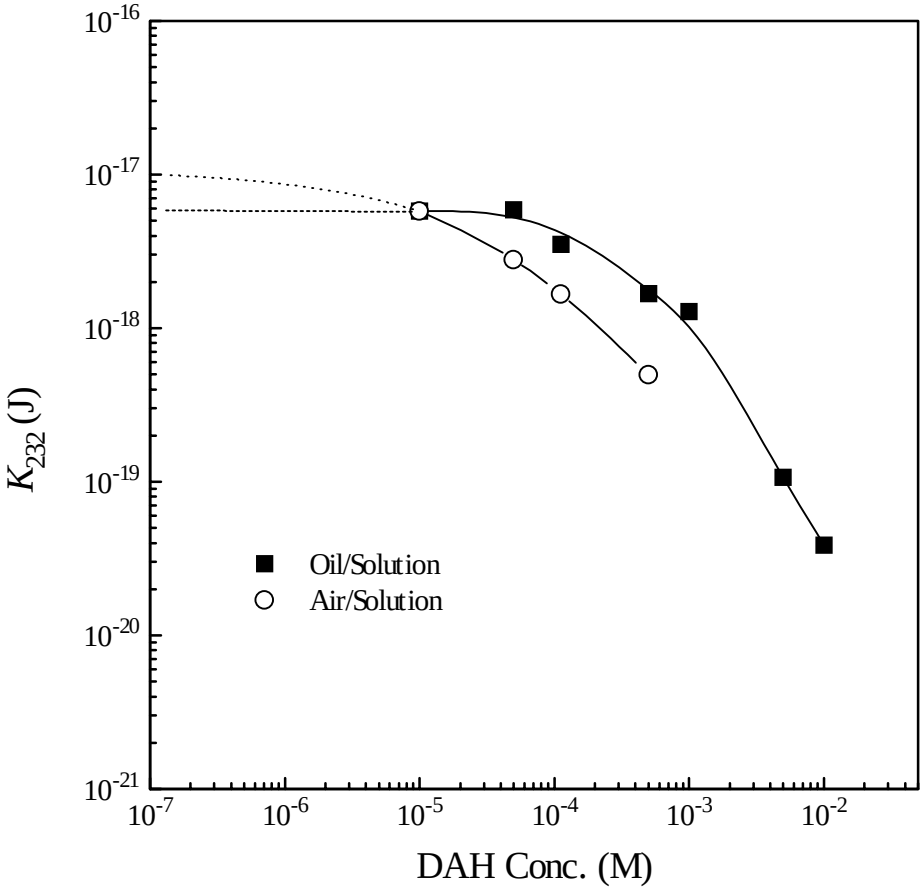

Figure 4.16. Comparison of K_{232} values for oil/solution and air/solution interfaces

interface (72.4 mN/m) is higher than that at oil/water interface (52.1 mN/m). Since water is excluded more completely from the more hydrophobic interface, a higher interfacial tension can be produced. One may expect that the hydrophobicity of the interface is a function of the interfacial tension.

The effect of the surfactant is different for two kinds of interfaces. The decreasing of K_{232} for air/solution interface with increasing DAH concentration is more significant than that for oil/solution interface, which may be attributed to the presence of dodecane molecules at oil/solution interface, as discussed in previous section. Similar to the neutral amine $RNH_2(aq)$ in the solution, these oil molecules are less hydrated, their existence at the oil/solution interface produces more closely packed hydrocarbon layer (44) and also changes the ordering of the hydrocarbon chains which directly affect the hydrophobic force (65). As the results, the hydrophobicity of the interface is improved and the effect of the highly hydrated polar heads of the RNH_3^+ ions is reduced. Therefore, the value of K_{232} for oil/solution interface is less sensitive to the addition of DAH than that for air/solution interface.

Figure 4.17 shows coalescence of two bubbles or oil droplets, the volume reservation gives:

$$2\left(\frac{4}{3}\pi {R_1}^3\right) = \frac{4}{3}\pi {R_2}^3, \qquad [4.18]$$

thus,

$$R_2 = \sqrt[3]{2}\, R_1. \qquad [4.19]$$

The decrease of the free energy (ΔG) is:

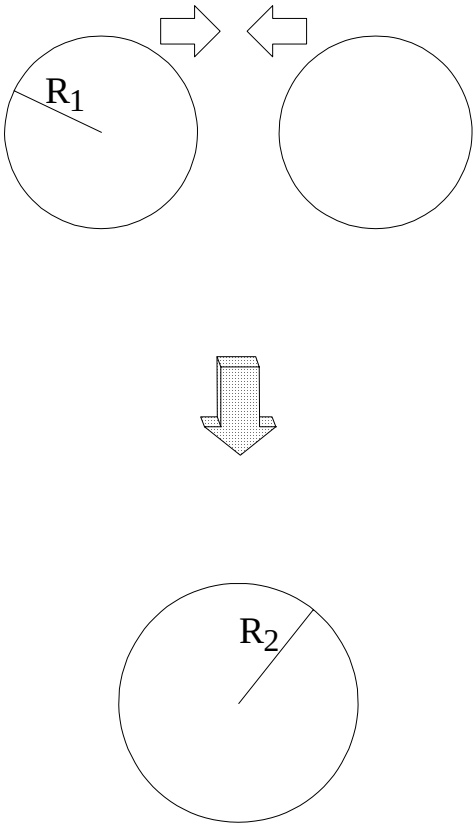

Figure 4.17. Coalescence of droplets dispersed in aqueous solution.

$$\begin{aligned}\Delta G &= \gamma\left(4\pi R_2{}^2 - 2\times 4\pi R_1{}^2\right) \\ &= 4\pi\gamma\left(R_2{}^2 - 2R_1{}^2\right)\end{aligned}, \qquad [4.20]$$

in which γ is the interfacial tension. Substitute Eq. [4.19] to Eq. [4.20],

$$\begin{aligned}\Delta G &= 4\pi\gamma\left(\sqrt[3]{4}R_1{}^2 - 2R_1{}^2\right) \\ &= -1.6504\pi\gamma R_1{}^2\end{aligned}. \qquad [4.21]$$

Eq. [4.21] indicating that, the decreasing of the free energy is proportional to interfacial tension. Since the surface tension of water (72.4 nN/m) is higher than that of dodecane/water interface (52.1 mN/m)(66), the magnitude of ΔG for bubble coalescence is larger than that for oil coalescence. Therefore, the air bubbles have more tendency to combine each other than oil droplets, which may attribute or relate to the better hydrophobicity of air bubbles than that of dodecane droplets dispersed in pure water. One may expect that, there may exist a relationship between hydrophobicity and interfacial tension, the higher the interfacial tension, the better the hydrophobicity. More investigation is necessary to validate this conclusion.

4.4 Summary and Conclusions

For the first time, the hydrophobic force between two oil/solution interfaces has been quantified in present investigation. The modified Thin Film Balance (TFB) technique was used to measure the equilibrium thickness of the aqueous film immerging in dodecane in the presence of dodecylammonium hydrochloride (DAH). The results show that, the aqueous film is stabilized by the repulsive double layer force, which increases with increasing surfactant concentration. However, the interfacial potentials obtained based on the classical DLVO theory are significantly lower than those calculated using Gibbs' adsorption equation and those at the Outer Helmholtz Plane (OHP),

indicating that there exists an attractive force, called hydrophobic force, which must be included in the classical DLVO theory to determine the stability of the aqueous film. A power law is used to represent the hydrophobic force for convenience. The value of the only parameter K_{232} decreases steadily with increasing DAH concentration and thus the stability of the aqueous film is increased. This is attributed to the increasing adsorption of RNH_3^+ ions at the oil/solution interface. An extrapolation of the experimental data shows that, in the absence of surfactant, the value of K_{232} is about 6×10^{-18} J, which is much larger than the Hamaker constant. Therefore the oil surface is inherently hydrophobic.

Changing the pH from 5.8 to 9.0 increases the concentration of the neutral amine RNH_2(aq) in the solution. These species co-adsorb at the oil/solution interface, change the interfacial composition and slightly increase the hydrophobicity of the interface. The presence of the supporting electrolyte also obviously changes the hydrophobicity of the interface, which is attributed to the increasing concentration of the strongly hydrated electrolyte ions at the oil/solution interface.

The area occupied by each RNH_3^+ ion at oil/solution interface suggests that, the dodecane molecules may present between two RNH_3^+ ions which reduces the effect of the highly-hydrated polar heads of the RNH_3^+ ions on the interfacial hydrophobicity. This new adsorption model provides an explanation for the fact that the value of K_{232} for oil/solution interface is less sensitive to the addition of DAH than that for air/solution interface.

The hydrophobicity of air bubbles is better than that of dodecane droplets dispersed in pure water, which may be related to the difference of the interfacial tensions. It is expected that, higher interfacial tension may results in a stronger hydrophobic force between the droplets dispersed in aqueous solution.

4.5 References

1. Jeffreys, G. V., and Davies, G. A., in: Recent Advances in Liquid-Liquid Extraction, Hanson, C. Ed., Pergamon, New York, p. 495(1971).

2. Easan, D. T., Shah, S. M., Chan, M., Sampath, K., and Shah, R., in: Chemistry of Oil Recovery, R. T. Johansen and R. L. Berg. Eds., ACS Symposium Series 91, American Chemical Society, Washington, DC, p.91(1979).

3. Dahami, M. A., Constant, W. D., and Wolcott, M., *Fuel* **67**, 1242(1988).

4. Wolfgang, R., Eckhart, B., and Walter, M., *Chem. Eng. Sci*. **47**, 555(1992).

5. Miller, A., and Stavans, J., *Langmuir* **12**, 301(1996).

6. Tambe, D. E., and Sharma, M. M., *Advances in Colloid and Interface Sci*. **52**, 1(1994).

7. Anon, *J. Colloid Interface Sci*. **163**, 512(1994).

8. Harald, F., Yannick, S., Johan, S., and Luc, V. J., *Colloids and Surfaces A: Physiochemical and Engineering Aspects* **106**, 33(1996).

9. Medrzycka, K., and Zwiezykowski, W., *Sep. Sci. Technol*. **22**, 1637(1987).

10. Dickinson, E. and Stainsby, G., Colloid in Food, Elsevier Applied Science, London, 1982.

11. Dickinson, E., *Colloids Surf*. **42**, 191(1989).

12. Chen, J. D., Hahn, P. S., and Slattery, J. C., *AIChE J*. **34**, 140(1988).

13. Jeelani, S. A. K., and Hartland, S., *J. Colloid Interface Sci*. **156**, 467(1993).

14. Chen, J. D., *J. colloid Interface Sci*. **107**, 209(1985).

15. Platikanov, D., *J. Phys. Chem*. **68**, 3619(1964).

16. Blake, T. D., and Kitchener, J. A., *J. Chem. Soc. Faraday Trans*. **68**, 1435(1972).

17. Aronson, M. P., and Princen, H. M., *Colloid Polym. Sci*. **256**, 140(1978).

18. Yoon, R. H., and Yordan, J. L., *J. Colloid Interface Sci*. **146**, 565(1991).

19. Burrill, K. A., and Woods, D. R., *J. Colloid Interface Sci*. **42**, 15(1973).

20. Burrill, K. A., and Woods, D. R., *J. Colloid Interface Sci*. **42**, 35(1973).

21. Derjaguin, B. V., and Kussakov, M. M., *Acta Physicochim. URSS* **10**, 25(1939).

22. Derjaguin, B. V., and Landau, L. D., *Acta Physicochim. URSS* **14**, 633(1941).

23. Verwey, E. J. W., and Overbeek, J. Th. G., Theory of the Stability of Lyophobic Colloids, Elsevier, Amsterdam., (1948).

24. Sanders, R. S., Chow, R. S. and Masliyah, J. H., *J. Colloid Interface Sci*. **174**, 230(1995).

25. Groeneweg, F., Vader, F. van V., and Agterof, W. G. M., *Chemical Engineering Sci*. **48**, 229(1993).

26. Hazlet, R. D., and Schechter, R. S., *Colloids Surf*. **29**, 53(1988).

27. Cho, W. G. and Fletcher, D. I., *J. Chem. Soc. Faraday Trans*. **93**(7), 1389(1997).

28. Deshiikan, S. R., and Paradopoulos, K. D., *J. Colloid Interface Sci*. **174**, 302(1995).

29. Deshiikan, S. R., and Paradopoulos, K. D., *J. Colloid Interface Sci*. **174**, 313(1995).

30. Exerowa, D., Kolarov, T. and Khristov, KHR., *Colloids Surf*. **22**, 171(1987).

31. Bergeron, V., Waltermo, R., and Cleasson, P. M., *Langmuir* **12**, 1336(1996).

32. Joye, J. L., and Miller, C. A., *Langmuir* **8**, 3083(1992).

33. Ruckenstein, E., and Bhakta, A., *Langmuir* **12**, 4134(1996).

34. Pugh, R. J., *Advances in Colloid and Interface Sci*. **64**, 67(1996).

35. Rabinovich, Y. I. And Yoon, R. H., *Langmuir* **10**, 1903(1994).

36. Tchaliovska, S., Manev, E., Radoev, B., Eriksson, J. C. and Claesson, P. M., *J. Colloid Interface Sci*. **168**., 190(1994).

37. Scheludko, A., *Proc. Kon. Ned. Akad. Wetensch* **B65**, 76(1962).

38. Scheludko, A., *Adv. Colloid Interface Sci*. **1**, 391(1967).

39. Aksoy, B. S., "Hydrophobic Forces in Free Thin Films of Water in the Presence and Absence of Surfactants", Ph. D. Thesis, Dept. of Mining Minerals Eng., Virginia Polytechnic Institute and State University, 1997.

40. Adamson, A. W., Physical chemistry of surface, 5th Edition, John Wiley & Sons, Inc., 1990.

41. Andreas, J. M., Hauser, E. A. and Tucker, W. B., *J. Phys. Chem*. **42**, 1001(1938).

42. Niederhauser, D. O. and Bartell, F. E., Report of progress-fundamental research on the occurrence and recovery of petroleum, Publication of the American Petroleum Institute, The Lord Baltimore Press, Baltimore, 114(1950).

43. Fuerstenau, D. W., *Trans. AIME* **208**, 1365(1957).

44. Yoon, R. H. and Ravishankar, S. A., *J. Colloid Interface Sci*. **166**, 215(1994).

45. Rutland, M., Waltermo, A., and Claesson, P., *Langmuir* **8**, 176(1992).

46. Somasundaran, P., *Int. J. Miner. Process*. **3**, 5(1976).

47. Bergeron, V., Langevin, D., and Asnacios, A., *Langmuir* **12**, 1550(1996).

48. Kolarov, T., Cohen, R. and Exerowa, D., *Colloid. Surf*. **42**, 49(1989).

49. Israelachvili, J. N., Intermolecular and Surface Force with Applications to Colloid and Biologocal Systems, Academic Press, Orlando, FL., (1985).

50. Usui, S., Electrical Double Layer, In: Kitahara, A. and Watanabe, A. (Editor), Electrical Phenomena at Interfaces: Fundamentals, Measurements and Applications, Marcel Dekker, Inc., New York and Basel, (1984).

51. CRC Handbook of Chemistry and Physics, 76th Edition, CRC Press, Inc. Boca Raton, Florida. 1995.

52. Gouy, L., *J. Phys*. (4), **9**, 457(1910); *Ann. Phys*. (9), **7**, 129(1917).

53. Chapman, P. L., *Philos. Mag.* (6), **25**, 475(1913).

54. Kjellander, R. and Marcelja, S., *Chem. Phys. Lett*. **112**, 49(1984); and *J. Phys. Chem*. *90*, 1230(1986).

55. Guldbrand, L., Jönsson, B., Wennerström, H. and Linse, P., *J. Chem. Phys*. **80**, 2221(1984).

56. Attard, P., Mitchell, J. and Ninham, B. W., *J. Chem. Phys*. **89**, 4358(1984).

57. Pugh, R. J. and Yoon, R. H., *J. Colloid Interface Sci*. **163**, 169(1994).

58. Israelachvili, J. N. and Pashley, R., *Nature* **300**, 341(1982).

59. Pashley, R. M., McGuiggan, P. M., Ninham, B. W. and Evans, D. F., *Science* **229**, 1088(1985).

60. Claesson, . M., Blom, C. E., Herder, P. C. and Ninham, B. W., *J. Colloid. Interface Sci*. **114**, 234(1986).-

61. Tsao, Y., Yang, S. X. and Evans, D. F., *Langmuir* **7**, 3154(1991).

62. Rabinovich, Y. I. And Derjaguin, B. V., in: Proceed. 5th Hungarian Conference on Colloid Chemistry, Loránd Eötvös University, Budapest, Hungary, 1988.

63. Christensson, H. K., Claesson, P. M. and Parker, J. L., *J. Phys. Chem*. **96**, 6725(1992).

64. Tsao, Y. and Evans, D. F., *Langmuir* **9**, 779(1993).

65. Rabinovich, Y. I., Guzonas, D. A. and Yoon, R. H., *Langmuir* **9**, 1168(1993).

66. Dukhin, S. S., Kretzschmar, G., and Miller, R., Dynamics of Adsorption at Liquid Interfaces Theory, Experiment, Application, In: Mobius, D. and Miller, R. Eds. Studies in Interface Science. Elsevier, New York, (1995).

4.6 Appendix

The principle underlying the film thickness measurement is demonstrated in Figure A4.1. Light wave, reflected by the top surface of the film, interfere with reflected waves that reflect off the bottom surface of the film, the optical path differences between the interfering waves generates a phase difference that can be used to extract the film thickness. For normally incident light on a homogeneous film, the relationship between R and H is given by the Raleigh equation (1):

$$R = \frac{I^r}{I_0} = \frac{A^2 + B^2 + 2AB\cos\theta}{1 + A^2B^2 + 2AB\cos\theta} \qquad [A4.1]$$

where

$$A = \frac{n_1 - n_0}{n_1 + n_0} \qquad B = \frac{n_2 - n_1}{n_{12} + n_1}$$

$$\theta = \frac{4\pi n_1 H}{\lambda}$$

in which λ is the wavelength of the incident light. θ is the phase angle, I_0 is the intensity of the incident light and I^r is the reflected light intensity. n_0, n_1 and n_2 are the refractive indices corresponding to the incident, film and transmitting medium respectively, as shown in Figure A4.1. Table A4.1 shows the refractive indices of the phase involved in the present work. The relationship between reflectance and film thickness for dodecane-water-dodecane system is shown in Figure 4.3 when monochromatic light with wavelength of 602.1 nm is used.

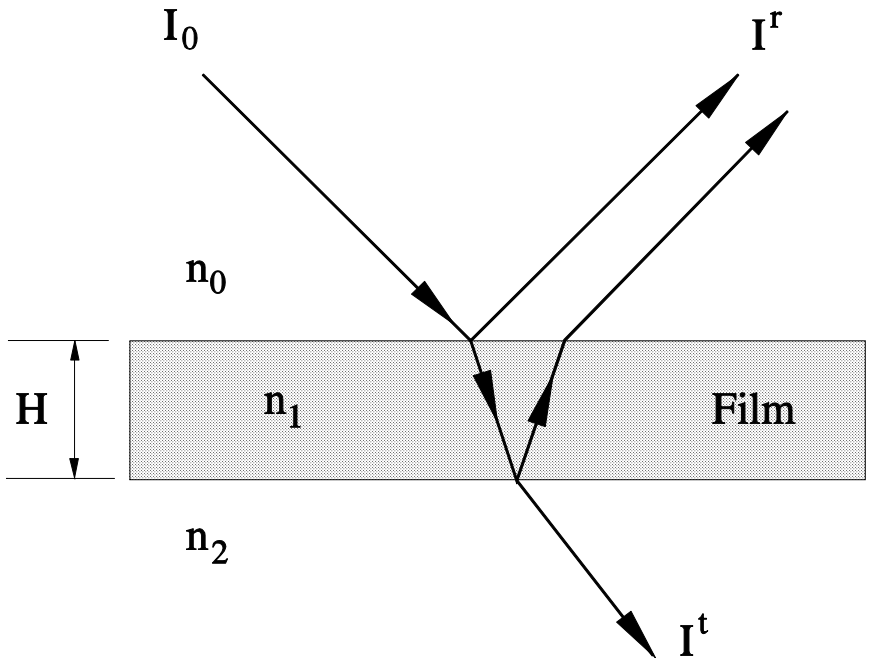

Figure A4.1 Thin film interference.

TABLE A4.1 The refractive indices of the interface involved in the thin film thickness measurement

Interface	n
Water	1. 331 *
Dodecane	1. 4216 **

* Reference (2)

** Reference (3)

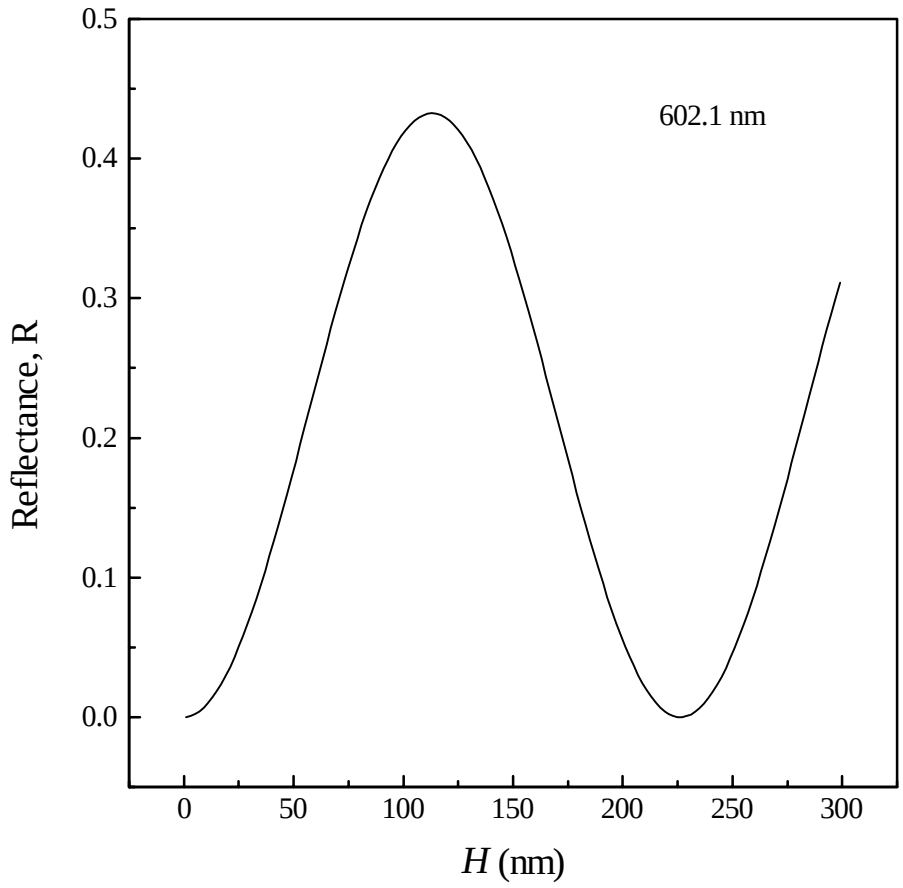

Figure A4.2 Reflectance as a function of the film thickness for the dodecane-water-dodecane system and monochromatic light with λ = 602.1 nm.

However, the image analysis system can't measure the reflectance of the interference pattern directly, it can only measure the gray level intensity of the digitized image. Therefore, a calibration curve, which connects the gray level intensity to reflectance, was determined by measuring the gravy level intensity of calibration standards of known reflectance. Figure A4.3 shows a typical calibration curves demonstrating a linear relationship between the gray level intensity and the reflectance, thus the reflectance of the interference pattern can be obtained from the measurement of gray level intensity.

References

1. Vasicek, A., Optics of Thin Films, North-Holland Pub. Co., Amsterdam, 60(1996)
2. Blake, T. D., and Kitchener, J. A., *J. Chem. Soc., Faraday Trans I* **68**, 1435(1972).
3. CRC Handbook of Chemistry and Physics, 76th Edition, CRC Press, Inc. Boca Raton, Florida. 1995.

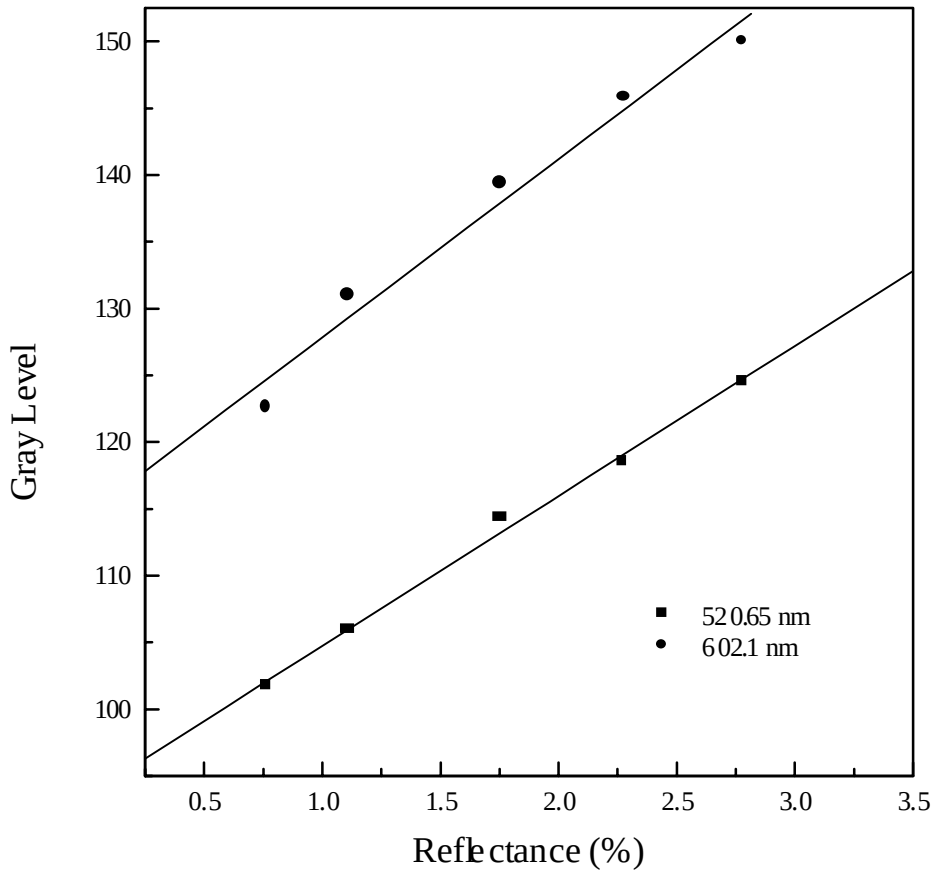

Figure A4.3 Reflectance versus gray level for monochromatic light with λ=602.1 nm.

CHAPTER 5: CONCLUSIONS

The major findings of the present investigation are summarized as following:

1. A first-principle flotation rate equation has been developed by considering both hydrodynamic and surface forces involved in bubble-particle interactions. The extended DLVO theory, which includes the hydrophobic force in addition to the electrostatic double-layer force and van der Waals dispersion force, is essential to understand the elementary subprocesses of flotation, from which the explicit expressions for probabilities of adhesion and detachment are derived, and thus a complete flotation model is obtained. The model can be used to predict the flotation rate from the hydrodynamic and surface chemistry parameters of the system.

2. The bubble-particle adhesion in flotation may be considered analogous to chemical reaction. The activation energy or energy barrier (E_1) can be determined from the extended DLVO theory, while the kinetic energy (E_k) for adhesion can be obtained from the tangential velocity of the particle moving around a bubble which can be calculated using the stream function of the system. The computation results showed that, E_k is a function of not only the hydrodynamic properties of particle, bubble and medium, but also the initial position of particle relative to the bubble surface and critical thickness of the disjoining film (H_1) which is dependent on the surface forces between bubble and particle. At a given H_1, there is a distribution of E_k values, and thus a mean kinetic energy should be used to determine the probability of adhesion.

3. The bubble-particle detachment can be considered as a reverse process of the attachment. Therefore, a corresponding Arrhenius-type expression is derived in present work for the probability of detachment. The activation energy for this process is the sum of the work of adhesion (W_a) and E_1. The kinetic energy (E_k') may be determined using French and Wilson's model for fine particles attached on the bubble surface. In addition to the hydrodynamic properties of bubble and particle, the contact angle of solid surface and the number of particles attached on the bubble surface also determine the value of E_k'. As a result, E_k' is a step function with respect to the bubble rising time in a flotation column.

4. The new model can also be used to determine one of the parameters involved in the system from flotation results. In the present investigation, the hydrophobic force parameter was calculated using the data of rate constants obtained from the single bubble flotation tests. The results show that, the hydrophobic force parameters for bubble-particle interaction (K_{132}) are substantially larger than those for particle-particle interaction (K_{131}) but smaller than those for air bubbles interacting with each other (K_{232}) in the absence of surfactant. In fact, the K_{132} values are close to the geometric means of K_{131} and K_{232}, i.e.

$$K_{132} = \sqrt{K_{131} \cdot K_{232}} \ .$$

This "combining rule", obtained for the first time in present work, reveals the relationship among the hydrophobic force parameters for different interfaces. It can be used to calculate the hydrophobic force parameter, which is difficult or impossible to be determined experimentally, from the other two hydrophobic force parameters which may be obtained much easily. Therefore, the combining rule has great potential application. Also, it is validated by asymmetric direct force measurement conducted after present investigation.

5. The model developed in the present investigation can also provide theoretic explanation for flotation responses, and suggest various methods to improve the behavior of flotation. The total energy curves show that, the hydrophobic force plays the most important role in decreasing the energy barrier for bubble-particle interaction, and hence increasing the flotation rate.

6. The model is used to simulate the flotation process as a function of various parameters and investigate the mechanisms involved. The results shows that, when the double layers of bubble and particle are of like charge, decreasing the magnitude of double layer potential enhances the flotation rate due to the decreasing of activation energy. On the other hand, the selectivity of separation becomes better when the potential is increased.

7. The hydrophobic force, the main driving force for bubble-particle adhesion, can be accurately represented by K_{132}. The simulation results show that, the rate constant is obviously increased with increasing K_{132}, which is attributed to the decreasing of the activation energy. In most cases, the contact angle is a good alternate representation of the hydrophobic force which can be easily determined experimentally. Higher contact angle indicates stronger hydrophobic force, which decreases the activation energy (E_1) and the probability of detachment (P_d), resulting in increasing of rate constant.

8. For given values of K_{132}, increasing the electrolyte concentration decreases both E_1 and E_k, resulting in a minimum value of k which is observed in the flotation tests when K_{132} is low. However, the presence of the electrolyte may also change the hydrophobic attraction between bubble and particle which can not be simulated without the relationship between K_{132} and electrolyte concentration.

9. The simulation results demonstrates a linear relationship between the logarithmic values of k and particle size, which are observed in many flotation systems when the particle is small and P_d is close to 1. The increasing of k with the particle size is primarily due to the increasing of the kinetic energy (E_k) and thus the probability of adhesion (P_a).

10. There is an optimum bubble size at which the maximum rate constant can be obtained. This is attributed to the increasing of P_c and S_b, and decreasing of P_a with decreasing of bubble size. The optimum shifts toward smaller bubble size as the particle hydrophobicity increases, which provides an appropriate bubble size to achieve the best selectivity of flotation.

11. The modified Thin Film Balance (TFB) technique was used to measure the equilibrium thickness of the aqueous solution immersing in dodecane in presence of dodecylammonium hydrochloride (DAH). It is shown that, the equilibrium thickness can be obviously decreased with increasing DAH concentration.

12. The aqueous film is stabilized by the repulsive double layer force, which increases with increasing surfactant concentration. However, the double layer potentials calculated using the classic DLVO theory are significantly lower than those obtained using Gibbs' adsorption and at the Outer Helmholtz Plane (OHP), which was attributed to the hydrophobic force not included in the classic DLVO theory.

13. For the first time, the hydrophobic force parameter K_{232} of two oil/solution interfaces has been determined using the extended DLVO theory. The results showed that, the value of K_{232} decreased obviously with increasing DAH concentration, resulting in an increasing of stability of the aqueous film, which was attributed to the increasing adsorption of RNH_3^+ ions at the oil/solution interface. In absence of surfactant, K_{232} is about 6×10^{-18} J, which is much larger

than the Hamaker constant, demonstrating the inherent hydrophobicity of oil/water interface.

14. The improvement of hydrophobicity of the interface with increasing pH from 5.8 to 9.0 is not significant, in spite of the fact that the concentration of the neutral amine $RNH_2(aq)$ in the solution is increased, which co-adsorbs at the interface and changes the interfacial composition.

15. Addition of the supporting electrolyte may obviously reduce the hydrophobic attraction, resulting in an increase of the film stability. This may be attributed to more strongly hydrated electrolyte ions present at the oil/solution interface.

16. An adsorption model at the oil/solution interface has been proposed. It is showed that, the dodecane molecules may present between two RNH_3^+ ions at the interface, which reduces the effect of the surfactant species on the interfacial hydrophobicity. As a result, the value of K_{232} for oil/solution interface is less sensitive to the addition of DAH than that for air/solution interface.

17. Thermodynamic analysis showed that, there might exist a relationship between the interfacial hydrophobicity and interfacial tension. A stronger hydrophobic force may be expected for the interfaces with higher interfacial tension.

CHAPTER 6: RECOMMENDATIONS FOR FUTURE RESEARCH

Based on the conclusions of the present work, further investigations into the following areas are recommended:

1. The flotation model developed in the present work was used to determine the hydrophobic force parameter K_{132} from the experimental data of rate constants. The calculation results suggested the combining rule, a relationship among the hydrophobic force parameters of different interfaces. This rule has been validated later in direct force measurement, providing a indirect verification of the flotation model. However, the model should be verified directly, which can be done by measuring the values of K_{132} using modified AFM, Thin Film Balance (TFB) or traditional bubble-against-plate technique. The values obtained, together with other hydrodynamic and surface force parameters, can be used in the flotation model to predict the rate constants which can be directly compare with the experimental results of single bubble flotation test. Also, the values of K_{132} can be compared with those of K_{131} and K_{232}, which can be readily obtained using AFM and TFB technique respectively, to verify the combining rule. Since the real bubbles are used in the experiments, this verification should be more directly, and then more reliable than that using hydrophobic solid surface to simulate air bubble.

2. In derivation of the expressions for P_c from the stream functions of the system, it was assumed that particles in the suspension were small enough that they could be considered inertialess and thus followed the streamlines of the liquid. This assumption becomes less valid as the ratio of particle to bubble diameter increases, large particles may have sufficient inertia to deviate from the streamlines and directly colloid with bubble surface, resulting in a higher value of

P_c. However, if the inertia of particle is considered in the bubble-particle collision, it is difficult to derive an explicit expression of P_c, thus numeric techniques usually have to be used which may cause other problems in the computation. More investigation is desired to develop analytical expression of P_c which incorporates the effect of particle inertia.

3. The general expression for bubble-particle detachment has been developed in present work, and French and Wilson's model is used to determine the kinetic energy for detachment (E_k'). The fluid pressure subjected by the particles on the bubble surface is considered as the driving force for bubble-article detachment, which is valid only for small particle. For large particle, the gravitational force, turbulent forces and bubble oscillations acting on attached particle should also be considered. Therefore, developing a method of determining E_k' is necessary when the flotation model is used for coarse particle flotation.

4. In order to analyze the elemental subprocesses of bubble-particle interaction, the flotation system considered in present work is extremely simplified. Actual flotation, of course, is more complicated by other variables, such as the concentration and distribution of air bubbles, particle shape, particle rotation on the bubble surface, etc. which may obviously change the efficiency of flotation. These influences should be quantitatively represented in the future research before the model is used in industrial practices. In addition, the model presented in this work only describes the bubble-particle interaction in the recovery zone, however, the characterization of the froth zone is also essential to completely describe the behavior of the actual flotation system, which should also be conducted in future investigation.

5. It has been shown that the disjoining pressure isotherm for oil/solution interfaces is difficult to be obtained using Thin Film Balance (TFB) technique, especially

when the concentration of surfactant is low. The apparatus designed recently by Aveyard *et al*, as described in Chapter 1, provide a new technique which can be used in the future research to measure the disjoining pressure as a function of distance. Since the film thickness is determined from the optical interference pattern obtained using a microscopy, the values obtained should be more reliable than that using modified Atomic Force Microscope.

6. The comparison of K_{132} values of air bubble and oil droplet conducted in present investigation showed that, the interfacial hydrophobicity might be related to the interfacial tension. A series of similar experiments should be carried out using other oils with different interfacial tension, from which a quantitative relationship between the hydrophobicity and the interfacial tension can be obtained. Such relationship can be used to predict the interfacial hydrophobicity from the interfacial tension, and may provide an explanation of the origin of hydrophobic force existing between two oil/water interfaces. Since the hydrophobic force often dominates the stability of the oil/water emulsions, this relationship may find very broad applications in industries.

VITA

Laiqun Mao was born in Qidong, Jiangsu Province, P. R. China, where he lived until graduation from the Donghai High School in September, 1980. He immediately enrolled himself in the Mineral Processing Engineering Program at Northeast University, Shenyang, Liaoning Province, P. R. China, and received his B.S. Degree in July, 1984 and his M.S. degree in January, 1987. During his undergraduate career, he was awarded four times of scholarship and three times of outstanding student for academic excellence. After teaching at the Northeast University for more than five years, he was awarded a research assistantship and enrolled in the doctoral program for Mining and Minerals Engineering at Virginia Polytechnic Institute and State University, Blacksburg, Virginia in May, 1992, where he won Outstanding Graduate Student award in 1995. He is a member of the Society of Mining, Metallurgy and Exploration, member of the Honor Society of Phi Kappa Phi, and member of the Phi Beta Delta Honor Society for International Scholars. He has six publications and six presentations on professional meetings to his credit.